Titre: Title:	Développement d'un analyseur thermogravimétrique à lit fluidisé : application à la gazéification catalytique du charbon
Auteur: Author:	Said Samih
Date:	2016
Type:	Mémoire ou thèse / Dissertation or Thesis
Référence: Citation:	Samih, S. (2016). Développement d'un analyseur thermogravimétrique à lit fluidisé : application à la gazéification catalytique du charbon [Thèse de doctorat, École Polytechnique de Montréal]. PolyPublie. https://publications.polymtl.ca/2111/

URL de PolyPublie: PolyPublie URL:	https://publications.polymtl.ca/2111/
Directeurs de recherche: Advisors:	Jamal Chaouki
Programme: Program:	Génie chimique

UNIVERSITÉ DE MONTRÉAL

DÉVELOPPEMENT D'UN ANALYSEUR THERMOGRAVIMÉTRIQUE À LIT FLUIDISÉ : APPLICATION À LA GAZÉIFICATION CATALYTIQUE DU CHARBON

SAID SAMIH

DÉPARTEMENT DE GÉNIE CHIMIQUE

ÉCOLE POLYTECHNIQUE DE MONTRÉAL

THÉSE PRÉSENTÉE EN VUE DE L'OBTENTION

DU DIPLÔME DE PHILOSOPHIAE DOCTOR

(GÉNIE CHIMIQUE)

AVRIL 2016

UNIVERSITÉ DE MONTRÉAL

ÉCOLE POLYTECHNIQUE DE MONTRÉAL

Cette thèse intitulée :

DÉVELOPPEMENT D'UN ANALYSEUR THERMOGRAVIMÉTRIQUE À LIT FLUIDISÉ : APPLICATION À LA GAZÉIFICATION CATALYTIQUE DU CHARBON

Présenté par : SAMIH Said

en vue de l'obtention du diplôme de : Philosophiae Doctor

a été dûment acceptée par le jury d'examen constitué de :

M. TAVARES Jason-Robert, Ph. D., président

M. CHAOUKI Jamal, Ph. D., membre et directeur de recherche

M. PERRIER Michel, Ph. D., membre

M. MACCHI Arturo, Ph. D., membre externe

DÉDICACE

A mes chers parents,

Que ce travail soit l'exhaussement de vos vœux, tant formulés, et de vos innombrables sacrifices.

A mes sœurs et frères,

Veuillez trouver, ici, le témoignage d'une fraternité indéfectible. Que ce travail soit aussi le vôtre.

A tous ceux qui me sont chers,

SAMIH Said

REMERCIEMNTS

J’aimerais tout d’abord exprimer mes profonds remerciements à mon directeur de recherche, Professeur Jamal Chaouki, pour m’avoir accompagné toutes ces années. Sa patience, son encouragement, ainsi que son aide compétente m’ont permis de mener à bien ce projet de doctorat. Ses critiques m’ont été précieuses tant pour structurer ce travail que construire ma vie personnelle.

Je tiens à remercier l’ensemble des techniciens, ainsi que le personnel administratif, du département génie chimique. La majorité de ce travail n’aurait pu être réalisée sans leurs précieuses aides. Je pense particulièrement au grand Robert Delisle, Sylvain Fleury-Simard, Gino Robin, Yazid, Martine Lamarche, Jean Huard, Daniel Pilon, Valérie Baudart, Hélène Chatillon, Mehdi Bentounes, Michelle McNicoll, Carole Massicotte, Sylvie Taillon, Josée Rivest, Évelyne Rousseau, Gagnon Brigitte et Carmen-Elena Membreno Aguilar.

J’exprime aussi ma gratitude à Madame Manon Leduc, du département génie civil, géologie et des mines, pour m’avoir permis d’utiliser son montage expérimental pour le broyage et tamisage du charbon.

J’ai une dette de reconnaissance infinie envers toute l’équipe de recherche PEARL, pour leur soutien agréable. L’accomplissement de cette thèse n’aurait pu être possible sans les nombreuses discussions avec mes collègues Rouzbeh, Milad, Farzam, Majid, Jaber, Omid, Pierre, Mohammad, Abdelmadjid, Rachid, Sepehr, Soumaya, El Mahdi, Abdelkamel, Bajil, Aziz, Carlos, Julie et toute la troupe de recherche PEARL.

Enfin, une pensée particulière à tous les amis et collègues avec qui j’ai partagé un café, un repas, une aventure ou une discussion : les Karim(s), Najlae, Imane, Fadoua, Saida, Kaouthar, Najma, Aamal, El Mustapha, Youness, Issmail, Omar, les Ilyas (s), Simona, Adnane et Abdellah Azimani, Mohamad Saidi, Saida, tous les Émistes ALEMI, les Hatim(s), Kamal, Hilal, Abdelmorhit, Najib et ses petits, Ibrahim et ses sœurs, Rhaouti, Oussama et sa famille, Hassan, Bensalem et sa famille, Sophie, James Abbott, ainsi que tous les autres dont j’ai pu avoir oublié de mentionner le nom.

RÉSUMÉ

Un analyseur thermogravimétrique (ATG) à lit fluidisé a été développé afin de surmonter les nombreuses limitations de l'ATG conventionnel. Une configuration spéciale des instruments de mesure a permis de mesurer le poids de l'échantillon, introduit dans l'ATG à lit fluidisé, en temps réel. Une autre particularité de cet équipement est le contrôle et la régulation des débits des gaz alimentés en fonction de la température. Cette technique a permis de garder un régime de fluidisation optimale pour obtenir un mélange approprié au sein du lit fluidisé, tout en minimisant les vibrations du système. De plus, cet ATG à lit fluidisé a été muni de plusieurs analyseurs des gaz produits : FTIR et chromatographie en phase gazeuse.

La décomposition thermique de l'hydroxyde de calcium a fait l'objet du test de validation de l'ATG à lit fluidisé. Les résultats ont été impressionnants : les limitations de transfert de matière et de chaleur, qui ont été observées dans l'ATG conventionnel, ont disparu de l'ATG à lit fluidisé. Cette conclusion a été consolidée par une analyse des échantillons produits par la technique de la diffraction des rayons X (XRD). Les résultats ont confirmé que l'ATG à lit fluidisé sera, dans le futur, un équipement idéal pour l'étude de la cinétique et de mécanismes des réactions chimiques gaz-solide.

Vu l'importance du charbon dans le portfolio énergétique mondial, il a été décidé de faire de la gazéification du charbon une première application dans l'ATG à lit fluidisé en décomposant les réactions associées au mécanisme de la réaction. Ainsi, une série de tests expérimentaux sur la pyrolyse du charbon, la gazéification du char et la gazéification du charbon dans l'ATG fluidisé a été effectuée. Les résultats ont été traités pour trouver les différents paramètres cinétiques de la dévolatilistaion totale du charbon, ainsi que ceux des principaux gaz produits de la pyrolyse. La cinétique de l'oxydation partiale du char a été étudiée dans l'ATG à lit fluidisé et les paramètres cinétiques ont été développés. Le modèle de la cuve parfaitement agitée a été utilisé pour décrire le fonctionnement du réacteur de l'ATG à lit fluidisé. Ce modèle a été alimenté par les paramètres cinétiques obtenus précédemment, et les résultats ont été comparés avec ceux obtenus expérimentalement. L'équilibre la gazéification du charbon a aussi été étudié dans l'ATG à lit fluidisé. Les résultats ont montré que les réactions de reformage du méthane, ainsi que celle du déplacement de monoxyde de carbone, ont été loin d'être en équilibre.

Les cendres et le soufre, contenus intrinsèquement dans le charbon, constituent un problème majeur pour le développement des technologies de gazéification du charbon. C'est pourquoi il a été décidé de faire de la gazéification catalytique du charbon sans cendre la deuxième application de l'ATG à lit fluidisé. Les cendres ont été éliminées du charbon grâce à un procédé développé par l'Université d'Alberta. Le charbon sans cendre a été gazéifié dans l'ATG à lit fluidisé. Le catalyseur (K_2TiO_3) a permis d'obtenir une meilleure conversion de carbone à basse température avec des gaz produits de grande valeur énergétique. Une diminution de la quantité du goudron, produite de la gazéification du charbon sans cendre, a été obtenue par l'application du catalyseur. L'effet catalytique a permis, aussi, de diminuer les énergies d'activation des principales réactions de gazéification, incluant le reformage du méthane et le déplacement de monoxyde de carbone.

ABSTRACT

A new fluidized bed thermogravimetric analyzer (TGA) was developed to overcome the various limitations of the conventional TGA. This is the first equipment that combines both fluidization and thermogravimetric analyzer technologies. A new concept of «the pseudo-variation» of the weight was introduced in the fluidized bed TGA. A novel model was developed to transform the energy loss, by the fluidizing agent, into weight. This pseudo variation of the weight was evaluated by measuring the pressure drop through the gas distributor and filter. A special configuration was used to obtain the real weight loss of the sample inside the reactor. Another particularity, which was introduced by the fluidized bed TGA, is the strategy for gas flow rate adjustment according to temperature. This program was used for controlling the gas flow rate as a function of temperature to maintain the minimum fluidization regime throughout all of the experiments. Calcium hydroxide decomposition was the standard test that was used for the validation of the fluidized bed TGA. The results were compared with those obtained from the conventional TGA. Diffusion control was eliminated by the application of the fluidized Bed TGA, which was confirmed by the X-Ray Diffraction (XRD) analysis on the treated samples. The reliability of the newly developed equipment was confirmed by such validation test.

Coal gasification was studied in the novel fluidized bed thermogravimetric analyzer. The weight loss obtained from the fluidized bed TGA was in general agreement with the total gas product. For coal pyrolysis, resulting activation energies for the individual gases were 3 to 4 times lower than those found in literature. For char gasification, the resulting kinetic parameters were in relative agreement with those found in literature. The Continuous Stirred-Tank Reactor (CSTR) model was used to describe the reaction chamber of the fluidized bed TGA. The experimental and the model results were in reasonable agreement. Equilibrium data were also compared with experimental results. The steam reforming and the CO shift reactions were far from equilibrium.

The application of potassium catalyst (K_2TiO_3) on ash free coal gasification was studied in the fluidized bed TGA. The total gas product was in general agreement with the total yield obtained from the fluidized bed TGA. The carbon conversion and the higher heating value of the gas product gas were significantly enhanced by the catalyst application on ash free coal gasification. The effect of catalyst on the kinetics of char gasification was neglected. The activation energy of the CO shift

reaction was decreased by 45%, from the previous one without catalyst, by applying catalyst. This value was decreased 19% from the one reported in literature in the case of catalytic gasification. The value of the activation energy of the methane reforming reaction was reduced by 40% from the one found in this work without catalyst. Higher heating value of the product gas and higher carbon conversion could be obtained in catalytic ash free coal gasification at low temperatures.

TABLE DES MATIÈRES

LISTE DES TABLEAUX

LISTE DES FIGURES

LISTE DES SIGLES ET ABRÉVIATIONS

AFC	Ash free coal
ATG	Analyseur thermogravimétrique à lit fluidisé
ATGF	Analyseur thermogravimétrique à lit fluidisé
CatAFC	Catalyst with ash free coal
DSC	Differential Scanning Calorimetry
FB-TGA	Fluidized Bed Thermogravimetric Analyzer
FTIR	Fourier Transform Infrared
GC	Gas Chromatography
HC	Hydrocarbons
HHV	Higher Heating Value
MFC	Mass Flow Controller
PCI	Pouvoir Calorifique Inférieur
TGA	Thermogravimetric Analyzer
XRD	X-Ray Diffraction
WGS	Water Gas Shift

LISTE DES ANNEXES

CHAPITRE 1 INTRODUCTION

L'influence de l'activté humaine sur le système climatique a été récement qualifiée par la plus élevée depuis les années 1950, début de l'époque préindustrielle. L'atmosphère et l'océan se sont rechauffés. Les eaux de mers se sont acidifiées en absorbant 30 % des émissions anthropiques de dioxyde de carbone. Au cours des dernières decennies, l'océan a stocké environ 93 % de l'augmentation de l'énergie dans le système climatique. Ce qui a entraîné une élévation du niveau de la mer ainsi qu'une dimunition de la couverture de neige et de glace [1-5].

En septembre 2015, un record des anomalies de température à la surface de la terre a été observée [3]. La température moyenne du globe terrestre a été la plus élevée depuis 136 ans, à 0,9 ° C au-dessus de la moyenne du 20ème siécle, qui est de 15,0 °C. Cette valeur est en augmentation de 0,06 ° C par décennie. Au Canada, les températures ont été supérieures à la moyenne jusqu'à 5 ° C dans toute la province de l'Ontario. Environ 2,1 ° C au-dessus de la moyenne du 20ème siécle a été observée aux États-Unis. Septembre 2015 a été, cependant, le plus froid en Espagne et au Royaume-Uni, à 0,8 ° C en dessous de la moyenne natioale dans la période 1981-2010 [2-4].

La cause principale du changement climatique observé est l'émission anthropique du gaz à effet de serre (GES), incluant le dioxyde de carbone (CO_2), le méthane (CH_4) et le protoxyde d'azote (N_2O). Le probleme principal réside dans le CO_2, même si le CH_4 a un impact sur l'effet de serre 21fois plus grand que celui de CO_2 sur une période de 100 ans. Due majoritairement aux croissances économique et démographique, le total des gaz à effet de serre anthropiques (GES) a continué d'augmenter d'une facon considérable, et ceci depuis la révolution industrielle. En 2011, les concentrations respectives de ces gaz à effet de serre ont atteint 391 ppm, 1 803 ppb et 324 ppb, dépassant les niveaux préindustriels d'environ 40 %, 150 % et 20 % [1, 3, 4]. Environ 78% de ces émissions sont dues à la combustion de combustibles fossiles [1, 2, 4]. Le charbon représente la plus grande source des émissions anthropiques de CO_2, à environ 44% [2, 4].

La majorité de CO_2 produit par des centrales thermiques, des cimentries, ainsi que des incinérateurs, est mélangé avec l'azote et la vapeur d'eau. Cette situation rend le captage de CO_2 complexe, car celui-ci devrait d'abord être séparé de l'azote. Ainsi, telque indiqué sur la Figure 1.1, quatre modes de séparations sont possibles : précombustion (gazéification), la séparation durant les differents procédés industriels responsables de la production des GES, et enfin l'oxycombustion, postcombustion [6].

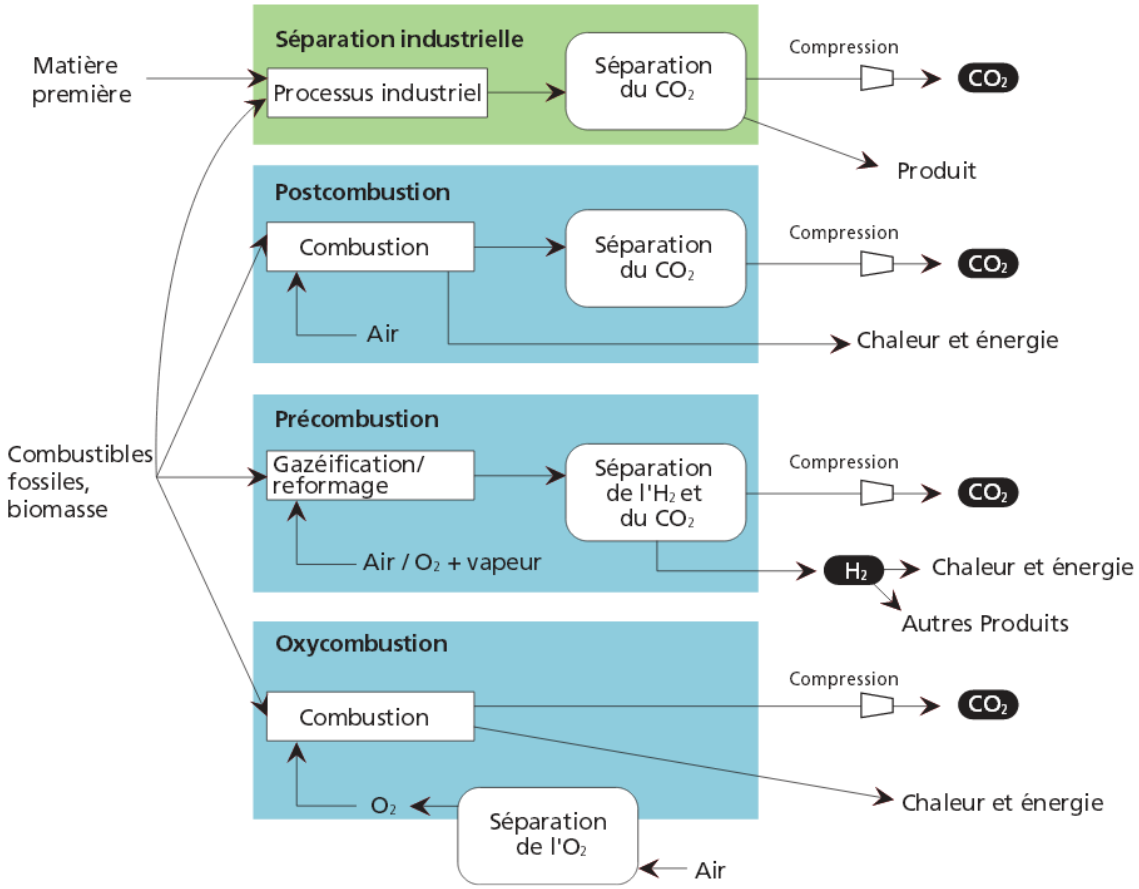

Figure 1.1 Système de piégeage de CO_2 [6]

Le dernière technique est celle la plus utilsée au point. Elle consite à plonger les gaz produits dans une solution d'amines pour dissoudre le CO_2 et éliminer l'azote sous forme gazeuse. Le CO_2 est libérée sous forme de gaz, en chauffant la solution, et la soution d'amines est recyclée. Toutefois, d'énormes quantités d'énergie sont exigées pour chauffer

une telle solution. Golobalement, 20 à 25% d'energie d'une centrale thermique au charbon est consommée pour séparer le CO_2, le comprimer et le stocker.

Par ailleurs, cette technique montre plusieures diffucultés: (1) technologiques, exemple de SaskPower, qui après 1 an d'opération (octobre 2015), fonctionne seulement à 40% de la séparation, (2) des coûts d'investissement élevés (550M$CAD pour 1Mt de CO_2 pour SaskPower), et (3) des coûts d'opération à cause de la perte du solvant.

La deuxième technologie, pendant la combustion, consiste à séparer l'azote alimenté avec l'oxygène directement dans un premier réacteur, et faire la combustion de l'hydrocarbure dans un autre compartiment. Comme indiqué sur la Figure 1.2, cette « boucle chimique de combustion » permet d'adsorber l'oxygène via un solide, sous forme réduite, dans un premier compartiment. Le solide est transporté dans un deuxième compartiment pour liberer l'oxygène à l'hydrocarbure pour combustion. Cette technique, testée sur plus que 1000 solides, s'avère limitée par la capacité du solide à transporter l'oxygène.

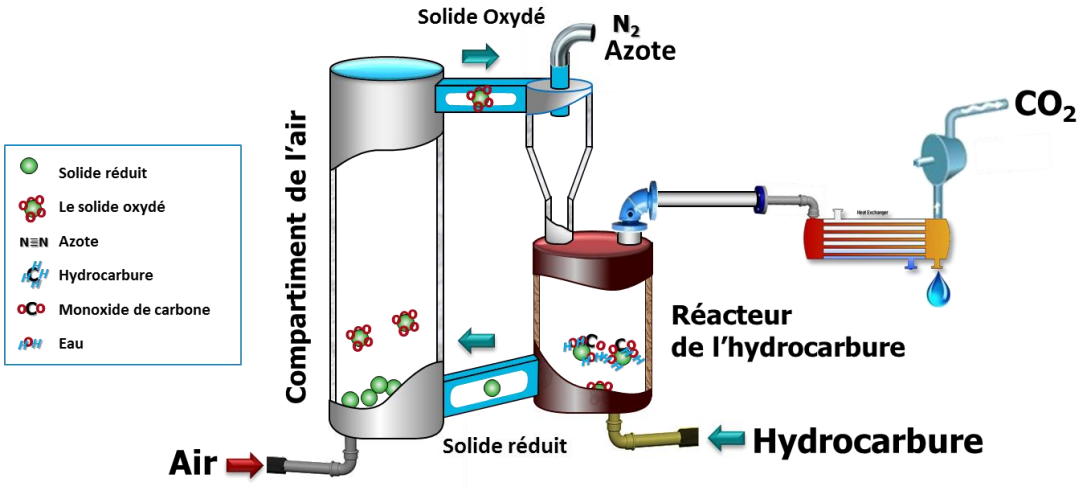

Figure 1.2 Boucle chimique de combustion

La première technique, l'oxycombustion, permet d'éliminer la production d'azote en brulant l'hydrocarbure à l'oxygène pur. Produire l'oxygène pur rend toutefois ce procédé excessivement dispendieux.

Le troisième mode est celui qui réside à faire une gazéification avant la combustion. Cette technologie propre, prometteuse et respectuese de l'enviroennemt, pourrait jouer un rôle

stratégique pour préserver l'avenir du globe terrestre. En 2007, il y avait 420 gazéifieurs dans 142 usines en exploitation à travers le monde. Le charbon et les résidus de pétrole comptent environ 55% et 32% de ces usines respectivement. Environ 44% du total des gaz de synthèse, produits à partir de ces gazéeifieurs, a été utilisé pour produire des produits chimiques, 30% pour produire des carburants liquides et 18% pour la production d'électricité. Il y avait 45 usines de gazéification du charbon, en exploitation, dans 212 gazéifieurs avec une capacité de 30,825 MWth de gaz de synthèse.

La chine compte la majorité de ces usines de gazéification du charbon construits récemment . Cette tendance est prévue de se maintenir dans le futur [7, 8].

Le charbon contribue majoritairement dans le protfolio energétique mondial. Comme indiuqé sur la Figure 1.3, le charbon compte près de tiers de la consommation mondiale de l'énergie [9].

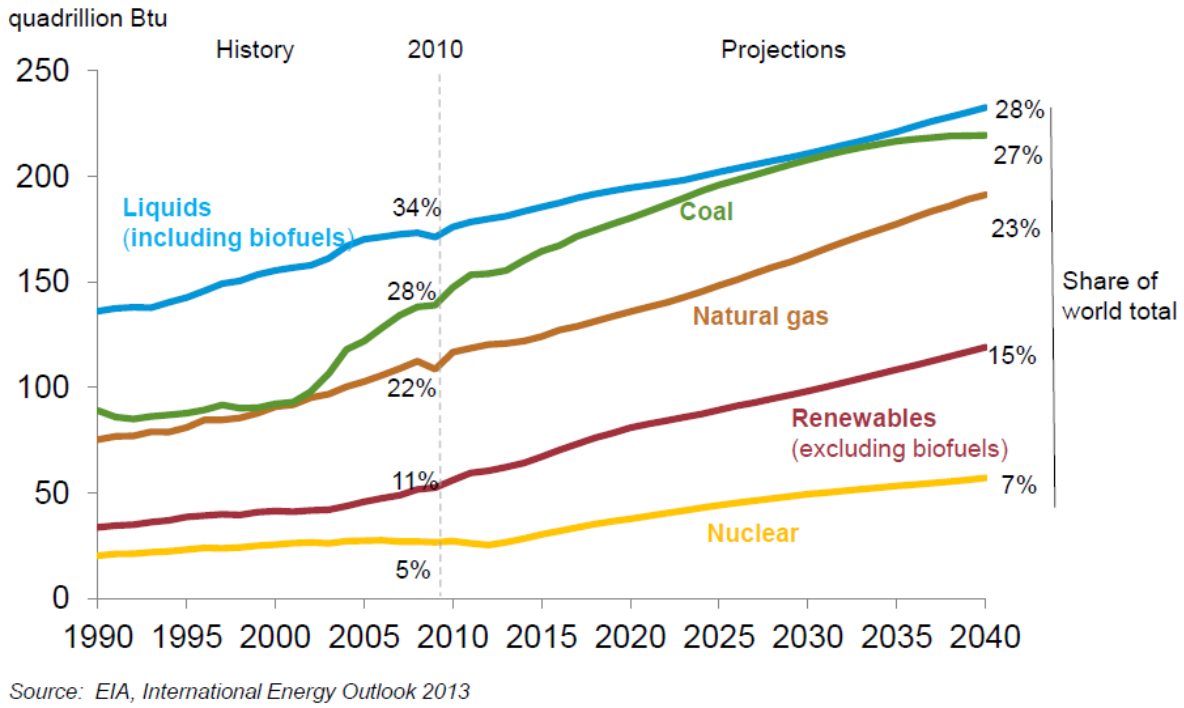

Figure 1.3 Évolution de la consommation énergétique mondiale [9].

Le défi majeur, actuel, pour la communaté scientifique internationale est de découpler la croissance économique et le développement social de l'augmentation des emissions anthropiques des gaz à effet de serre (GES) [2, 4, 5]. Pour réduire ces émissions et préserver

le systéme climatique, l'investissement dans l'innovation et dans des technologies propres, respectieuses de l'environnement, sont nécessaires [2, 5].

Canada, un des cinq pays les plus grands producteurs d'energie au monde, a adopté une stratégie de l'énergie qui vise à accélérer le développement et le déploiement de technologies de pointe qui favorisent l'utilisation de sources d'énergie propres et fossiles [10]. La stratégie canadienne mis aussi l'accent sur la formation du capital humain hautement qualifié [10].

C'est dans ce cadre que s'inscrit la présente thèse, faisant parti d'un grand projet Candian visant à développer une technologie de gazéification catalytique du charbon avec le piégeage du dioxyde de carbone via des sorbents. Le présent travail consiste à developper un analyseur thermogravimétrique à lit fluidisé (ATGF) ; et d'y faire de la gazéification catalytique du charbon une première application.

CHAPITRE 2 REVUE DE LA LITTÉRATURE

Bien que le coût du réacteur ne représente que 20%, environ, du coût total d'investissement dans une usine de gazéification, les performances de cette usine sont directement dictées par le bon fonctionnement du réacteur. En terme plus concrets, la conception, l'exploitation, le contrôle et l'optimisation du fonctionnement d'une installation de gazéification nécessitent une connaissance approfondie des phénomènes et mécanismes chimiques décrivant le fonctionnement du réacteur. Dans ce chapitre, deux aspects du procédé de gazéification seront abordés. La cinétique des différentes réactions chimiques ainsi que la technologie utilisée pour développer cette cinétique.

2.1 Technologie de l'analyseur thermogravimétrique

La technologie utilisée pour développer les mécanismes et la cinétique des réactions chimiques est dans la très grande majorité l'analyseur thermogravimétrique. Cette technique consiste à placer un échantillon dans un four afin de suivre et mesurer sa variation du poids dans le temps, ou température. Cette technologie est largement utilisée tant dans le milieu académique qu'industriel. Cependant, plusieurs phénomènes et limitations altèrent la fiabilité des paramètres cinétiques, obtenus à partir de cette technique d'analyse thermogravimétrique :

- La non-uniformité de la température tout au long de l'échantillon solide ;
- L'absence du mélange dans un échantillon hétérogène ;
- Le mauvais mélange du catalyseur pour les réactions catalytiques solide-solide et gaz-solide ;
- Le faible taux de chauffage de l'échantillon contrairement aux conditions opératoires industrielles : Dans les analyseurs thermogravimétriques conventionnels, cette valeur du taux de chauffe ne dépasse pas les 50K/min. Dans

les conditions opératoires industrielles, cette valeur pourrait facilement attendre les 1000 K/s, par exemple dans le cas des lits fluidisés ;

- La faible quantité de l'échantillon solide traité : La conception de l'analyseur thermogravimétrique conventionnel ne permet pas d'utiliser des masses des échantillons dépassant les 100 mg [11]. Cette quantité ne suffit pas pour représenter l'homogénéité des échantillons extrêmement hétérogènes, incluant le charbon, la biomasse et les déchets solides. L'effet de cette limitation quantitative de l'échantillon solide étudié s'amplifie lors de l'utilisation des catalyseurs solides en faible quantité, avoisinant les 1 à 5% de la masse totale de l'échantillon ;
- La limitation des réactions par les phénomènes de diffusion : la diffusion inter-particules et intra-particules constitue un problème majeur pour l'étude de la cinétique des réactions hétérogènes. Cette limitation diffusionnelle peut se manifester aussi au niveau de l'interface gaz-solide dans le cas des mécanismes impliquant le transfert de substances gazeuses du solide vers le film gazeux entourant la particule solide [11].

La Figure 2.1 illustre les différents types de limitation diffusionnelle dans le cas d'une réaction d'oxydation des poudres de SiC dans un ATG conventionnel [12].

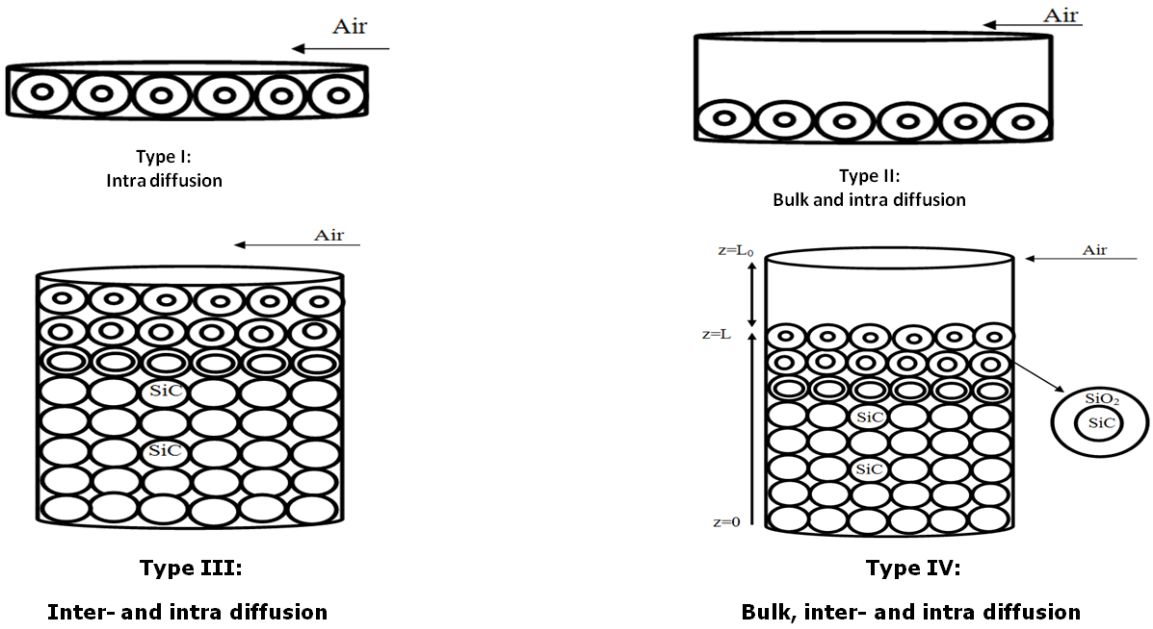

Figure 2.1 Différents types de diffusion. Reproduit avec permission de [12]

D'une manière générale , dans une réaction gaz-solide , quatre types de régimes peuvent contrôler la vitesse de réaction en fonction de la configuration expérimentale: (I) diffusion intra-particulaire, ou diffusion du réactif gazeux à travers la couche formée du produit (SiO_2), (II) la diffusion externe, ou transfert du réactif (O_2) par diffusion à travers le film gazeux air-particule solide de SiC, et la diffusion interne à travers la couche de SiO_2, (III) la diffusion inter-particulaire, ou diffusion du réactif gazeux entre les particules solides de SiC-SiO_2, et la diffusion interne du réactif gazeux à travers la couche formée de SiO_2, et enfin, (IV) les diffusions externe, interne et inter-particulaires. Selon le mécanisme de la réaction et les propriétés physiques du système, telles que la porosité et la hauteur du système (creuset), ces étapes peuvent limiter, séparément ou simultanément, la réaction globale [11, 12].

2.2 Mécanisme et réactions de la gazéification du charbon

Le charbon commence à se décomposer de 350 °C à 400 °C en un résidu riche en carbone et un riche en hydrogène volatile. La décomposition se poursuit jusqu'à une température

d'environ 950 °C [13]. Ainsi, la gazéification du charbon se déroule en trois étapes comme mentionné ci-dessous [14, 15].

$$\text{Étape } 1: Charbon \xrightarrow{Dévolatilisation} Volatiles\ \ lourds + Gaz(CO_2, H_2, CO, CH_4, H_2O, etc) + Char$$
$$\text{Étape } 2: Volatiles\ \ lourds \xrightarrow{Craquage} Liquide + gaz$$
$$\text{Étape } 3: Gazéification\ du\ char: C + H_2O + CO_2 + H_2 \rightarrow (CO, H_2, CH_4).$$

2.2.1 Étape 1 : pyrolyse

Dans une atmosphère inerte et sous l'effet du chauffage (350-600 ° C), le charbon est converti en un produit solide, appelé char, et plusieurs produits gazeux tels que H_2, CO, CO_2, H_2O, et CH_4. De plus, il y a formation d'autres hydrocarbures gazeux, huiles lourdes, et le goudron.

2.2.2 Étape 2 : craquage du goudron

Dans cette étape, les divers produits d'hydrocarbures gazeux et huiles lourdes de l'étape précédente sont craqués pour produire de l'hydrogène, de monoxyde de carbone, du méthane, ainsi que du dioxyde de carbone et le goudron inerte [16].

2.2.3 Étape 3 : gazéification du char

Le char et les composés gazeux, y compris H_2O , H_2 , CO_2 , produit par l' étape initiale de gazéification , réagissent pour produire une variété de gaz à haute et à basse énergie, telles que CO, H_2 et CH_4. Toutefois, il convient de noter que l'étape de dévolatilisation est terminée en quelques secondes à des températures élevées , alors que l'étape de gazéification nécessite des minutes ou plusieurs heures pour obtenir une conversion significative dans les conditions pratiques [16].

2.3 Cinétique de la gazéification

Un résumé des paramètres cinétiques de la pyrolyse et de la gazéification du charbon est présenté dans les paragraphes suivants.

2.3.1 Dévolatilization totale

Les différents paramètres cinétiques de la dévolatilization totale du charbon sont présentés dans le Tableau 2.1.

Tableau 2.1 Paramètres cinétiques de la dévolatilization totale du charbon

Charbon	Matière volatile	log ($k_{o,i}$/s)	E_i, (kcal/mol)	Déviation Std	Référence
Charbon lignite	52.6	-2.5	2.7	1.4 %	Ce travail
Différents charbons	39.5 to 51.0	-2.7 to 12.6	0.7 to 32.5	-	[17]

2.3.2 Pyrolyse du charbon

Les paramètres cinétiques de la pyrolyse du charbon, similaire aux charbons traités dans le présent travail, obtenus de la littérature sont regroupés dans le Tableau 2.2.

Tableau 2.2: Paramètres cinétiques de la pyrolyse du charbon [18]

Produit	**Étage**	**Log (**log ($k_{0,i}$ (s^{-1})))	**E_i (kcal/mol)**	**V_i* (mass. %)**	**n**
CO	1	12.26	44.4	1.77	1
	2	12.42	59.5	5.53	1
	3	9.77	58.4	2.26	1
CO_2	1	11.33	36.2	5.70	1
	2	13.71	64.3	2.70	1
	3	6.74	42.0	1.09	1
CH_4	1	14.21	51.6	0.34	1
	2	14.67	69.4	0.92	1
H_2O	1	13.90	51.4	16.5	1
H_2	1	18.20	88.8	0.50	1
Total	-	-	-	44.0	-

Ces paramètres regroupent essentiellement le facteur pré-exponentiel, $k_{0,i}$, l'énergie d'activation, $\mathbf{E_i}$, et la quantité totale de matière volatilisable V_i*. Les différents étages pour CO, CO_2, et CH_4 représentent, la pyrolyse primaire, le craquage des volatiles lourds et du

goudron respectivement. Les énergies d'activation du premier étage, pour chaque composé, sont les plus faibles par rapport aux deuxième et troisième étages.

2.3.3 Cinétique de la gazéification du charbon

Les cinétiques des différentes réactions chimiques gouvernant la gazéification sont illustrées dans le **Erreur ! Source du renvoi introuvable.**.

Tableau 2.3 Liste de réactions homogènes et hétérogènes

No	Réaction chimique	Cinétique	Référence
R1	$C+\alpha O_2 \rightarrow 2(1-\alpha)CO+(2\alpha-1)CO_2$	$r_1=\left(7.58\times10^4\right)\cdot\exp\left(-\frac{13592}{T}\right)\cdot P_{O_2}\cdot\left(1-X_{1c}\right)^{2/3}$ $\frac{2(1-\alpha)}{2\alpha-1}=(2400)\cdot\exp\left(-\frac{6234}{T}\right)$	s^{-1} [19, 20]
R2	$C+H_2O\rightarrow CO+H_2$	$r_2=\frac{k_1\cdot P_{H_2O}}{1+k_2\cdot P_{H_2O}+k_3\cdot P_{H_2}}$ $k_1=\left(4.93\times10^3\right)\cdot\exp\left(-\frac{18522}{T}\right)$ $k_2=\left(1.11\times10^1\right)\cdot\exp\left(-\frac{3548}{T}\right)$ $k_3=\left(1.53\times10^{-9}\right)\cdot\exp\left(\frac{25161}{T}\right)$	s^{-1} [19, 21] $bar\cdot s^{-1}$ bar^{-1} bar^{-1}
R3	$C+CO_2\rightarrow 2CO$	$r_3=\left(2\times10^{-8}\right)\cdot\exp\left(-\frac{360065}{T}\right)\cdot[CO_2]$	$kmol\cdot m^{-3}\cdot h^{-1}$ [19, 22]
R4	$C+2H_2\longrightarrow CH_4$	$r_4=\left(4.4.10^{-3}\right)\cdot\exp\left(-\frac{1.62.10^8}{T}\right)[H_2]$	$kmol\cdot m^{-3}\cdot s^{-1}$ [23, 24]
R5	$CO+1/2O_2\rightarrow CO_2$	$r_5=\left(8.83\times10^8\right)\cdot\exp\left(-\frac{99800}{RT}\right)\cdot[O_2].[CO\ ]$	$kmol\cdot m^{-3}\cdot s^{-1}$ [25, 26]
R6	$H_2+1/2O_2\leftrightarrow H_2O$	$r_6=\left(2.19\times10^9\right)\cdot\exp\left(-\frac{13127}{T}\right)\cdot[H_2]\cdot[O_2]$	$kmol\cdot m^{-3}\cdot s^{-1}$ [19, 21]

R7	$CH_4 + 2O_2 \rightarrow CO_2 + 2H_2O$	$r_7 = \left(1.58 \times 10^{10}\right) \cdot \exp\left(-\frac{24343}{T}\right) \cdot [CH_4]^{0.7} \cdot [O_2]^{0.8}$	$kmol \cdot m^{-3} \cdot s^{-1}$ [19, 21]
R8	$CO + H_2O \leftrightarrow H_2 + CO_2$	$r_8 = \left(10^3\right) \cdot \exp\left(-\frac{6370}{T}\right) \cdot \left([CO] \cdot [H_2O] - \left(\frac{[CO_2] \cdot [H_2]}{K^*}\right)\right)$ $K^* = 520 \times \exp\left(\frac{7230}{T}\right)$	$kmol \cdot m^{-3} \cdot s^{-1}$ [22, 27]
R9	$CH_4 + H_2O \rightarrow 3H_2 + CO$	$r_9 = \left(3 \times 10^2\right) \cdot \exp\left(-\frac{15000}{T}\right) \cdot [CH_4] \cdot [H_2O]$	$kmol \cdot m^{-3} \cdot s^{-1}$ [24, 28]
R10	**Craquage du goudron** $CH_{1.522}O_{0.0228} + 0.867O_2 \rightarrow CO + 0.761H_2O$	$r_{10} = \nu_i 10^{4.98} \exp\left(-\frac{93}{RT}\right) \cdot (\rho_{tar})$	$kg \cdot m^{-3} \cdot s^{-1}$ [29]
R11	**Combustion du goudron** $Tar \rightarrow \nu_{CO} CO + \nu_{CO_2} CO_2 + \nu_{CH_4} CH_4 + \nu_{H_2} H_2 + \nu_{tar} tar_{inert}$	$r_{11} = M_{HC} 9.2.10^6 T \exp\left(-\frac{9650}{T}\right) [HC]^{0.5} [O_2]$	$kg \cdot m^{-3} \cdot s^{-1}$ [30]

Les différents coefficients pour la réaction de combustion du goudron sont indiqués dans le Tableau 2.4.

Tableau 2.4: Coefficients stœchiométriques du craquage du goudron [29]

Component	**Coefficient**
CO	0.56
CO_2	0.11
CH_4	0.09
H_2	0.02
Goudron secondaire	0.22

2.4 Problématique du goudron

Le goudron est un mélange complexe d'hydrocarbures condensables. Divers groupes de recherche le définissent différemment. Il a été convenu par un certain nombre d'experts d'associer le nom du goudron à tous les contaminants organiques ayant un poids moléculaire plus grand que le benzène [31]. La formation du goudron constitue un problème majeur pour la technologie de gazéification. Ce composé lourd se condense à basse température, ce qui pourrait conduire au bouchage et blocage des différents équipements tels que les conduites, les filtres, les moteurs et les turbines. En général, le goudron peut être éliminé par des techniques physiques, non catalytique (craquage thermique), et catalytiques. Les paramètres de fonctionnement tels que la température, l'agent de gazéification, le rapport d'équivalence, le temps de séjour sont à optimiser pour réduire la quantité du goudron produite. Certains catalyseurs tels que la dolomite, les métaux alcalins et le nickel, peuvent également être utilisés à cet effet [32]. L'injection d'air secondaire dans le gazéifieur, dans la gazéification à deux étages, est également d'une importance primordiale pour éliminer le goudron des gaz sortants [32-34].

2.5 Gazéification catalytique

Divers catalyseurs ont été utilisés pour la gazéification du charbon. Parmi les principaux catalyseurs, il y a lieu de citer K_2CO_3, Na_2CO_3, KCl, NaCl et CaO.

Il est important de préciser que deux aspects principaux doivent être distingués dans l'évaluation de l'effet des catalyseurs : la conversion du carbone et l'efficacité thermique d'un gazéifieur. L'efficacité thermique diminue généralement lorsque la conversion du carbone augmente dans une gazéification catalytique. Ainsi, plus la réactivité d'un catalyseur est élevée, plus il aura un impact négatif sur l'efficacité thermique. Exemples de catalyseurs triés par ordre décroissant de réactivité : KCl, K_2CO_3, NaCl, $LiCO_3$, Fe_3O_4, Pb_3O_4, MgO et Ni.

L'effet des catalyseurs, K_2CO_3 et Na_2CO_3, sur gazéification du charbon, avec CO_2, est illustrée dans le Tableau2.5 [35].

Tableau2.5 Effet des catalyseurs sur les paramètres cinétiques: K_2CO_3 vs. Na_2CO_3

Catalyseur	Énergie d'activation (kJ/mol)	Facteur pré-exponentiel (min^{-1})
None	122.0	1480
K_2CO_3	75.3	18.4
Na_2CO_3	80.3	75.1

Le Tableau2.6 montre l'effet des différents catalyseurs sur la réaction de déplacement de monoxyde de carbone [36-40].

Tableau2.6 Effet des catalyseurs sur la réaction de déplacement de CO [36-40]

Catalyseur	Énergie d'activation ($kJ.mol^{-1}$)	Référence
Fe_2O_3/ZrO_2	105-111	[36]
$13.5Ni{-}2K/10CeO_2{-}Al_2O_3$	155.3	[38]
Pt@SiO2	70	[39]
Li/MgO	158	[40]
K_2TiO_3	**56.5**	Ce travail
Sans catalyseur	**101.9**	Ce travail

L'effet des différents catalyseurs sur la réaction de reformage catalytique du méthane est illustré sur le Tableau 2.7 [41-46].

Tableau 2.7 Effet des catalyseurs sur la réaction de reformage de méthane

Catalyseur	Énergie d'activation ($kJ.mol^{-1}$)	Référence
À base de K	113-124	[41-44]
Ni/y-Al2O3	133.9	[43]
Rh/Al_2O_3	111	[44]
Platine	114	[47]
$Ce_{0.9}Gd_{0.1}O_{2-x}$ (CGO)	153	[45]
Ni/Mg/K/Al2O3	93	[46]
Ni/La/Al2O3	85.2	[42]
Ni/La-Co/Al2O3	99.4	[42]
K_2TiO_3	**77**	Ce travail
Sans catalyseur	**108**	Ce travail

2.6 Différentes chambres de gazéification

Cette section résume les différentes chambres de gazéification : (1) gazéifieur à contre-courant, (2) gazéifieur à co-courant, (3) gazéifieur «cross draft», (3) gazéfieurs à lit fluidisé ; circulant et à bulles.

2.4.1 Gazéifieur à contre-courant

Ce type du réacteur est le plus ancien. Le solide est alimenté du haut du réacteur tandis que l'air entre par le bas du gazéifieur. Les gaz produits sortent du haut du réacteur, alors que les cendres se sont élimnées de son bas.

Ainsi, du bas en haut du réacteur, les réactions de combustion se passent d'abord dans la zone de combustion, suivies par celles de gazéification du char produit dans une deuxième zone plus eleveé. Quand il n'y a plus d'oxygène, le solide rentrant le réacteur se pyrolyse sous l'action de la chaleur transférée, par convection et radiation, des zones de combustion et de gazéification.

2.4.2 Gazéifieur à co-courant

La raison principele d'apparution de ce type de gazéifieur est d'éviter la présence du goudron dans les gaz produits. Ce qui se fait en introduisant l'air primaire de gazéification au niveau , ou un peu en haut, de la zone d'oxydation. Produire les gaz sans goudron constitue l'avantage majeur de ce procédé [48, 49].

2.4.3 Gazéifieur «cross draft»

La gazéification du charbon conduit à une température très élevée à la zone d'oxydation (1500 ° C ou plus) , ce qui nécessite une haute stabilité thermique pour le matériau . Dans ce contexte , cette technologie permet du char d'agir comme un matériau isolant contre la paroi , ce qui assure une protection suffisante pour que le réacteur soit exposé à des températures élevées. Un autre avantage de cette technologie est qu'elle donne la possibilité de fonctionner à très faible capacité (< 10 kW) [48, 49].

2.4.4 Gazéifieurs à lit fluidisé: circulant et à bulles

Les gazéifieurs à lit fluidisé peuvent être divisés en deux grandes catégories: lit fluidisé à bulles et lit fluidisé circulant. En raison du mélange approprié dans ce type de gazéifieur, l'uniformité de la température dans le lit est assurée. En outre, le contrôle de la température peut se faire facilement en changeant le rapport air-carburant contrairement au lit fixe. Dans un lit fluidisé à bulles , la conversion élevée en solides ne peut pas être atteinte en raison du mélange inverse des solides partiellement gazéifiés dans le courant solide. Une perte importante de matières solides est également due à l'entraînement des particules par les bulles provenant du lit fluidisé. En outre, la diffusion lente de l'oxygène des bulles de la phase d'émulsion conduit à un faible rendement de gazéification pour créer des conditions d'oxydation dans le lit entier. La technologie à lit fluidisé circulant est venu pour contourner ce problème ; en fournissant un temps de séjour plus elevé au solide à l'intérieur de sa boucle de circulation [15].

Par ailleurs, il convient de signaler que le premier gazéifieur à lit fluidisé a été inventé, construit et commercialisé en 1921 Fritz Winkler de l'Allemagne [15].

Le Tableau 2.8 résume la différence entre les gazéifieurs à lit fluidisé et ceux à lit fixe. Le facilité du contrôle ainsi que le bon mixing gaz-solide sont parmi les points les plus avantagaeux des gazéifieurs à lit fluidisé. Les problème de démarrage ainsi que le faible mixing font les points les plus faibles de la technologie à lit fixe.

Tableau 2.8 Caractéristiques principales des différents gazéifieurs [15, 48, 49]

	Lit fixes			Lits fluidisés	
Sensibilité à:	Co-courant	Contre-courant	«cross draft»	Bulles	Circulant
Spécification du fuel	Moderé	Spécifique	Moderé	Flexible	Flexible
Cendre	Pauvre	Pauvre	Pauvre	Très bien	Très bien
Température	1000°C	1000°C	900°C	850°C	850°C
Mixing du fuel	Pauvre	Pauvre	Pauvre	Très bien	Excellent
Température des gaz	250°C	800°C	900°C	800°C	850°C
Goudron dans le gaz	Très élevé	Très bas	Très élevé	Modéré	Faible
Poussières dans les gaz	Bien	Moderé	élevé	Très élevé	Très élevé
Potentiel de	Bien	Pauvre	Pauvre	Bien	Très bien
Démarrage	Pauvre	Pauvre	Pauvre	Bien	Bien
Contrôle	Bien	Bien	Bien	Très bien	Très bien
Conversion du carbone	Très bien	Très bien	Pauvre	Bien	Très bien
Efficacité thermique	Excellent	Très bien	Bien	Bien	Très bien
PCI des gaz	Pauvre	Pauvre	Pauvre	Pauvre	Bien

2.4.5 Gazéifieur à lit entrainé

La particularité de cette technologie est qu'il n'y a pas de matériel inerte. Les particules solides, qui sont très fines (80-100 µm), sont pulvérisées est suspendues dans un mélange gazeux air-oxygène et vapeur d'eau. Le taux de production est très élevé dans ce type de réacteur car le temps de résidence du solide est trés faible, étant donné que la vitesse du gaz est elevée. À haute temperature, 1200-1500°C, les cendres produites sont éliminés sous forme liquide. Ces conditions opératoires, de haute température, permettent une conversion elevée du carbone avec des gaz produits sans goudron [15, 49].

Enfin, cette technologie offre la possibilté de traiter de grande quantité, plus de 100 MWe, du charbon et du fuels solides [15, 49].

2.7 Modélisation des réacteurs à lits fluidisés

La modélisation des réacteurs à lits fluidisés pourrait être classifiée en deux catégories. La première approche est basée sur l'équilibre pour estimer la composition des gaz produits [50-55]. Cette approche ne prend pas en considération le transfert de matière et chaleur, en particulier la pyrolyse et la formation du goudron. Cette première approche englobe deux sous catégories : stœchiométrique et non stœchiométrique. La maitrise des mécanismes ainsi que toutes les réactions chimiques et les composées impliqués est primordiale pour l'approche stœchiométrique. Cette condition n'est toutefois pas nécessaire pour la méthode non-stœchiométrique, se basant sur la minimisation de la fonction de Gibbs du système [51, 52, 56]. Les seules données nécessaires sont l'analyse élémentaire du charbon.

La seconde approche utilise la cinétique des différentes réactions chimiques ainsi que l'hydrodynamique du lit fluidisé. Cette technique de modélisation regroupe l'étape de la pyrolyse, les réactions homogènes, les réactions hétérogènes, ainsi que les phénomènes de transfert. En outre, les différents paramètres hydrodynamiques gouvernant le fonctionnement d'un lit fluidisé devraient être spécifiés [57-60].

Par ailleurs, il convient de noter les différents modèles qui ont été utilisés pour la seconde approche. Les modèles à deux phases, avec ou sans dispersion axiale, et avec transfert de matière entre les deux phases [59, 61-63]. En outre, il y a lieu de noter les modèles à 3 phases : la phase principale du solide, la phase d'émulsion descendante, et une autre phase descendante, proche de paroi du réacteur [62-64].

2.8 Conclusion de la revue de littérature

Les performances et la fiabilité de toute usine de gazéification sont fortement affectées par la présence de cendre dans le charbon et de goudron à l'intérieur du gazéifieur, et à d'autres équipements de l'usine. Le prétraitement du charbon pourrait aider à réduire la quantité de cendre ou produire un charbon sans cendre. La quantité du goudron produite par la gazéification pourrait être réduite par l'utilisation du catalyseur.

Étant donné que le gazéifieur est le cœur d'une usine de gazéification du charbon, une analyse réussie des performances globales de cette usine est directement liée à la fiabilité de la modélisation du réacteur. En outre, la robustesse d'une modélisation du réacteur est associée au fait qu'elle est

basée sur une bonne partie de la compréhension des phénomènes fondamentaux, y compris la cinétique et les mécanismes de pyrolyse et de gazéification du charbon.

La conception d'un gazéifieur est basée sur la fiabilité de la cinétique utilisée à cet effet. Un des problèmes de toutes les technologies de gazéification est de concevoir un appareil pour développer la cinétique appropriée. Afin de surmonter les diverses limitations de l'ATG conventionnel mentionnées précédement, et de proposer des modèles cinétiques précises et plus complètes, un nouveau ATG à lit fluidisé (ATGLF) a été développé. Le chapitre 3 présente les objectifs de ce travail ainsi que la structure de la présente thèse.

CHAPITRE 3 OBJECTIFS ET STRUCTURE DE LA THÈSE

3. 1. Objectifs

L'objectif principal de la présente thèse de doctorat est de développer un analyseur thermogravimétrique à lit fluidisé, et d'y étudier la cinétique et les mécanismes de la gazéification catalytique du charbon et du charbon sans cendre. Pour ce faire, trois sous objectifs ont été fixés :

- Développer un analyseur thermogravimétrique (ATG) à lit fluidisé ;
- Étudier la cinétique et les mécanismes de la gazéification du charbon dans l'ATG à lit fluidisé ;
- Déterminer l'effet du prétraitement du charbon et du catalyseur sur la gazéification du charbon et du charbon sans cendre dans l'ATG à lit fluidisé.

3. 2. Structure de la thèse

Le travail est ainsi structuré est reparti en neuf chapitres. Après une introduction générale du projet, une revue détaillée de la littérature sur la cinétique de la gazéification du charbon et la technique de l'analyseur thermogravimétrique conventionnel a fait l'objet du deuxième chapitre. Le quatrième chapitre sera consacré à la méthodologie adoptée, incluant le matériel et les techniques utilisés, pour la réalisation du présent travail. Le premier article, portant sur le développement de l'ATG à lit fluidisé, sera présenté dans le cinquième chapitre. Le sixième chapitre mettra la lumière sur le deuxième article, objet de l'étude de la gazéification du charbon dans l'ATG à lit fluidisé. Le troisième article, mettant l'accent sur la gazéification catalytique du charbon et du charbon sans cendre dans l'ATG à lit fluidisé, sera développé dans le septième chapitre. Une discussion générale du travail sera présentée dans le huitième chapitre, suivie par une conclusion et des recommandations au neuvième chapitre.

CHAPITRE 4 MÉTHODOLOGIE

La première partie de ce chapitre fera l'objet d'une description détaillée de l'analyseur thermogravimétrique à lit fluidisé (ATGLF), ainsi que les difficultés techniques rencontrées lors de son design. La deuxième partie, quant à elle, décrit brièvement les différents matériaux ainsi que les principales méthodes et techniques utilisées pour mener les expériences, générer les données et atteindre ainsi les objectifs tels que définis précédemment.

4.1 Analyseur thermogravimétrique à lit fluidisé

La Figure 4.1 montre une photo de l'ATGLF. L'équipement consiste en trois parties : réacteur, four, cellule de charge et les différents instruments de mesure. Un schéma détaillé de l'ATGLF sera présenté dans le chapitre 5.

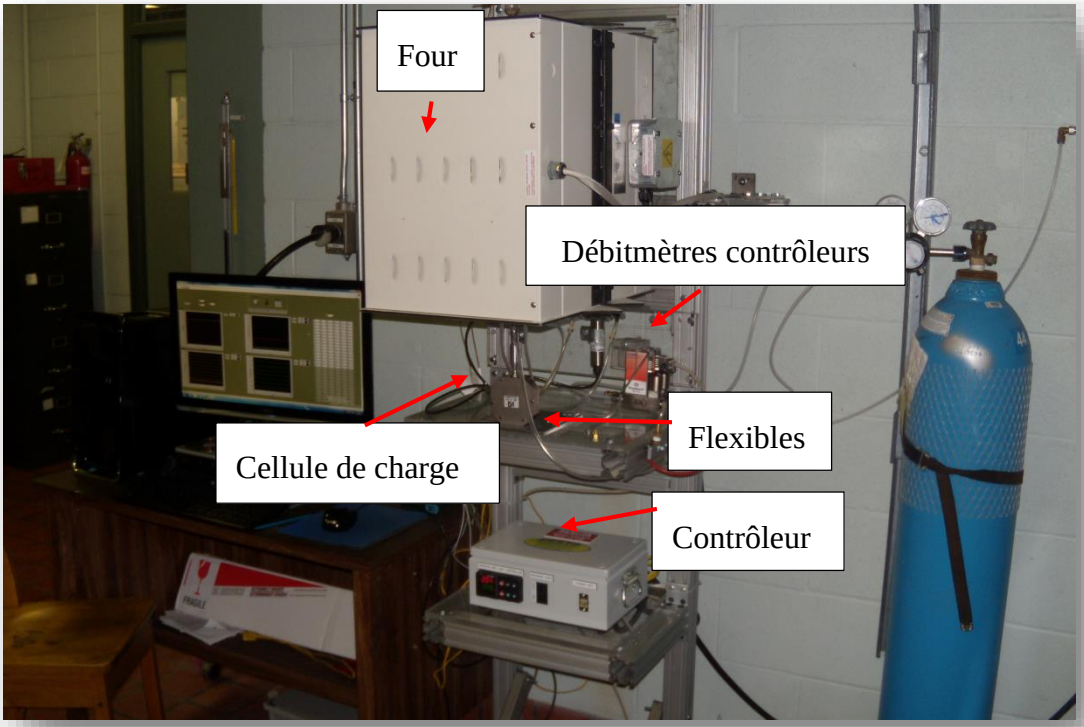

Figure 4.1 photo de l'analyseur thermogravimétrique à lit fluidisé

4.3.1 **Cellule de charge**

La mesure du poids apparent du réacteur a été effectuée à l'aide d'une cellule de charge, Honeywell Model 101AH. La mesure pourrait se faire par compression et/ou par contraction. Cette cellule est dotée d'un système antichoc et anti-vibration. La capacité maximale de la dite cellule est de1 kg et sa précision absolue est de 0.1%. Voir annexe B pour le certificat de calibration.

4.3.2 **Thermocouples**

Les thermocouples utilisés pour la mesure de température de l'ATGLF sont des types K (Chromel/Alumel), avec une gaine métallique composée d'un alliage Nickel-Chrome. Les deux diamètres utilisés sont 1/16 et 1/32 pouce. Une des particularités de ces thermocouples est qu'ils sont dotés des flexibles, permettant une liberté du réacteur de l'ATGLF.

4.3.3 **Four et éléments chauffants**

Le four Zesta et ctrl Wattlow a une puissance de 2260 Watts. Le taux de chauffe maximal qui pourrait être atteint avec le design actuel est de 50°C/min. Le contrôleur est de type ZCP560. Le système est certifié CSA. Voir annexe C pour plus de détails.

4.2 Difficultés rencontrées lors de la conception de l'ATGLF

Cette partie présente succinctement quelques difficultés rencontrées lors de la conception et le développement de l'ATGLF.

4.2.1 **Liberté du réacteur**

Afin de pouvoir mesurer le poids du réacteur de l'ATGLF, celui-ci déposé sur la cellule de charge, devrait être libre de tout le reste de l'équipement incluant le four, les thermocouples ainsi que les différentielles de pression. Ainsi, toute connexion du réacteur avec le reste devrait être flexible. Tel qu'illustré sur la Figure 4.2, les tubings, ou flexibles, utilisés pour les gaz d'alimentation et de fluidisation, prises de mesure de pertes de charge à travers le distributeur et la pression du réacteur, ainsi que pour les gaz sortant du réacteur sont de type Tygon B-44-3.

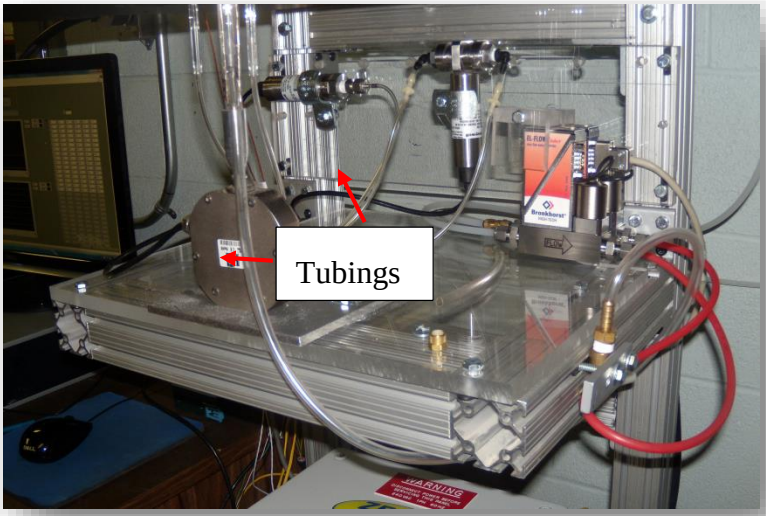

Figure 4.2 Tubings pour l'ATGLF

4.2.2 **Étanchéité à haute température**

La Figure 4.3 indique la partie supérieure du réacteur de l'ATGLF incluant le thermocouple. Le ruban en nickel est le matériau utilisé pour assurer une étanchéité à haute température au niveau des thermocouples. Ce matériau pourrait résister à une température maximale allant jusqu'à 1316°C.

Figure 4.3 Ruban en nickel pour l'étanchéité à haute température

4.2.3 **Emplacement de la cellule de charge**

Tel qu'indiqué précédemment, la mesure du poids du réacteur par la cellule de charge pourrait se faire par compression ou contraction. La contraction est la méthode choisie initialement. Par conséquent, la cellule de charge a été placée initialement en haut du réacteur, tel que mentionné sur la Figure 4.4 (a).

Les premiers tests ont toutefois permis de conclure que la température de la cellule a atteint 85°C quand celle du réacteur a été seulement 216°C. En effet, le chauffage de la cellule s'est fait rapidement par convection de l'air chaud sortant du réacteur.

Afin de remédier à cette situation, la cellule de charge a été placée en bas du réacteur, comme illustrée sur Figure 4.4 (b). La mesure du poids du réacteur s'est faite cette fois-ci par compression. Ainsi, la température n'a pas dépassée 50°C au niveau de la cellule de charge quand celle du réacteur a été 800°C.

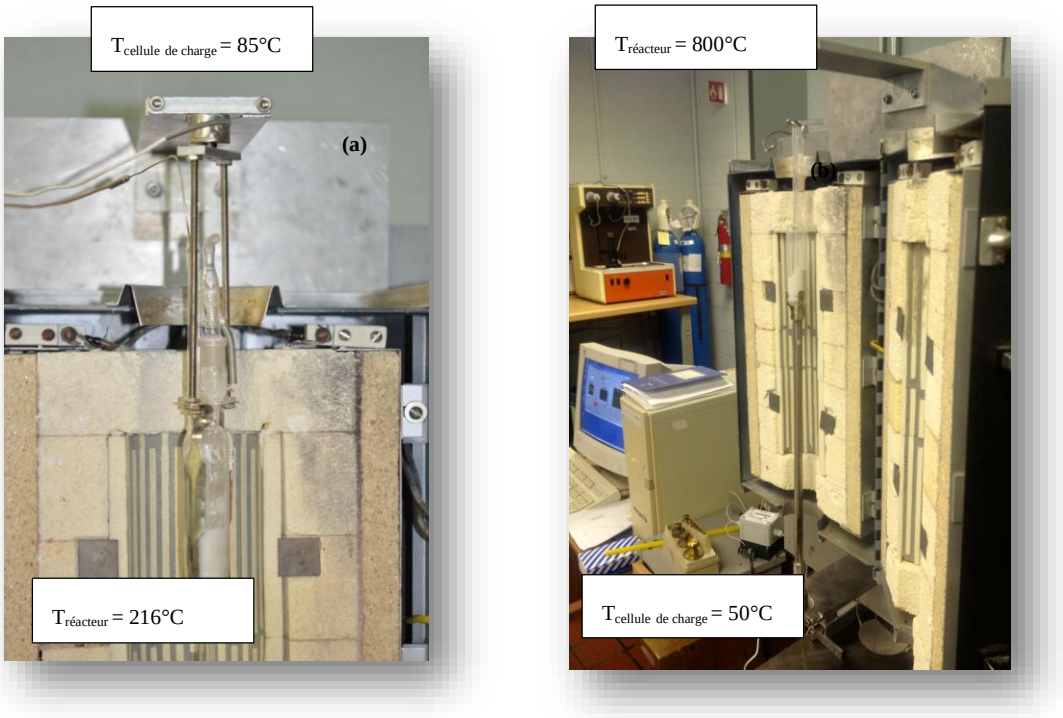

Figure 4.4 Emplacement de la cellule de charge : (a) en haut du réacteur, (b) en bas du réacteur

4.2.4 **Alimentation du réacteur par l'échantillon solide**

Afin de pouvoir alimenter le réacteur par l'échantillon solide, le réacteur de l'ATGLF a été conçu en deux parties : (1) principale, contenant la chambre de réaction, le distributeur du gaz, et les conduites pour mesurer les pertes de charges à travers le distributeur et la pression à l'intérieur du réacteur. (2) secondaire contenant le filtre et des trous pour les thermocouples. L'assemblage des deux parties se fait via des ressorts en acier trempé, plaqué en Zinc.

4.2.5 **Variation de la vitesse de fluidisation en fonction de température**

La température du réacteur de l'ATGLF augmente en fonction du temps. La vitesse du gaz de fluidisation augmente aussi. Cependant, la vitesse minimale de fluidisation diminue quand la température augmente. Afin d'éviter les vibrations de l'équipement, et d'éliminer l'effet des bulles sur l'étude de la cinétique, la vitesse du gaz de fluidisation devrait être contrôlée pour garder un régime de fluidisation autour de celui de la fluidisation minimale. Pour ce faire, un programme a été développé sur LabVIEW pour contrôler le débit en fonction de la température. Plus de détails sur ce programme seront fournis au chapitre 5.

4.3 Matériaux

Les différents matériaux utilisés dans ce projet de doctorat sont le sable, l'hydroxyde de calcium, le charbon, le charbon sans cendre, le catalyseur (K_2TiO_3), et les gaz. Plus de détails seront fournis dans les chapitres 5, 6 et 7.

4.3.1 **Analyse détaillée du charbon et du charbon sans cendres**

Le charbon et le charbon sans cendre, utlisés dans toutes les expériences reportées dans le présent travail, ont été obtenus de l'Ouest du Canada. Les charbons ont été broyés et tamisés. La taille des particules utilisées ont été de 500 à 600 µm.

L'analyse par activation neutronique (AAN) a été effectuée dans le laboratoire SLOWPOKE de Polytechnique Montréal. Cette technique d'analyse chimique nous a permis de mesurer les concentrations de plus de 50 éléments dans le charbon et charbon sans cendre. Il s'agit de rendre l'échantillon radioactif, en le bombardant par des neutrons, pour pouvoir détecter les rayons gamma émis par les différents éléments, contenus dans l'échantillon.

Les éléments mentionnés en **format italique** dans le Tableau 4.1 jouent le rôle de catalyseur, tandis que ceux indiqués en **format gras** constituent un véritable inhibiteur à la gazéification du charbon. Le charbon sans cendre contient plus d'éléments catalyseurs que le charbon original. Ce dernier contient également moins d'éléments inhibiteurs.

Tableau 4.1 Analyse complète des charbons

Analyse par activation neutronique (ppm)	**Charbon (lignite)**	**Charbon sans Cendre**
U	0.13	2.53
Ti	24	977
Sn	<2	<160
I	0.11	<4
Ag	<1	<1
Mn	0.82	9.4
Mg	50	2321
Cu	1.29	<86
In	0.0013	<0.2
Si	1171	74270
V	0.99	10.71
Cl	10.9	< 86
Al	392	15201
Ca	379	11614
S	1713	<10000
Hg	<0.05	<0.05
Se	<1	<1
Mo	0.12	0.8
U	0.13	1.6
Th	0.25	4.1
Cr	0.83	6.9
Cd	<0.2	<0.2
Au	0.015	0.0056
HF	0.162	1.28
Ba	38	821
As	0.48	1.67

Sb	6.89	0.44
W	2.83	5.25
Zr	<19	<71
Cs	0.37	1
Rb	<1	6.14
Fe	172	3240
Zn	15	11
Co	4.38	18
Na	147	5503
K	48	961
La	0.22	6.36
F	<53	<290

4.4 Analyse des gaz produits

Les gaz produits de la pyrolyse et de la gazéification du charbon et du charbon sans cendre ont été analysés, continuellement et conjointement, à l'aide d'un spectromètre infrarouge à transformée de Fourier (FTIR, MuliGas^{TM} 2030 Series) et d'un chromatographe gazeux (CP-4900 Varian). Ces deux techniques permettent une analyse complète et en temps réel des gaz produits. Les deux appareils ont été calibrés, et vérifiés, en utilisant des gaz standards de concentrations différentes, couvrant la marge des concentrations des gaz produits.

CHAPITRE 5 ARTICLE 1: DEVELOPMENT OF A FLUIDIZED BED THERMOGRAVIMETRIC ANALYZER

5.1 Présentation de l'article

Ce chapitre reprend l'article intitulé **'Development of a fluidized bed thermogravimetric analyzer'**. Cet article a été publié dans la prestigieuse revue AIChE Journal.

Au troisième chapitre, nous avons souligné l'importance et la nécessité de développer un équipement idéal pour étudier la cinétique et les mécanismes des réactions catalytiques gaz-solide. C'est dans cette optique que l'analyseur thermogravimétrique à lit fluidisé a été développé.

Pour ce faire, une description détaillée de l'équipement, nouvellement développé, a été nécessaire. Un intérêt particulier a été donné aux instruments et techniques de mesure du poids, de perte de charges, de température et de débits de gaz. Ensuite, le nouveau concept de la pseudo-variation du poids de l'ATG à lit fluidisé (ATGLF) a été introduit. Cette variation du poids a été formulée par un modèle, transformant les pertes de charges à travers le distributeur et le filtre du réacteur en une pseudo-masse. Le modèle a été d'abord validé à température ambiante et ensuite à hautes températures. La procédure expérimentale, incluant tous les tests et protocoles expérimentaux, ainsi que les différents matériaux utilisés, a été grandement détaillée dans cet article et dans le chapitre 4. La validation expérimentale de l'ATGLF a été réalisée par la décomposition thermique de l'hydroxyde de sodium ($Ca(OH)_2$). Une comparaison des résultats expérimentaux des tests effectuées dans les ATG conventionnel et à lit fluidisée a effectuée. Les tests ont montré que l'utilisation de l'ATGLF a permis d'éliminer les limitations diffusionnelles de matière. Cette conclusion a été renforcée en analysant les différents échantillons traités, dans les deux ATGs, par la technique de la diffraction des rayons X. Ces résultats obtenus ont confirmé que l'ATG à lit fluidisé, nouvellement développé, pourrait constituer un équipement idéal pour l'étude de la cinétique et mécanismes des réactions chimiques gaz-solides.

5.2 Development of a Fluidized Bed Thermogravimetric Analyzer

Said Samih and Jamal Chaouki[1]

Revue : AIChE journal [ISSN : 0001-1541] — année : 2015 v : 61 no : 1 pg : 84 -89

5.2.1 Abstract

A new fluidized bed thermo-gravimetric analyzer (FB-TGA) was developed that introduces two major particularities: the pseudo variation of the weight of the reactor and the special strategy for gas flow rate adjustment according to temperature. A momentum balance was performed on the reactor and the pseudo variation of the reactor weight was evaluated by measuring the pressure drop through the gas distributor and filter. The real weight loss of the reactor was obtained by subtracting the pseudo variation of the weight from the total weight loss measured by the load cell. In addition, a special program for the gas flow rate as a function of temperature was developed and used; so the minimum fluidization regime is maintained throughout all of the experiments. The validation test of the Fluidized Bed TGA was carried out on calcium hydroxide decomposition and the results were compared with those obtained from the conventional TGA. Diffusion control was suppressed by the application of the Fluidized Bed TGA, which was confirmed by the X-Ray Diffraction (XRD) analysis on the treated samples.

5.2.2 Introduction

The kinetics and mechanism of thermally activated catalytic gas-solid reactions are usually obtained from Thermal Gravimetry Analysis (TGA), Differential Thermal Analysis (DTA) and Differential Scanning Calorimetry (DSC) [65-70]. These experimental techniques have

[1] Corresponding author : Dr. Jamal Chaouki, jamal.chaouki@polymtl.ca

been commonly applied to characterize a wide range of reactions, such as solid fuels pyrolysis, gasification and combustion [71-75], thermal decomposition of different materials [67, 68, 71], crystallization of polymers, regeneration of deactivated catalysts and oxidation-reduction of metal oxides [75, 76].

In spite of a wide range of applications in academia and the industry, the thermo-gravimetric (TG) technique shows some limitations, which may reduce the reliability of kinetic models. In more concrete terms, studying kinetics in the conventional TGA suffers seriously from (1) the non-uniformity of the temperature throughout the sample, (2) poor mixing and distribution of gas-solid and solid-solid throughout the sample, (3) the low heating rate, (4) the small amount of solid sample, which is not enough to represent its homogeneity, (5) and the bulk, inter-particle and intra-particle diffusion control [12, 65].

Recently, our research group investigated the diffusional effects in TGA during the oxidation of SiC powders under air (gas reactant) in a cylindrical crucible [12]. In general, in the gas-solid reaction, four types of regimes can control the reaction rate (figure 1) according to the experimental configuration: (1) intra-diffusion (diffusion of the gaseous reactant through the product layer) and surface reaction, (2) bulk diffusion (diffusion of the gaseous reactant from the bulk to the surface of the bed), intra-diffusion, and surface reaction, (3) inter-particle diffusion (diffusion through the pore space between particles), intra-diffusion, and surface reaction and, finally, (4) bulk, inter-, and intra-diffusion, and surface reaction. Depending on the mechanism of the reaction and physical properties of the system, such as porosity and height of the system (crucible), these diffusional steps may limit separately or simultaneously the overall reaction.

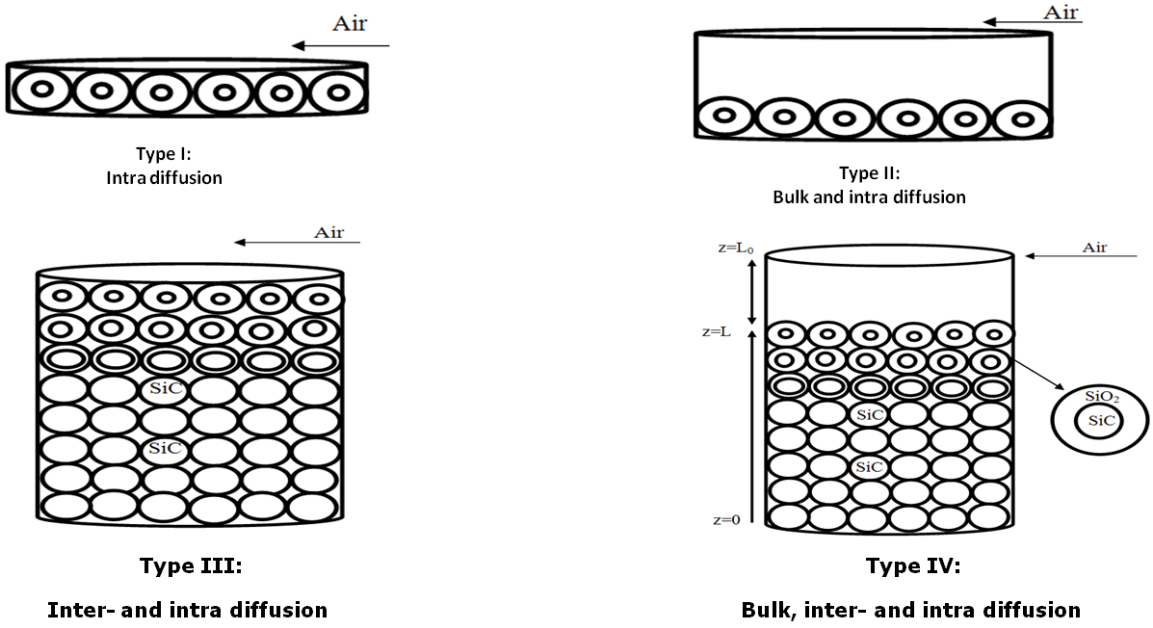

Figure 5.1 Different types of diffusion. Reproduced with permission from [12]

To overcome these issues and offer accurate and more comprehensive kinetic models, a new fluidized-bed-thermo-gravimetric-analyzer (FB-TGA) was developed. Consequently, due to the proper mixing and the uniform distribution of gas-solid and solid-solid that fluidization provides, the fluidized bed reaction chamber can easily ensure (1) the uniformity of the temperature throughout the sample, (2) the use of a sufficient amount of the solid sample, (3) the real elimination of the bulk and inter-particle diffusion controls, and (4) the use of a higher heating rate, which can represent the reality of what is happening in catalytic gas-solid reactions on an industrial scale. Morever, by playing with the solid inerts and reactant particle size, the intra-particle diffusion control could be partially suppressed.

The primary application of the newly developed equipment was carried out on calcium hydroxide decomposition. The results obtained were compared with those obtained from the conventional TGA.

5.2.3 Apparatus description

As shown in Figure 5.2, the fluidized bed reactor (FB-TGA) includes three main parts: the micro-reactor, the furnace and the various measuring instruments. The quartz fluidized bed reactor measures 1 inch in diameter and 6 inches in length (or height). The measuring instruments consist of (1) a load cell for weight measurement, (2) a thermocouple for temperature measurement of the bed, (3) pressure transducers for pressure drop measurement and (4) two mass flow controllers for gas flow rate adjustment depending on the temperature. The equipment is linked to a data acquisition system and the gas outlet is connected to a GC/FT-IR system.

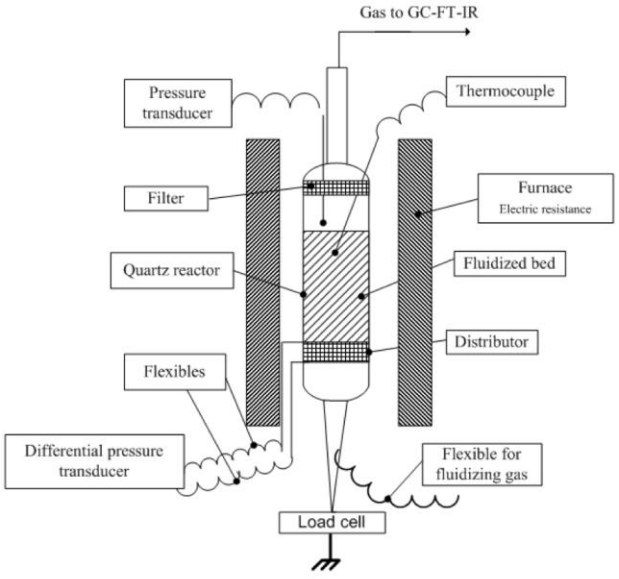

Figure 5.2 Schematic of the Fluidized Bed TGA

Furthermore, software was developed for the FB-TGA in order to keep the system at approximately minimum fluidization at any temperature. The software includes a program for gas flow rates as a function of temperature. Also, the two mass flow controllers are linked to the thermocouple, which permits decreasing the gas flow rates when the temperature is increasing.

5.2.4 Concept of the "pseudo variation" of the weight of the fluidized bed TGA

Figure 5.3 illustrates the concept of the pseudo variation of the weight of the reactor. As shown in this curve, two zones can be identified as follows: (1) the first one where the reactor was empty, so the mass of sand was 0g, and (2) the second zone where 25 g of sand was used in the bed. For the two experiments, three different gas velocities were tested: U_g= 0 U_{mf}, U_g = U_{mf} and U_g = 1.25 U_{mf}. The results suggest that the whole weight of the reactor decreases when the gas velocity increases. Thus, when the gas velocity changes from 0 U_{mf} to U_{mf}, the variation of the weight of the reactor remains the same for the two different masses of sand; 0g and 25 g. The same conclusion was observed by changing the gas velocity from U_{mf} to 1.25 U_{mf}.

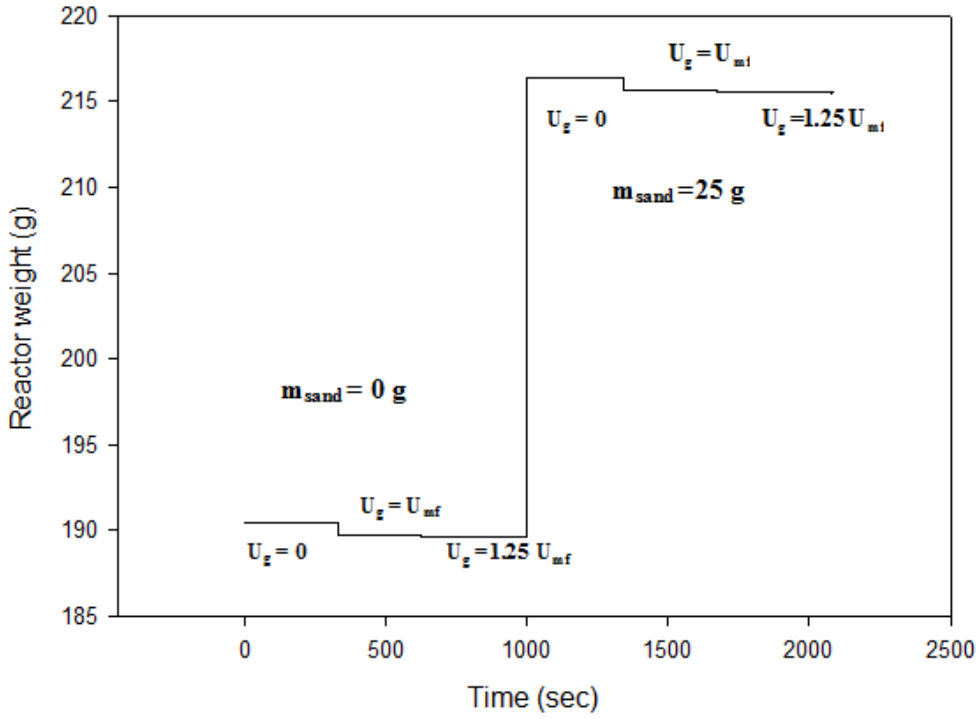

Figure 5.3 Pseudo variation of the reactor weight: Mass of sand = 0; 25 g

Regarding this experimental conclusion, the measured weight of the reactor or apparent weight could be described by equation 1.

$$m_{app} = m_{real} - \Delta m_P \qquad (1)$$

Where, m_{app} and m_{real} represent the apparent and real weight of the reactor and Δm_p denotes the variation of the weight of the reactor.

This "pseudo variation" of the weight of the reactor, shown in Figure 5.3, is due to the pressure drop through the distributor and filter. Modeling the pseudo variation of the weight of the fluidized bed reactor will be developed in the next section.

5.2.5 Modeling the pseudo variation of the weight of the reactor

It is important to keep the fluidization regime at “around” minimum in order to (1) profit from the fluidization advantages and to avoid (2) the vibration effect of fluidization on weight measurement and (3) the hydrodynamics effect on the study of kinetics.

Nevertheless, the gas and the minimum fluidization velocities change with the temperature. Hence, the control and regulation of the gas flow rate with the temperature is necessary in order to keep the system near the minimum fluidization regime. For this reason, the fluidized bed TGA is equipped with two (2) mass flow controllers (MFC). Using a special program, the MFCs adjust the gas flow rate instantaneously when the temperature increases.

On the other hand, by changing the gas velocity, the pressure drop through the distributor and filter will be affected. Therefore, modeling the pseudo variation of the weight of the reactor is required.

By performing a momentum balance on the micro-fluidized bed reactor, and neglecting the convection term and the weight of the fluid inside the reactor, the force applied by the fluidizing gas on the reactor can be expressed as follows:

$$F_{fluid \rightarrow reactor}\big|_z = \left(\Delta P_{dist.} + \Delta P_{filter}\right) \times S \qquad 2$$

Hence, the pseudo variation of the weight of the reactor is due to the force expressed by equation 2. Therefore, equation 3 gives the expression of the "pseudo variation of the weight of the reactor", denoted Δm_P, as a function of the pressure drop across the distributor and filter of the reactor.

$$\Delta m_P = \alpha_P \times \left(\Delta P_{dist} + \Delta P_{filter}\right); \alpha_P = \frac{S}{g} \quad (3)$$

Furthermore, the apparent weight of the reactor, which is measured by the load cell, can be expressed by equation 4.

$$m_{app.}\left(t,T,U_g\right) = m_{real}\left(t,T,U_g\right) - \Delta m_P\left(t,T,U_g\right) \quad (4)$$

Where:

$$m_{real}\left(t,T,U_g\right) = m_{reactor}\left(t,T,U_g\right) + m_{bed}\left(t,T\right) \quad (5)$$

and Δm_P denotes the pseudo variation of the reactor weight that is given by equation 3.

In more concrete terms, the model gives the real weight of the reactor in the fluidized bed TGA and is expressed in equation 6.

$$m_{real}\left(t,T,U_g\right) = m_{app}\left(t,T,U_g\right) + \Delta m_P\left(t,T,U_g\right) \quad (6)$$

To include the effect of the pseudo variation of the reactor weight in the FB-TGA results, the pressure drop along distributer and filter should be measured, converted to weight, and subtracted from the total weight loss of the reactor.

5.2.6 Experimental Procedures

For the experiments shown in Figure 5.3, which illustrates the concept of the pseudo variation of the reactor weight in the fluidized bed TGA, the used fluidizing agent was air. The experiments were carried out at 25C (room temperature), and 0g and 25g of sand were used. The minimum fluidization velocity was determined by measuring the pressure drop across the bed.

However, for the validation of the pseudo variation of the weight at ambient temperature, two different strategies were used. For the results represented in Figure 5.4, it was proposed

to validate that the pseudo variation of the weight, explained above in the paper, is only due to the pressure drop across the distributor. Therefore, according to the Ergun equation, which gives the pressure drop as a function of the square of the gas velocity ($\Delta P \propto U_g^2$) for the turbulent regime, this experimental pseudo variation of the weight should follow the same law. Hence, by changing the fluidizing gas velocity and measuring the weight of the reactor by the load cell, the experimental resulting low weight of the reactor should be proportional to the square of the gas velocity ($\Delta m \propto U_g^2$). It should be indicated that, during the experiments presented in Figure 5.4, different masses of sand were tested (0g, 10g, 20 g and 30 g) and there was no filter at the top of the reactor.

As indicated in figure 4, the results were modeled and the model is: $\Delta m=0.0025\ U_g^2$. It should be remembered that the model shown in Figure 5.4 is completely different from the one mentioned in Figure 5.5.

Furthermore, Figure 5.5 (Measuring the weight of the bed: Model vs. Bed pressure drop) indicates the second strategy for confirmation and validation, at ambient temperature, which is the pseudo variation of the reactor weight is due to the pressure drop along the distributor and filter of the reactor. For these experiments, the fluidizing agent used was air and 20 g of tested sand. The air velocity was changing and three parameters were measured: (1) the weight of the reactor that was measured by the load cell, (2) the pressure drop along the distributor and (3) the pressure drop across the bed. The load cell indicates the apparent bed weight that is corrected by the model, which gives the pseudo variation of the reactor as a function of pressure drop along the distributor (equations 3 and 6). The results are shown in Figure 5.5 (Real bed weight (model)). Moreover, the pressure drop across the bed was converted to weight that is illustrated by Figure 5.5 (Bed weight (bed pressure drop)). The initial weight of the bed (20g) is shown in figure 5 (Bed weight (sample)). Finally, it should be indicated that the fluidized bed TGA operates at ambient pressure and the pressure drop across the filter is negligible.

For the section (pseudo variation of the weight: Validation at high temperature), three different masses of sand were tested: 20, 25, and 30 g. For all experiments, the fluidizing agent used was air and the reactor heated up according to the following temperature profile:

(1) Isothermal for 10 min at 25C (ambient temperature), (2) temperature ramp rate of 20°C/min up to 600°C and (3) isothermal for 20 min at 600°C. The values of minimum fluidization velocities, at different temperatures, were determined by measuring the pressure drop of the bed at the corresponding temperatures. The corresponding gas flow rate for the minimum fluidization regime, at different temperatures, was used as shown in Figure 5.6 (Gas flow rate adjustment vs. temperature).

At any temperature, the load cell measures the apparent weight of the reactor and the pressure transducer gives the pressure drop across the distributor. The results are given in Figure 5.8. The apparent weight, which is obtained from the load cell, is corrected by the model giving the pseudo variation of the reactor weight as a function of the pressure drop along the distributor (equations 6 and 9). For the different masses of sand used, the obtained results are shown in Figure 5.8 (corrected weight from the model (20-25-30g). The bed weights obtained from the pressure drop across the bed are also represented in Figure 5.8 (bed weight from the bed pressure drop).

For the section (Experimental validation: Calcium hydroxide decomposition), the experiments were carried out in argon (Ar) atmosphere and according to the following temperature profile: (1) Isothermal for 10 min at 25C (ambient temperature), (2) temperature ramp rate of 20C/min up to 650C, (3) isothermal for 30 min at 650C. The conventional TGA that was used for the experiments presented in figure 10 was the TGA Q-50 instrument type. Three (03) different masses of calcium hydroxide were tested: 10, 25 and 140 mg. The mean particle size of $Ca(OH)_2$ was 45 microns and the particle density was 2340 $kg.m^{-3}$. However, for the decomposition of calcium hydroxide in the fluidized bed TGA, 4g of $Ca(OH)_2$ was mixed with 30 g of sand. The mean particle size was 45 microns for $Ca(OH)_2$ and 75 microns for sand. The particle density for the sand used was 2650 $kg.m^{-3}$, while the one for $Ca(OH)_2$ was 2340 $kg.m^{-3}$.

The values of minimum fluidization velocities of the mixture were calculated by measuring the bed pressure drop at different temperatures. Also, two thermocouples were used, at

different z and r positions in the fluidized bed, in order to confirm that the bed was well fluidized at all times during the experiments.

5.2.7 Pseudo variation of the weight: Validation at ambient temperature

It is well known that the pressure drop across the distributor is proportional to the square of the gas velocity ($\Delta P_{distr.} \alpha U_g^2$). For confirmation and validation of the model converting the pressure drop of the distributor into reactor weight loss, experiments were carried out at ambient temperature and the results are shown in Figure 5.4 and Figure 5.5.

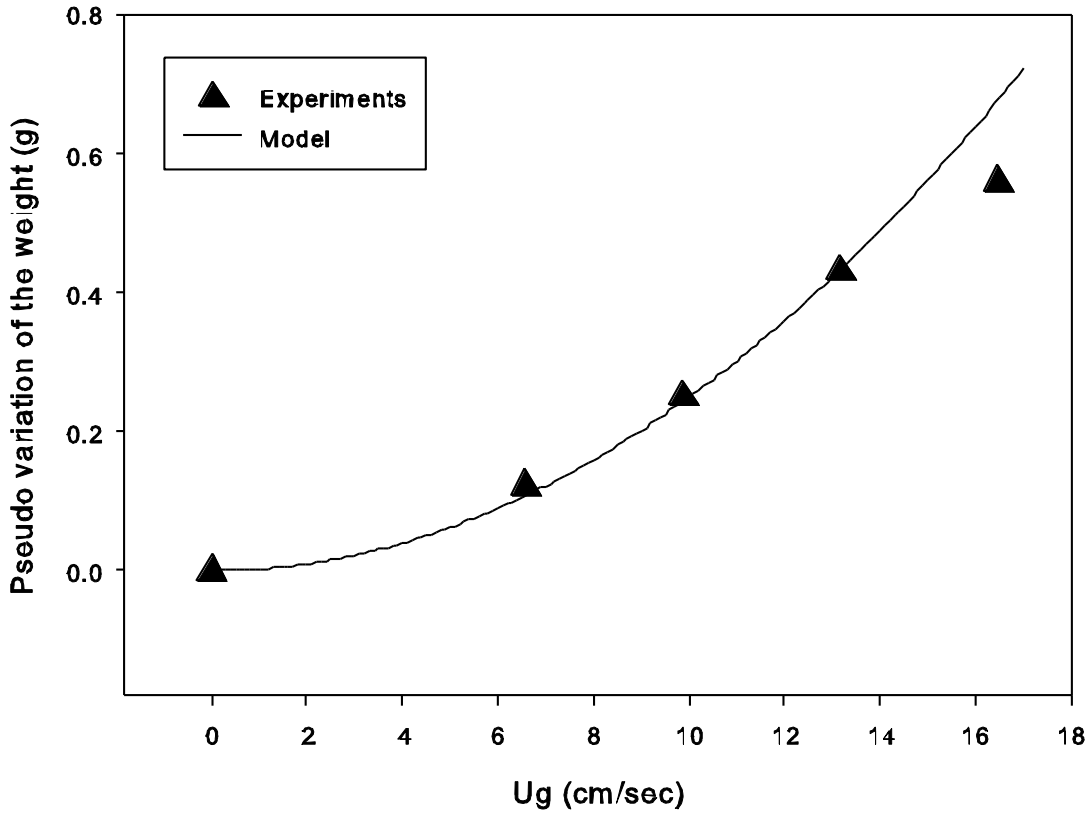

Figure 5.4 Modeling the pseudo variation of the reaction weight: Validation (T=25°C)

It should be indicated that, depending on the particle size of the fluidization material, the gas velocity for the experiments could range from 2 to 14 cm/s.

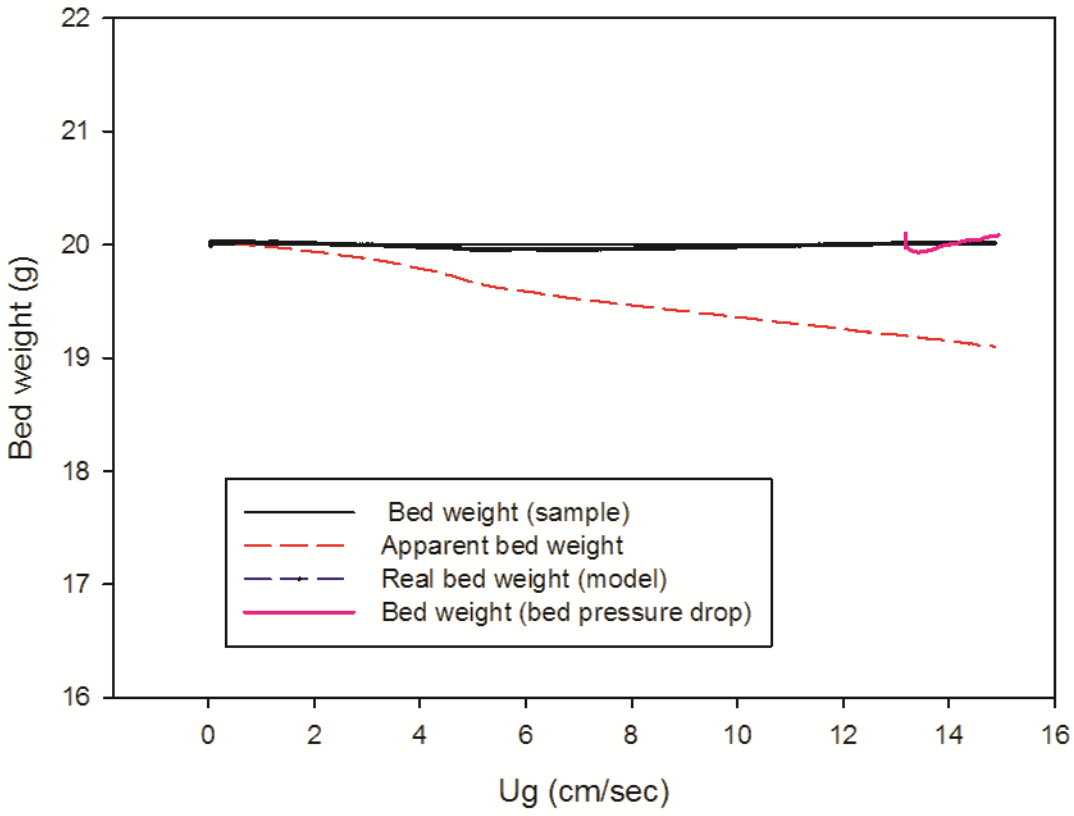

Figure 5.5 Measuring the weight of the bed: Model vs. Bed pressure drop

Moreover, the bed weight measured by the pressure drop of the bed shows some fluctuations, contrary to that obtained from the model. The validation of the model at high temperature is given in the next section.

5.2.8 Pseudo variation of the weight: Validation at high temperature

The objectives of this section focus on validating the modeling of the pseudo variation of the reactor weight at high temperature and the use and confirmation of the strategy for the gas flow rate adjustment versus temperature.

Figure 5.6 shows the flow rate adjustment versus temperature. The gas flow rate decreases when the temperature is increasing and remains constant for each 50°C segment of temperature. This segment of temperature was chosen so that the fluidization regime remains steady at around minimum fluidization.

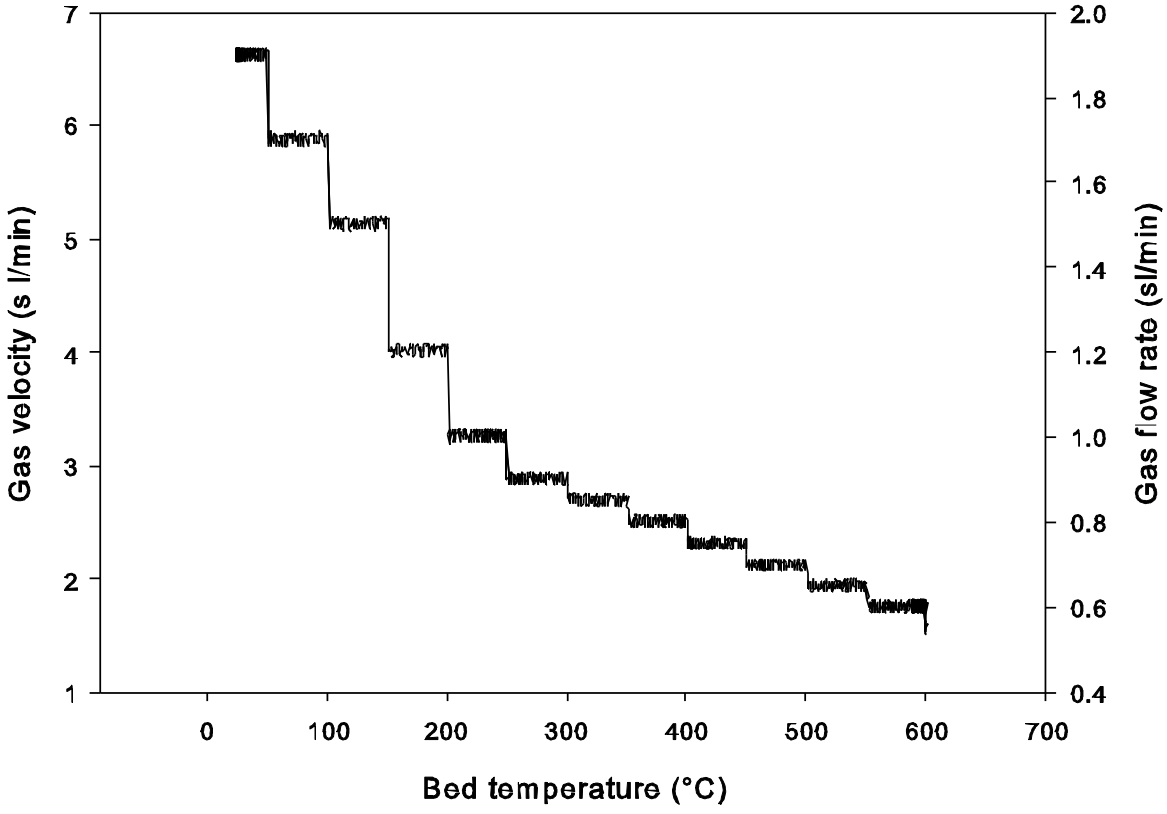

Figure 5.6 Gas flow rate adjustment vs. temperature

Figure 5.7 illustrates the variation in pressure drop throughout the distributor depending on the temperature. For each 50°C segment of temperature where the temperature remains constant, the pressure drop increases gradually. When the gas flow rate decreases, however, the pressure drop decreases instantaneously.

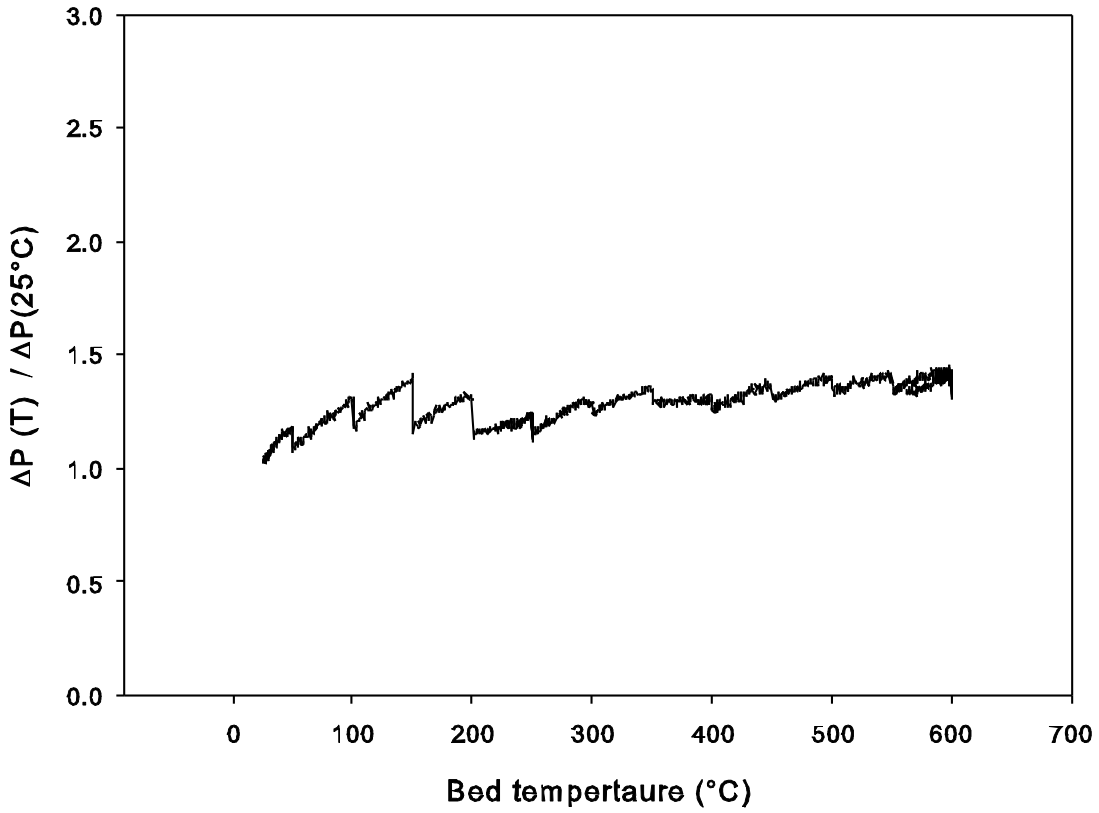

Figure 5.7 Pressure drop vs. temperature

The validation, at high temperature, of the model developed for the pseudo variation of the reactor weight is demonstrated in Figure 5.8. The reactor for the FB-TGA was tested with three different masses of sand: 20, 25, and 30 g. The heating rate was 20°C/min and the reactor was heated up to 600°C.

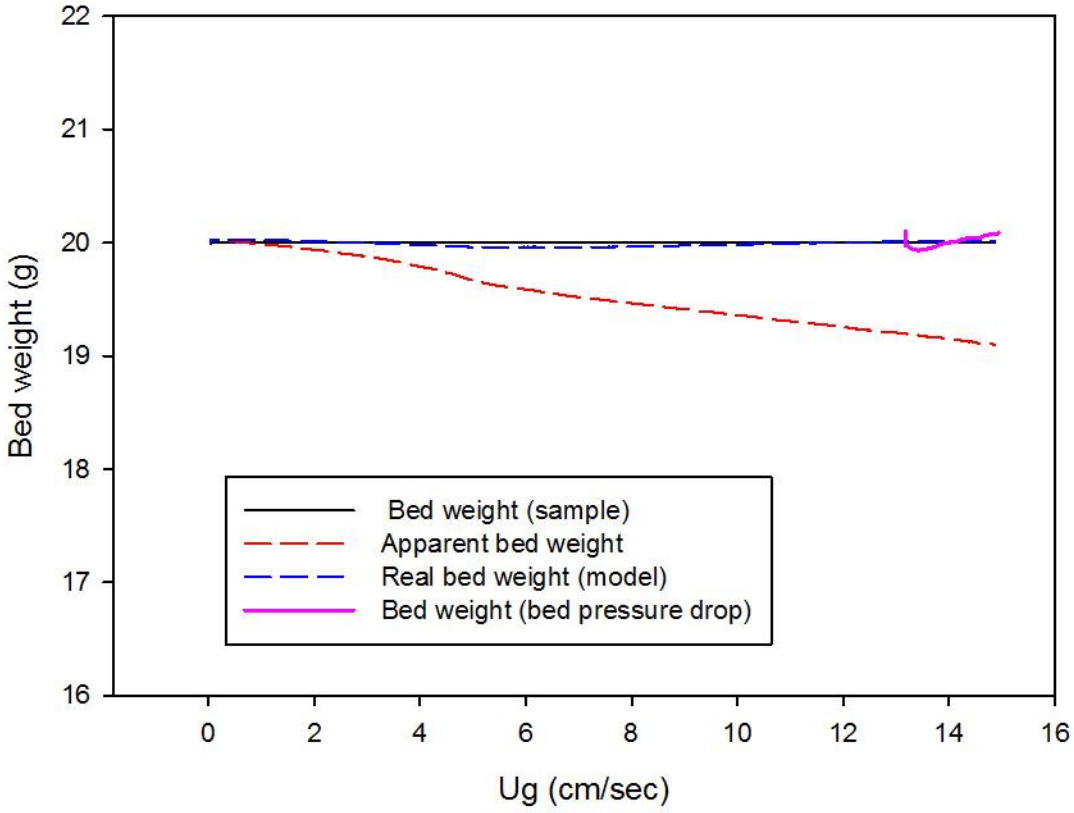

Figure 5.8 Pseudo variation of weight vs. temperature

The obtained results suggest that the weight of the reactor decreases roughly with the temperature. By converting the value of the pressure drop throughout the distributor, the corrected weight of the reactor (bed), according to the developed model, remained constant with the temperature.

Hence, by using these strategies, the weight loss due to thermal transformation is

measured precisely, which makes the developed FB-TGA an accurate standard piece of equipment for the kinetics study of catalytic gas-solid reactions.

5.2.9 Experimental validation: Calcium hydroxide decomposition

Application and validation of the newly developed fluidized bed TGA were carried out on the calcium hydroxide ($Ca(OH)_2$) decomposition. The validation tests were done in an Argon (Ar) atmosphere with a heating rate of 20°C/min. The results obtained from the conventional TGA and the FB-TGA are shown in Figure 5.9.

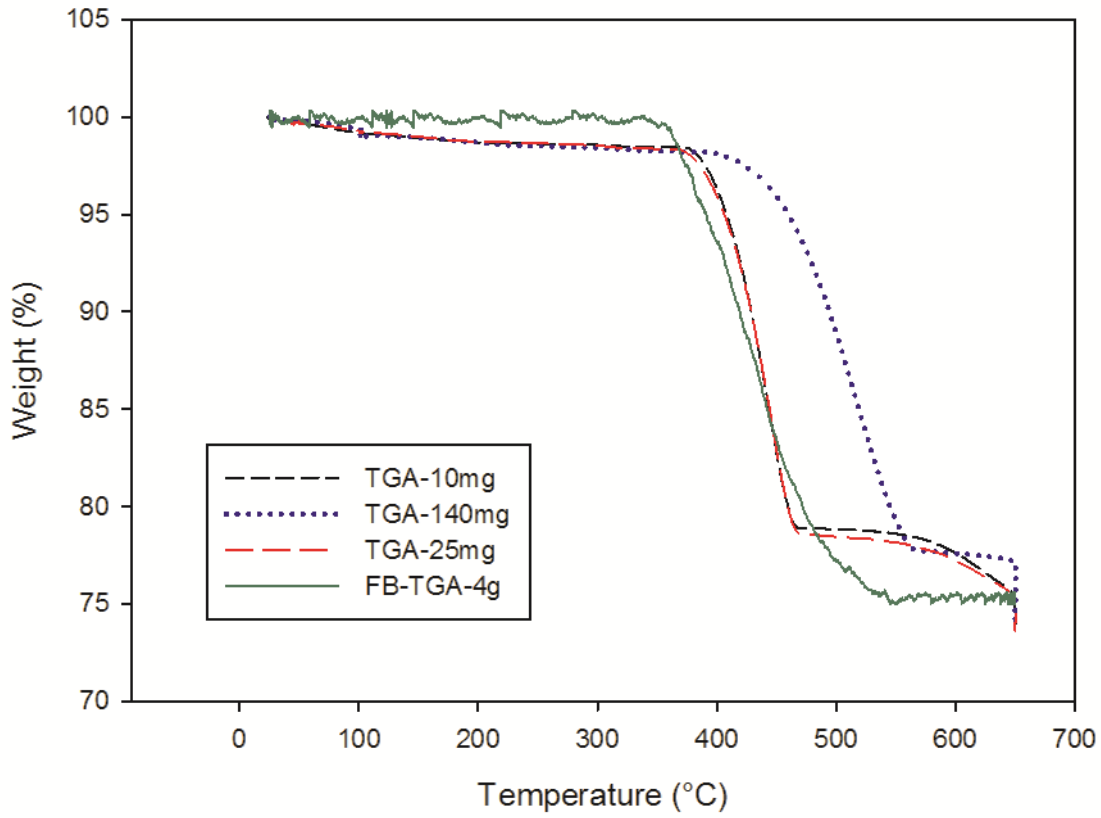

Figure 5.9 Ca(OH)2 decomposition: Comparison between Conventional and Fluidized Bed TGAs

Three (3) amounts of $Ca(OH)_2$ were tested on the conventional TGA: 10 and

25 mg to validate that there is no diffusion (bulk and inter-particle) control and 140 mg to demonstrate the diffusion limitation on the conventional TGA. However, 4 g of $Ca(OH)_2$ were tested on the FB-TGA to confirm that there is no diffusion control limitation.

For the conventional TGA, the results obtained for 10 and 25 mg are similar but different from those obtained for140 mg. The obtained curves can be divided into two major parts, denoting two different reaction stages. The first zone can be represented by 370-470°C for 10 and 25 mg and 395-565°C for 140 mg, while the second zone can be delimitated by 470-650°C for 10 and 25 mg and 565-650°C for 140 mg.

The overall process of conversion of solid $Ca(OH)_2$ into CaO and water vapor, involving the sub processes of heat transfer, mass transfer and thermal decomposition kinetics, is driven by the rate of thermal energy flux received by the inner core of $Ca(OH)_2$ surrounded by the shell of CaO(s) in a solid (say) spherical particle. For a given particle, the product species, water vapor would issue out of the particle through pores in the core of $Ca(OH)_2$ and shell of CaO in the form of jets (involving convective flow due to the build-up of pressure gradient between the particle interior and its exterior surface) or via the Knudsen/bulk molecular diffusion depending on the rate of thermal energy flux and particle pore size.

Accordingly, during the first stage, the difference shown between the results obtained from 10-25 mg and 140 mg is due to the heat transfer limitation and/or the temperature gradient throughout the sample (140 mg). Nevertheless, the intra-particle diffusion of H_2O through a small layer of CaO that was formed around the $Ca(OH)_2$ particle and, its external diffusion through the gas film around the particle, gradually became the rate-controlling step of the thermal decomposition reaction during the second part.

On the other hand, the results obtained from 4 g of $Ca(OH)_2$ in the fluidized bed TGA are in agreement with those obtained from 25 mg of $Ca(OH)_2$ in the conventional TGA, but only during the first zone. In fact, only one stage for the thermal decomposition of Ca(OH)2 in the FB-TGA can be considered (360-540°C).

These results suggest that, in the case of FB-TGA, it is quite likely that the thickness of CaO(s) shell layer would be less than that in the case of fixed, conventional bed TGA due to spalling of the CaO(s) shell layer in the FB-TGA. This affects both the heat and species mass transfer resistances. Also, the effect of turbulence in the FB-TGA would be to decrease the effective thickness of the gas film (or, concentration boundary layer) around

the particle. Its effect on the intra-particle diffusion mass transfer coefficient would be negligibly small, if any. One way to minimize or eliminate the effect of intra-particle diffusion mass transfer of a species, such as water vapor, is to decrease the solid $Ca(OH)_2$ particle size so that the concentration of water vapor as a function of the radial distance in the particle pores is almost flat.

In addition, the obtained samples were analyzed by X-Ray Diffraction (XRD). The results are demonstrated in Figure 5.10. The scores for $Ca(OH)_2$ are 26 for the sample treated in the conventional TGA (25 mg), and 3 for the one treated in FB-TGA. These results confirm that (1) the effective thickness of the gas film around the particle was greatly decreased, and (2) the intra-particle diffusion of H_2O throughout the formed layer of CaO was relatively suppressed in the case of the FB-TGA. Consequently, the heat and water vapor mass transfer were significantly enhanced by using the FB-TGA.

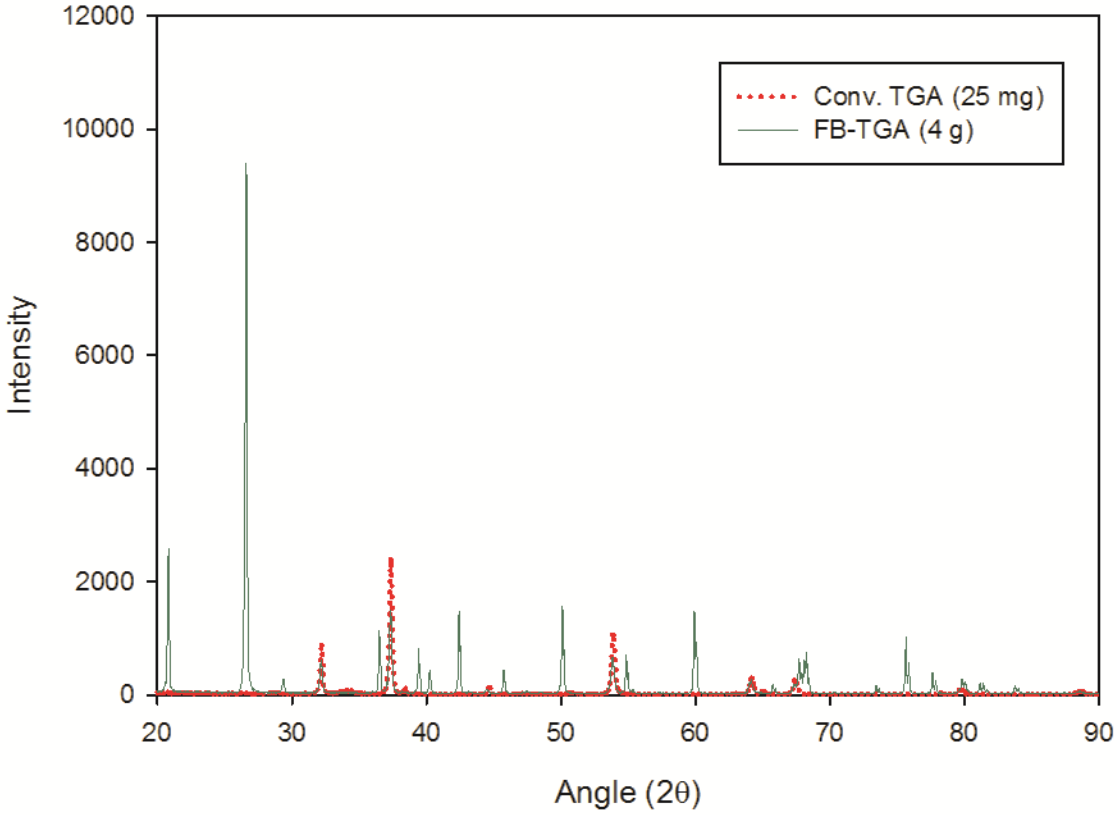

Figure 5.10 XRD results of the treated samples from Conv. TGA and FB-TGA

Furthermore, the overall decomposition of $Ca(OH)_2$ in the FB-TGA was 75.4%. This experimental value, obtained from the FB-TGA, is in perfect agreement with the calculated value (75.6%) from the decomposition reaction of dry $Ca(OH)_2$, which confirms the reliability and the repeatability of the newly developed FB-TGA.

5.2.10 Conclusion

To provide accurate and more comprehensive kinetic models for gas-solid reactions, the Fluidized Bed TGA (FB-TGA) was developed. The standard equipment was validated and applied to calcium oxide decomposition. The experiments demonstrated that FB-TGA

provided good and more reliable results for the thermal decomposition of $Ca(OH)_2$ than the conventional TGA. Bulk and inter-particle diffusion were perfectly suppressed by the application of FB-TGA. The treated samples were analyzed by XRD and the results confirmed that, by applying the FB-TGA, both heat and species mass transfer limitations were almost eliminated.

Studying kinetics and the mechanism of catalytic pyrolysis, combustion and gasification of coal, biomass, and waste solid in the newly developed FB-TGA are in progress and the results will be published in the near future.

5.2.11 Acknowledgments

The authors are grateful for the financial support of Carbon Management Canada. Acknowledgments are also extended to Dr. Rouzbeh Jafari, Mr. James Abbott, Mr. Yazid Belkhir and Mr. Robert Delisle for their precious help.

5.2.12 Nomenclature

U_g	Superficial Gas velocity (m/s);
U_{mf}	Minimum fluidization velocity (m/s);
m_{sand}	Mass of sand; (kg)
m_{bed}	Mass of bed; (kg)
$\Delta P_{dist.}$	Pressure drop across the distributor; (Pa)
ΔP_{bed}	Pressure drop across the bed; (Pa)
ΔP_{filter}	Pressure drop across the filter; (Pa)
ΔP_{mf}	Pressure drop across the bed at minimum fluidization; (Pa)
S	Transversal area of the reactor; (m^2)
U_{g0}	Gas velocity at the inlet of the distributor; (m/s)
U_{g1}	Gas velocity at the outlet of the distributor; (m/s)

U_{g2}	Gas velocity at the inlet of the filter; (m/s)
U_{g3}	Gas velocity at the outlet of the filter; (m/s)
g	Gravity acceleration; (m^2/s)
Δm_P	Pseudo variation of the weight of the reactor; (kg)
α_P	Pressure drop to weight conversion factor; (kg/Pa)

CHAPITRE 6 ARTICLE 2: COAL GASIFICATION IN A FLUIDIZED BED THERMOGRAVIMETRIC ANALYZER

6.1 Présentation de l'article

Ce chapitre reprend l'article intitulé **'Coal gasification in a fluidized bed thermogravimetric analyzer'**. Cet article a été soumis à la revue Fuel Journal (manuscript number: JFUE-D-16-01226).

Nous avons vu, dans le chapitre précédent, l'importance et la nécessité de développer un équipement idéal pour étudier la cinétique et les mécanismes des réactions catalytiques gaz-solide. Vu la contribution majeure du charbon dans le secteur énergétique mondial, nous avons décidé de faire de la gazéification du charbon une première application dans l'analyseur thermogravimétrique à lit fluidisé (ATGF). Dans cet article, une analyse complète du charbon a été présentée. Ensuite, un rappel des principales composantes de l'ATGF a été exposé. Une description des différentes étapes de la gazéification du charbon, comprenant la pyrolyse, la gazéification du char et le craquage du goudron a été réalisée. Les principales réactions, ainsi que leurs cinétiques, gouvernant la gazéification du charbon dans l'ATGF ont été listées. Une série de tests indépendants expérimentaux sur la pyrolyse du charbon, la gazéification du char et la gazéification du charbon dans l'ATGF a été effectuée. Les différents paramètres cinétiques, obtenus, lors de la dévolatilistaion totale du charbon, ainsi que ceux des principaux gaz produits de la pyrolyse du charbon, ont été montrés. La cinétique de l'oxydation partiale du char a été étudiée dans l'ATGF et les paramètres cinétiques ont été estimés. Ensuite, le modèle de la cuve parfaitement agitée a été proposé pour décrire le fonctionnement du réacteur de l'ATGF. Les paramètres cinétiques, obtenus précédemment, ont alimentés le modèle et les résultats ont été comparés avec ceux obtenus expérimentalement. La dernière partie de l'article a été consacrée à une étude de l'équilibre des principales réactions homogènes de la gazéification du charbon. Les résultats expérimentaux ont été comparés avec les constates d'équilibre des différentes réactions chimiques de la gazéification.

6.2 Coal gasification in a fluidized bed thermogravimetric analyzer

Said Samih and Jamal Chaouki

(Soumis à Fuel Journal, manuscript number: JFUE-D-16-01226)

6.2.1 Abstract

Kinetics and the modeling of coal gasification were studied in the newly developed fluidized bed thermogravimetric analyzer. The weight loss obtained from the fluidized bed TGA was in good agreement with the total gas product. The presented model for the micro fluidized bed reactor encompasses the kinetics of coal pyrolysis as well as the char gasification reaction rate. For coal pyrolysis, resulting activation energies for the individual gases were 3 to 4 times lower than those found in literature. However, the resulting kinetic parameters basically agree with those found in literature for char gasification in a fluidized bed reactor. The effects of temperature on the yield and the composition of the gas product are studied. Equilibrium data were also compared with experimental results. The model shows reasonably good agreement with the experimental results, except for water gas shift reaction.

6.2.2 Introduction

Gasification is technology that thermally converts coal and waste feed stocks, including refinery residues, petroleum coke, biomass, and municipal and other solid carbonaceous materials to a gaseous product with a useable heating value [57, 77, 78]. In 2007, there were 420 operating gasifiers worldwide, of which 55% used coal as feed and 32% petroleum residue. With a gasification capacity of 30,825 MWth of syngas, there were 212 operating coal gasifiers. China accounts for the majority of coal gasification plants built in recent years [7].

Gasification technology includes pyrolysis, partial oxidation, and hydrogenation [57, 77, 79]. Partial oxidation is the dominant one that produces syngas consisting of carbon monoxide and hydrogen in varying ratios.

Modeling the process of coal gasification is key for its scale up, design, operation and control. This requires a robust knowledge of chemical phenomena and the hydrodynamics taking place in the gasifier [23, 57].

A widely used technique to characterize the kinetics and mechanism of gaz-solid reactions is the thermogravimetric analysis (TG). However, the technique has some limitations, such as the small amount of sample that can be used (mg), the poor mixing and distribution of the gas-solid-catalyst throughout the sample, the lower heating rate, the non-uniformity of the temperature throughout the sample, and the inter- and intra-particle diffusion limitations. The above major limitations reduce the relaibility of the kinetic parameters found using the conventionnal thermogravimetric analyzer (TGA) [11, 12, 80].

Recently, the innovative fluidized bed thermogravimetric analyzer (FB-TGA) was developed to characterize the kinetics and mechanism of gas-solid reactions [11]. In the present paper, the kinetics of coal pyrolysis and gasification are investigated in this newly developed fluidized bed TGA. The experimental results are used to evaluate a model for the micro-fluidized reactor. The proposed model unifies the two stages of gasification, pyrolysis and char gasification, and evaluates the individual gas yield at different temperatures and a moderate heating rate.

6.2.3 Experimental

6.2.3.1 Feed Material

Western Canadian lignite coal (WLC) was used as the solid fuel for the experiments reported in this paper. The proximate and utlimate analyses of the coals are presented in Table 6.1. More information on the bed material is given in the apparatus descritpion and procedures section. As can be seen in Table 6.1, the proximate and the ultimate analysis for the two coals are similar. The lignite coal was chosen, from literature, for comparison.

Table 6.1 Analysis of the lignite coals

Coals	**Canadian Lignite Coal**	**Lignite Coal [18]**
Proximate analysis (wt. % a.r.)		
Fixed carbon	34.3	46.4
Volatile matter	39.3	36.9
Ash	15.4	9.9
Moisture	11.1	6.8
Ultimate analysis (wt. % a.r.)		
C	57.2	59.3
H	4.3	3.8
N	1.2	0.9
O	21.1	18.2*
S	0.1	1.1

a.r. as received; * by difference

6.2.3.2 Apparatus description and procedures

Figure 6.1 shows a schematic diagram of the experimental apparatus that includes the fluidized bed TGA and the gas analyzing system. The newly developed equipment consists of a quartz reactor 1 inch in diameter and 6 inches in length, a furnace, and various measuring instruments. The measuring instruments include (1) a load cell for weight measurement, (2) thermocouples for measuring the temperature of the bed, (3) pressure transducers for pressure drop measurement and (4) two mass flow controllers for the gas flow rate adjustment. The two mass flow controllers are linked to the thermocouple, which permits decreasing the gas flow rates when the temperature is increasing[11]. The apparatus uses a software for the FB-TGA in order to keep the system at approximately minimum fluidization at any temperature. The gas outlet is connected to a GC/FT-IR system.

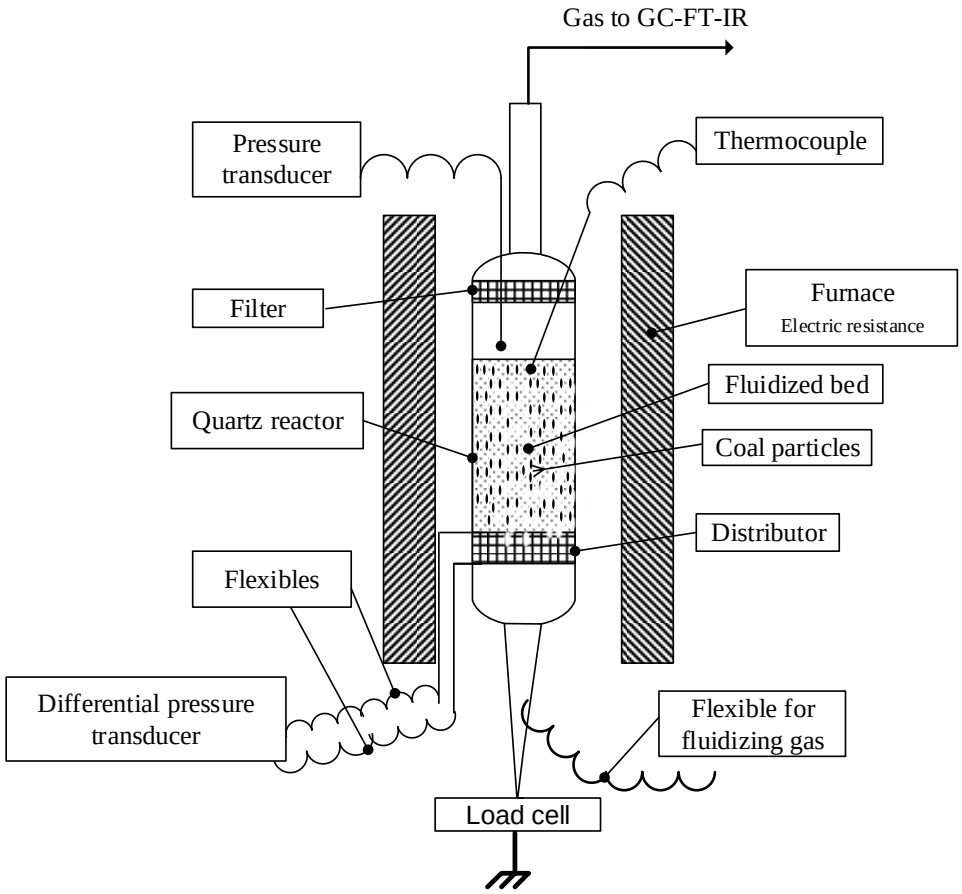

Figure 6.1 Fluidized bed TGA. Adapted from [11]

6.2.3.3 Experimental procedures

For all the experiments reported in the present article, 35 g of silica sand, > 125 μm and < 150 μm in size, were mixed and fluidized with 5 g of lignite coal, > 500 μm and < 600 μm in size. The particle density for the used sand was 2650 $kg.m^{-3}$. It should be noted that both the coal and the used sand are categorized as Geldart group B particles.

The heating rate used was about 40°C/min. The gas flow rate was changing depending on the temperature in order to keep the bed at the minimum fluidization regime at any temperature according to the strategy developed for the FB-TGA [11].

The values of minimum fluidization velocity of the mixture were calculated by measuring the bed pressure drop at different temperatures. Also, two thermocouples were used, at different z and r positions inside the reactor, in order to make sure that the bed was well fluidized at any temperature during the experiments.

Furthermore, there was no opportunity for segregation in the experimentally studied conditions. In fact, under moderate bubbling conditions, the bulk of jetsam develops the characteristic convective motion. Therefore, the flotsam particles are drawn down into the depth of the bed with no opportunity for segregation until disturbed by bubbles [81-84].

At any temperature, the load cell measures the apparent weight of the reactor and the pressure transducers give the pressure drop across the distributor and the filter. The apparent weight, which is obtained from the load cell, is corrected by the model giving the pseudo variation of the reactor weight as a function of the pressure drop along the distributor [11].

The exiting gases from the FB-TGA were analyzed by means of a GC/FT-IR system. A two-point external calibration, using standard gases composed of 8 gas components at different concentrations, was employed for all the FB-TGA experiments.

6.2.3.4 Experimental strategy

Performing the experiments separately, for the different steps of gasification, is the strategy that was used for studying the kinetics and mechanism of coal gasification in the fluidized bed TGA. First, the pyrolysis of coal was carried out in nitrogen (alpha 1) atmosphere. The mixed solid, including Canadian lignite coal (see Table 6.1) and sand, was heated up to 700°C at a heating rate of 40°C/min. Then, the fluidized bed reactor was kept under isothermal conditions, at 700°C, for more than three hours. Experimental data, including solid weight loss measurements and gas product compositions, were continuously collected to derive kinetic parameters for coal pyrolysis.

The produced char was then partially oxidized with a gas mixture, 5% oxygen-balance nitrogen, in the second step. At a heating rate of 40°C/min, the mixed char and sand were heated up to 700°C. The mixed solid bed was kept under isothermal conditions, at 700°C, for more than three hours. The solid weight loss and the gas product compositions, mainly CO and CO_2, were continuously measured. The experimental data was used to develop kinetic parameters for the char gasification reaction.

The third experimental step was the gasification of coal in the fluidized bed TGA. The gasification agent was a gas mixture of 5% oxygen-balance nitrogen. Five grams of coal and 35 g of sand were heated up to 750°C and 650°C respectively at a heating rate of 40°C/min. Then, the reactor was kept under fixed temperature conditions at 650°C and 750°C separately for more than three hours. The solid weight loss was measured by the fluidized bed TGA, while the gas product compositions, mainly CO, CO_2, H_2, CH_4 and H_2O, were continuously measured by means the GC/FT-IR system.

The last experimental step was to remove the condensed tar on the outlet part of the reactor. The experiments were conducted, after each test, in an atmosphere of air at 750°C.

6.2.4 Kinetic modeling

6.2.4.1 Coal pyrolysis

Coal pyrolysis leads to three different products: (1) volatile gases, including essentially H_2O, CO_2, CO, CH_4 and H_2, (2) char and (3) tar.

Total devolatilization

Total devolatilization of coal can be represented by the following overall single-reaction model[85]:

$$\boldsymbol{Coal \rightarrow y_{dev}\, V + (1 - y_{dev})S} \qquad (1)$$

where V equals total volatile yield and S equals char. The assumed first-order rate can be expressed as follows:

$$\boldsymbol{\frac{d(y_{dev})}{dt} = r_{dev} = k_{0,dev} e^{-E_{dev}/RT}(1 - y_{dev});\ y_{dev} = \frac{w_0 - w(t)}{w_0 - w_\infty}} \qquad (2)$$

where y_{dev} represent the yield of devloatilization up to time t, and $w_0, w(t), w_\infty$ stand respectively for the initial, the instantaneous and the final weight of coal.

6.2.4.2 Gas release

Coal pyrolysis can be modeled as a set of independent parallel reactions having a statistical distribution of activation energies [18, 73]. Hence, for each key product i from the reaction

$$\boldsymbol{Coal\ (V) \rightarrow \text{Product i}} \qquad (3)$$

The assumed n_i-order rate is as follows:

$$\boldsymbol{\frac{d(y_i)}{dt} = r_{p,i} = k_{0i} e^{-E_i/RT}(1 - y_i)^{n_i};\ y_i = \frac{V_i}{V_i^*}} \qquad (4)$$

Where V_i is the amount of product i produced up to time t (kg), V_i^* is the amount of product i, which could potentially be produced (kg), k_{0i} is the pre-exponential factor, E_i and n_i are respectively the activation energy and the order of reaction i, T is the absolute temperature, and R is the gas constant. V_i and V^*_i can be calculated as follows:

$$\boldsymbol{V_i = \frac{M_i}{24}\int_0^t Q_S y_i\, dt \;\; and \; V_i^* = \frac{M_i}{24}\int_0^\infty Q_S y_i\, dt} \qquad (5)$$

Where Q_s is the total gas volumetric flow rate at standard temperature and pressure conditions (15°C and 1 atm), and i could be CO, CO_2, H_2, CH_4, or H_2O.

6.2.4.3 Char production

Char production can be determined directly from the weight measurement obtained from the fluidized bed TGA. Furthermore, it can be deducted from the following equation :

$$\boldsymbol{Char\ production = 100 - total\ devolatilization} \qquad (6)$$

6.2.4.4 Tar production

Tar production, or unconverted tar, was to be estimated from the following equation:

$$\boldsymbol{tar\ production = 100 - total\ devolatilization\ - total\ gas\ produced} \qquad (7)$$

It should be indicated that the total gas produced comes from the total devolatilization and the amount of tar cracked inside the reactor. Since the residence time was short enough, the concentration of tar in the gas and the temperature were low, the conditions were not appropriate for complete tar cracking. The tar production may stand for the 'uncracked tar', including inert ant the unconverted tar.

6.2.4.5 Coal gasification

The principal chemical reactions governing the coal gasification process are those involving carbon (C), carbon monoxide (CO), carbon dioxide (CO_2), hydrogen (H_2), steam

water (H_2O), and methane (CH_4) [57, 78]. These reactions are listed in Table 6.2. More comments are given in the results and discussion section.

Table 6.2 List of Heterogeneous and Homogeneous reactions

No	Chemical Reaction	Kinetic	Reference
R1	$C+\alpha O_2 \rightarrow 2(1-\alpha)CO+(2\alpha-1)CO_2$	$r_1=\left(7.58\times10^4\right)\cdot\exp\left(-\frac{13592}{T}\right)\cdot P_{O_2}\cdot\left(1-X_{1c}\right)^{2/3}$ $\frac{2(1-\alpha)}{2\alpha-1}=(2400)\cdot\exp\left(-\frac{6234}{T}\right)$ $r_1=\left(14.5\times10^{-3}\right)\cdot\exp\left(-\frac{13180}{T}\right)\cdot P_{O_2}\cdot\left(1-X_{1c}\right)^{2/3}$ $\frac{2(1-\alpha)}{2\alpha-1}=(2400)\cdot\exp\left(-\frac{6234}{T}\right)$	s^{-1} [19, 20] This work
R2	$C+H_2O\rightarrow CO+H_2$	$r_2=\frac{k_1\cdot P_{H_2O}}{1+k_2\cdot P_{H_2O}+k_3\cdot P_{H_2}}$ $k_1=\left(4.93\times10^3\right)\cdot\exp\left(-\frac{18522}{T}\right)$ $k_2=\left(1.11\times10^1\right)\cdot\exp\left(-\frac{3548}{T}\right)$ $k_3=\left(1.53\times10^{-9}\right)\cdot\exp\left(\frac{25161}{T}\right)$	s^{-1} [19, 21] $bar\cdot s^{-1}$ bar^{-1} bar^{-1}
R3	$C+CO_2\rightarrow 2CO$	$r_3=\left(2\times10^{-8}\right)\cdot\exp\left(-\frac{360065}{T}\right)\cdot[CO_2]$	$kmol\cdot m^{-3}\cdot h^{-1}$ [19, 22]
R4	$C+2H_2\longrightarrow CH_4$	$r_4=\left(4.4.10^{-3}\right)\cdot\exp\left(-\frac{1.62.10^8}{T}\right)[H_2]$	$kmol\cdot m^{-3}\cdot s^{-1}$ [23, 24]
R5	$CO+1/2O_2\rightarrow CO_2$	$r_5=\left(8.83\times10^8\right)\cdot\exp\left(-\frac{99800}{RT}\right)\cdot[O_2].[CO\ ]$	$kmol\cdot m^{-3}\cdot s^{-1}$

			[25, 26]
R6	$H_2 + 1/2\,O_2 \leftrightarrow H_2O$	$r_6 = (2.19\times10^{9})\cdot\exp\left(-\frac{13127}{T}\right)\cdot[H_2]\cdot[O_2]$	$kmol\cdot m^{-3}\cdot s^{-1}$ [19, 21]
R7	$CH_4 + 2O_2 \rightarrow CO_2 + 2H_2O$	$r_7 = (1.58\times10^{10})\cdot\exp\left(-\frac{24343}{T}\right)\cdot[CH_4]^{0.7}\cdot[O_2]^{0.8}$	$kmol\cdot m^{-3}\cdot s^{-1}$ [19, 21]
R8	$CO + H_2O \leftrightarrow H_2 + CO_2$	$r_8 = (10^{3})\cdot\exp\left(-\frac{52960}{RT}\right)\cdot\left([CO]\cdot[H_2O]-\left(\frac{[CO_2]\cdot[H_2]}{K^*}\right)\right)$ $K^* = 520\cdot\exp\left(-\frac{7230}{T}\right)$ $r_8 = (2.89\times10^{2})\cdot\exp\left(-\frac{162607}{RT}\right)\cdot\left([CO]\cdot[H_2O]-\left(\frac{[CO_2]\cdot[H_2]}{K^*}\right)\right)$ $K^* = 12.64\cdot\exp\left(-\frac{23591}{T}\right)$ $r_8 = (2.95)\cdot\exp\left(-\frac{101847}{RT}\right)\cdot\left([CO]\cdot[H_2O]-\left(\frac{[CO_2]\cdot[H_2]}{K^*}\right)\right)$ $K^* = 5.5\times10^{3}\cdot\exp\left(-\frac{9000}{T}\right)$	$kmol\cdot m^{-3}\cdot s^{-1}$ [22, 27] [19, 86] This work
R9	$CH_4 + H_2O \rightarrow 3H_2 + CO$	$r_9 = (3\times10^{2})\cdot\exp\left(-\frac{15000}{T}\right)\cdot[CH_4]\cdot[H_2O]$ $r_9 = (8\times10^{3})\cdot\exp\left(-\frac{13000}{T}\right)\cdot[CH_4]\cdot[H_2O]$	$kmol\cdot m^{-3}\cdot s^{-1}$ [19, 86] This work
R10	Tar cracking $Tar \rightarrow \nu_{CO}CO + \nu_{CO_2}CO_2 + \nu_{CH_4}CH_4 + \nu_{H_2}H_2 + \nu_{tar}tar_{inert}$	$r_{10} = \nu_i 10^{4.98}\exp\left(-\frac{93}{RT}\right)\cdot(\rho_{tar})$	$kg\cdot m^{-3}\cdot s^{-1}$ [29]
R11	Tar combustion $CH_{1.522}O_{0.0228} + 0.867O_2 \rightarrow CO + 0.761\,H_2O$	$r_{11} = M_{HC}\,9.2.10^{6}\,T\exp\left(-\frac{9650}{T}\right)[HC]^{0.5}[O_2]$	$kg\cdot m^{-3}\cdot s^{-1}$ [30]

The molecular weight of tar, $M_{HC,}$ is 90 kg/kmol, and ρ is the density of the tar (kg of tar/m^3 of gas), HC, in the gas stream. The stoichiometric coefficients for tar cracking reaction are reported in Table 6.3.

Table 6.3 Stoichiometric coefficients for tar cracking [23]

Component	**Coefficient**
CO	0.56
CO_2	0.11
CH_4	0.09
H_2	0.02
Secondary tar	0.22

6.2.5 Modeling of the fluidized bed TGA reactor

The experiments in the fluidized bed TGA were carried out at approximately the minimum fluidization regime. The solid mixing induces the mixing of the gas in the fluidized bed zone [87-89]. Therefore, the reactor can reasonably be modeled as follows: a continuous stirred-tank model for the fluidized bed zone and a plug-flow model for the freeboard region [87-91].

6.2.5.1 Fluidized bed zone

For each gas species in the fluidized bed zone, the mass balance can be written as follows:

$$\frac{d(C_{i,g}V)}{dt} = \dot{w}_{i,in} - \dot{w}_{i,out} + \sum_{\substack{g-g \\ g-s}} \nu_{ij} r_j^* V \qquad (8)$$

The molar composition of gas (i) can be deducted as follows:

$$\dot{w}_i = C_{i,g} Q \qquad (9)$$

Hence, the mass balance could be re-arranged as follows:

$$\frac{d(C_{i,g}V)}{dt} = C_{i,g} Q_{in} - C_{i,g} Q_{out} + \sum_{\substack{g-g \\ g-s}} \nu_{ij} r_j^* V \qquad (10)$$

where, $C_{i,g}$ is the concentration of gas i (kg/m^3), V is the volume of the fluidized bed zone (m^3), r_j represents the rate of reaction j ($kg.\ m^{-3}.s^{-1}$), $\dot{w}_i$ stands for the mass flow rate of the specie i (kg/s). Q represents the gas volumetric flow rate ($m^3.s^{-1}$).

One can relate the molar composition (y_i) and the yield of gas i ($Y_{d,i}$) by using the following relations:

$$y_i = \frac{C_{i,g}}{M_i c_{mol}} \qquad (11)$$

$$Y_{d,i}(t) = \frac{1}{w_0} \int_{t_0}^{t} (C_{i,g} Q) dt \qquad (12)$$

$$c_{mol} = \frac{1}{24}\left(\frac{T_S}{T}\right) \qquad (13)$$

where, c_{mol} is the molar concentration, M_i is the molar mass of gas i, w_0 represents the initial weight of coal (kg), and T_S is the standard temperature (15 °C).

It should be noted that only reaction R1 was to be taken into account in the gas-solid reactions (see appendix A). Moreover, the pyrolysis reactions were included in the reactions taking place in the fluidized bed zone.

6.2.5.2 Freeboard zone

The mass balance for each gas species in the freeboard zone could be expressed as follows:

$$\frac{\partial C_{i,g}}{\partial t} = \sum_{g-g} \nu_{ij} r_j^* - \frac{\partial (u_g C_{i,g})}{\partial z} \qquad (14)$$

where $C_{i,g}$ is the concentration of gas i (kg/m^3), r^*_j represents the rate of reaction j (kg. m^{-3}.s^{-1}), and u_g stands for the gas velocity (m/s).

It should be indicated that the homogenous reactions in the freeboard zone were shown to be negligible because of: (1) the short residence time, (2) the low temperature and, (3) the low gas concentration in the freeboard zone.

6.2.5.3 Solid in the fluidized bed

The mass balance for solid conversion, however, could be expressed as follows:

$$\frac{dw_s}{dt} = R_S \qquad (15)$$

Where w_s is the weight of the reacted solid in the reactor (kg), and R_s represents the total solid reaction rate (kg/s), including total devolatilization and char gasification rates.

Rate terms

In the conditions under which coal was gasified, atmospheric pressure and the temperature range 300-1023 K, only 7 species, CO, CO_2, H_2, CH_4, H_2O (i = 1, 2, 3, 4, 5), tar and char need to be considered. Also, the expressions for the rate terms are presented in Table 6.4.

Table 6.4 List of rate terms

Component	Rate terms
CO	$\sum \left(\upsilon_{ij} r_i\right) V = 2(1-\alpha)\, w_{char} \left(\frac{M_{CO}}{M_C}\right) r_1 + V^*_{CO}\, r_{p,CO} - M_{CO}\, r_8\, V + M_{CO}\, r_9\, V + \upsilon_{CO} r_{10}$
CO_2	$\sum \left(\upsilon_{ij} r_i\right) V = (2\alpha - 1)\, w_{char} \left(\frac{M_{CO_2}}{M_C}\right) r_1 + V^*_{CO_2}\, r_{p,CO_2} + M_{CO_2}\, r_8\, V + \upsilon_{CO_2} r_{10}$
H_2	$\sum \left(\upsilon_{ij} r_i\right) V = V^*_{H_2}\, r_{p,H_2} + M_{H_2}\, r_8\, V + 3 * M_{H_2}\, r_9\, V + \upsilon_{H_2} r_{10}$
CH_4	$\sum \left(\upsilon_{ij} r_i\right) V = V^*_{CH_4}\, r_{p,CH_4} - M_{CH_4}\, r_9\, V + \upsilon_{CH_4} r_{10}$
H_2O	$\sum \left(\upsilon_{ij} r_i\right) V = V^*_{H_2O}\, r_{p,H_2O} - M_{H_2O}\, r_8\, V - M_{H_2O}\, r_9\, V$
Char (S)	$R_S = \left(w_0 - w_\infty\right) r_{dev} + \left(w_0 * F.C.\right) r_1$
	$w_{char} = w_0 * F.C.$

where, F.C. is the fixed carbon in the coal sample, as presented in Table 6.1. It should be noted that the expressions of r_i are as indicated in Table 6.2.

6.2.6 Results and discussion

In this section, the obtained results from the various experiments, mentioned in the experimental strategy section, will be discussed.

6.2.6.1 Coal pyrolysis

Coal pyrolysis was carried out in a fluidized bed TGA as shown in Figure 6.2. The experimental conditions are mentioned in the experimental strategy section. The total measured gas and the total yield, obtained from the fluidized bed TGA, are in good agreement.

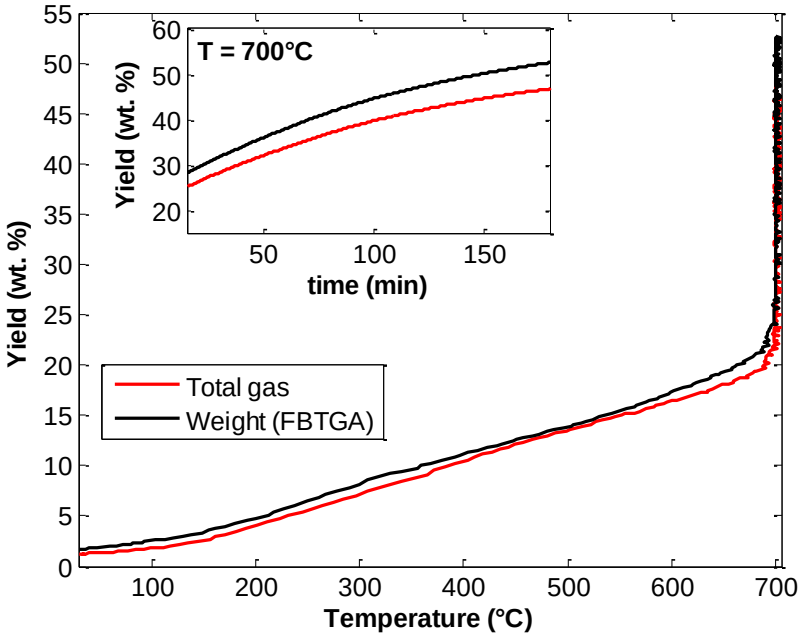

Figure 6.2 Weight loss of coal pyrolysis from fluidized bed TGA

Kinetic parameters for coal pyrolysis, found in the fluidized bed TGA, are listed in Table 6.5 and Table 6.6. The parameters were obtained by applying the technique of minimizing the square errors on the experimental and modeling results. As explained in details by one member of our reaserch group [92], the equation of the n_i-order reaction rate was implemented in Matlab program codes. In order to decrease the correlation between

the pre-exponential factor and the energy activation, the Arrhenius equation was written as $k = k_0{}^* exp\left(-\frac{E}{R}\left(\frac{1}{T}-\frac{1}{\bar{T}}\right)\right)$, where $\bar{T}$ is the average temperature over the experimental temperature data range. The initial conditions for the matlab codes were obtained from the experimental data. The optimal values of the kinetic parameters were chosen amoung all the suitable ones. Indeed, the coefficents of the correlation matrix were less than 0.5, which confims that this correlation was low.

The experimental results, shown in Figure 6.9, suggest that there are two stages for coal pyrolysis in the fluidized bed TGA: (1) primary pyrolysis from up to 750°C and (2) tar cracking, from 575 to 750°C. The CO produced during the second stage comes from the primary pyrolysis as well as the tar cracking reactions. However, only a small amount of CO_2 could potentially come from tar cracking, during the second stage. The results are in agreement with the ones reported in Table 6.3, CO and CO_2 could represent 56% and 11% of the product of tar cracking (R10) respectively.

As indicated in Table 6.5, the obtained kinetic parameters for total devolatilization are in the same range with those found in literature for similar coal [17]. For the individual gases, the obtained activation energies range from 2.7 to 34.1 kcal/mol. The results are significantly lower than those listed in Table 6.6 found in the literature[18]. The same conclusions were drawn from previous kinetic studies in a micro-fluidized bed analyzer for biomass pyrolysis: lower energy activations with lower pre-exponential factors [93].

Moreover, the ratio V'/VM, where V' represents the experimental volatile matter yield, excluding tar and hydrocarbons other than methane, and VM stands for the proximate volatile matter content, is about 0.90. This value is in agreement with previous works that were obtained from fluidized reactor experiments[85].

In sum, the results confirm that the newly developed fluidized bed TGA is an impressive equipment for analyzing gas-solid reactions, including pyrolysis.

Table 6.5 Kinetic parameters for coal devolatilization

Coal	Volatile matter	$\log(k_{o,i}/s)$	E_i, (kcal/mol)	Std Deviation	Reference
Lignite Coal	52.6	-2.5	2.7	1.4 %	This work
Various coals	39.5 to 51.0	-2.7 to 12.6	0.7 to 32.5	-	[17]

Table 6.6 Kinetic parameters of coal pyrolysis in fluidized bed TGA

Product	Stage	$\log(k_{o,i}/s)$	E_i,kcal/mol	V_i^*, wt. %	Std Deviation
Weight loss	1	-2.5	2.7	52.6	1.4
CO	1[a]	-3.06	7.34	18.4	2.5
	2[b]	-4.9	4.8		4.9
CO_2	1	-5.4	1.4	15.6	0.3
CH_4	1	2.6	13.2	2.4	0.8
H_2O	1[c]	-8.1	0.2	9.5	0.4
	2[d]	-7.8	1.0		0.3
H_2	1	0.9	22.3	2.2	0.5
Tar and MHC*	-	-	-	4.6	
TOTAL				48.0	
a: up to 700°C; b: 560°C - 700°C; c: up to 700°C; d: 330 -700°C					
MHC*: Minor hydrocarbons					
One stage: up to 700°C					

Table 6.7 Kinetic parameters for lignite pyrolysis [11]

Product	Stage	log (ko,i (s-1))	Ei, kcal/mol	Vi* %
CO	1	12.26	44.4	1.77
	2	12.42	59.5	5.35
	3	9.77	58.4	2.26
CO_2	1	11.33	36.2	5.70
	2	13.71	64.3	2.70
	3	6.74	42.0	1.09
CH_4	1	14.21	51.6	0.34
	2	14.67	69.4	0.92
H_2O	1	13.90	51.4	16.5
H_2	1	18.20	88.8	0.50
Total				44.0

6.2.6.2 Char gasification

The obtained char from coal pyrolysis was gasified in the fluidized bed TGA under the experimental conditions shown in the experimental strategy section. The results are illustrated in Figure 6.3**Erreur ! Source du renvoi introuvable.**. It can be seen that there is generally good agreement between the total yield, obtained from the fluidized bed TGA, and the total gas product.

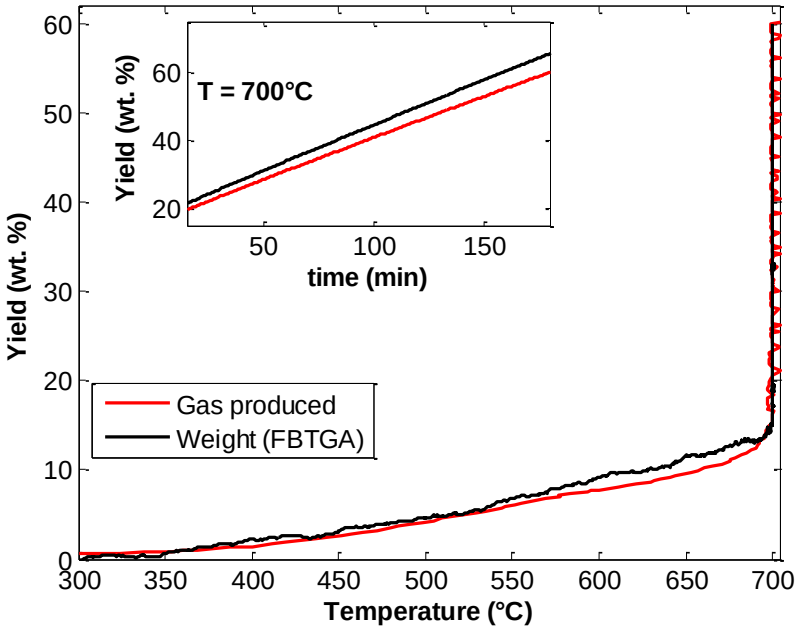

Figure 6.3 Char gasification in fluidized bed TGA: weight vs. total gas

Furthermore, the kinetics of char gasification (R1) was studied in the fluidized bed TGA. The obtained kinetic parameters are shown in Table 6.8. The obtained activation energy is in agreement with the one reported in the literature. However, the found pre-exponential factor is considerably lower than the one obtained from a similar coal in the literature. The results are however in agreement with those studied in a micro-fluidized bed analyzer, suggesting lower activation energy values with lower pre-exponential factors [93, 94].

Table 6.8 Kinetics of char gasification from fluidized bed TGA

Product	log(ko,i/s)	Ei, kcal/mol	Vi*, wt. % (as-received)	N	Std Deviation	Reference
Char	-1.84	3.15	34.30	2/3	0.26	This work
Char	11.24	3.25	-	2/3	-	[19, 20]

6.2.6.3 **Coal gasification in fluidized bed TGA**

Gasification of the western Canadian lignite coal was carried out in fluidized bed TGA. The proximate and elemental analyses of the studied coal are shown in Table 6.1. The experimental conditions are illustrated in the experimental strategy section.

Gasification of coal (carbon) can be carried out in four ways that are illustrated by reactions R1 to R4. Reactions R2 and R3 are important for the water gas and CO_2/O_2 mixture gasification processes, respectively, while reaction R4 plays a predominant role in the hydrogenating gasification process.

However, as shown in Figure 6.4, only reaction R1 can be taken into account in the studied experimental data range.

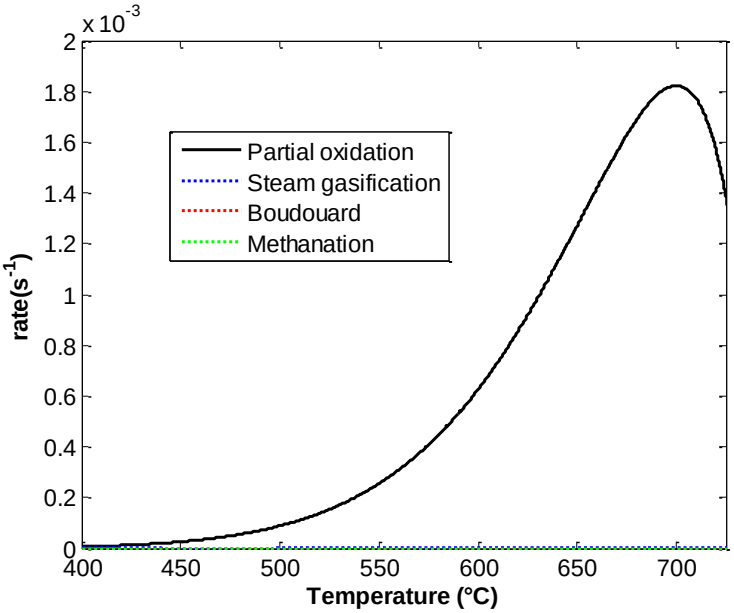

Figure 6.4 Comparison of gas-solid reaction rates

Figure 6.5 demonstrates a comparison of the homogenous reaction rates. For the homogeneous reactions, only methane reforming and water shift reactions can be taken into account in the experimental data range. Indeed, the reactions R5 to R6 are considered to be instantons in the experimental data range. Furthermore and as shown in Figure 6.5, the methane reforming reaction rate can be neglected in comparison with the water shift one, in the experimental data range.

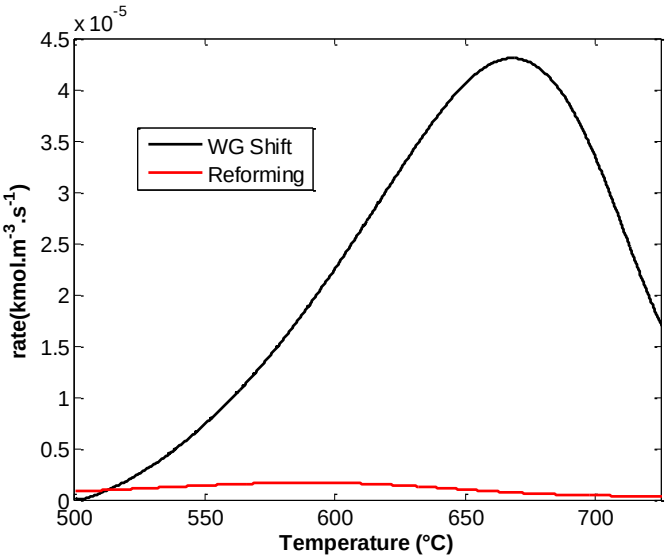

Figure 6.5 Comparison of reforming and water gas shift reaction rates

For CO shift reaction (R8), two different reaction rates were found in the literature. As shown in Table 6.2, the activation energies were different: 53 vs. 162.6 kJ/mol. The first value (53 kJ/mol) was not considered in this article since it is too low. The value of the activation energy, for the CO shift reaction, found in this work was 101.8 kJ/mol.

The CO shift reaction (R8) is more predominant than the methane reforming (R9) one in the studied experimental data range. In light of this, the model describing the coal gasification of the fluidized bed TGA is substantially simplified such that the gases were to be produced from pyrolysis, char partial oxidation (R1), CO shift (R8), methane reforming (R9), and tar cracking reactions.

The experimentally obtained weight loss and the total gas product yield are presented in Figure 6.6.

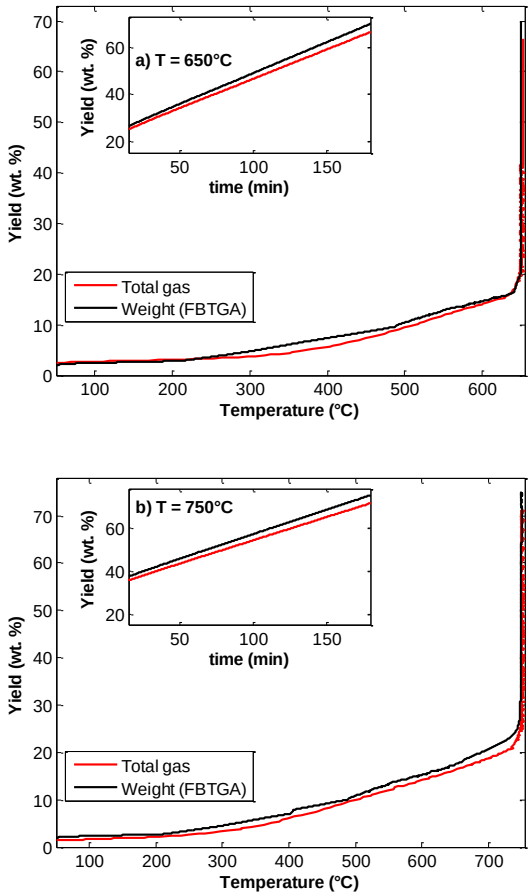

Figure 6.6 Coal gasification in fluidized bed TGA: weight loss vs. total gas

a) 650°C and b) 750°C

The obtained results from the fluidized bed TGA are in good agreement with those representing the total gas produced. The difference shown in Figure 6.6 could be attributed to the amount of tar produced from coal gasification. It should be noted that a total amount of 4.6% from the initial weight of the coal sample could potentially be considered as unconverted tar product.

Modeling the solid conversion in the fluidized bed TGA is shown in Figure 6.7.

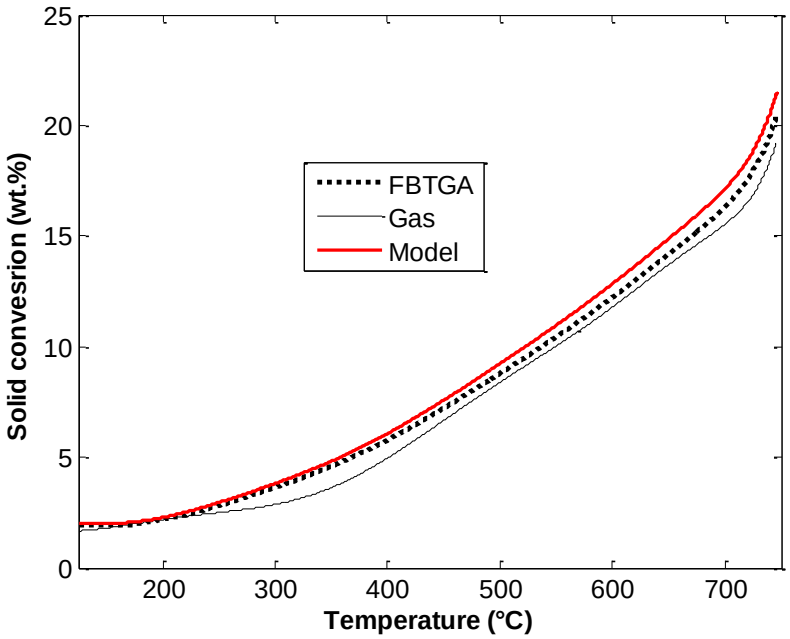

Figure 6.7 Solid conversion in fluidized bed TGA: (-) model and (.) experiments

The experimental conditions were explained in the experimental strategy section. The model for the solid conversion encompasses the total devolatilization and char gasification reactions. The kinetic parameters obtained previously for total devolatilization and char gasification reactions are used in the model. The results are generally in good agreement. The difference shown between the model and the experimental results can be attributed to the amount of tar condensed on the outlet part of the reactor. This minor amount of solid was inversely accounted for the weight loss measured by the fluidized bed TGA.

6.2.6.4 Comparison of experiments and model results

The experimental conditions for this section are detailed in the experimental strategy section. The comparison of the model and the experiments results is carried out in two parts: (1) the first stage from 25 up to 750°C and (2) the second stage, where the temperature was fixed at 750°C for 3 hours.

For the first stage, the experimentally observed effect of temperature on the mass yields and composition of the major components of the gas product is shown in Figure 6.8 and Figure 6.9. The solid and marked lines, in each figure, represent the results obtained from the model and the experiments respectively.

As can be seen from Figure 6.8, the simulated and experimental results are in reasonably good agreement in the range of temperature presented.

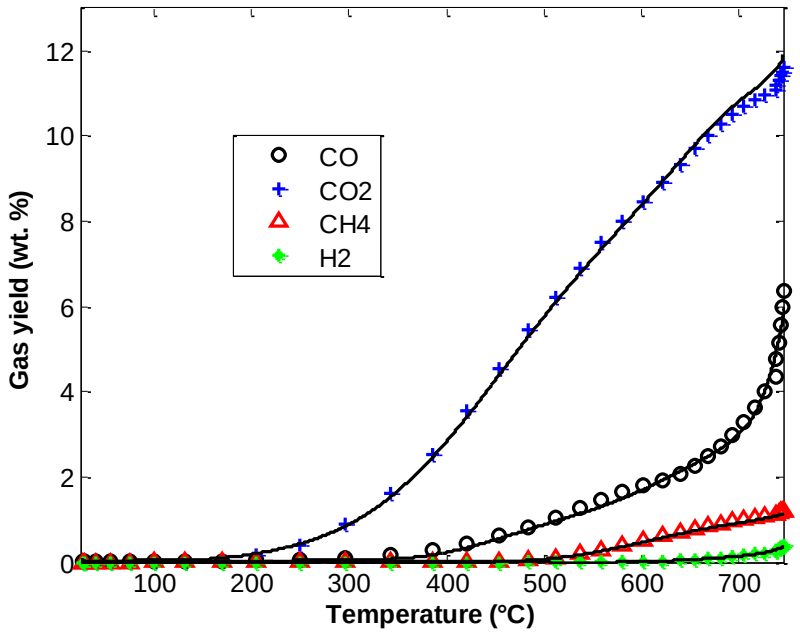

Figure 6.8 Model (o) vs. experiments (-): Temperature effect on individual gas product yields

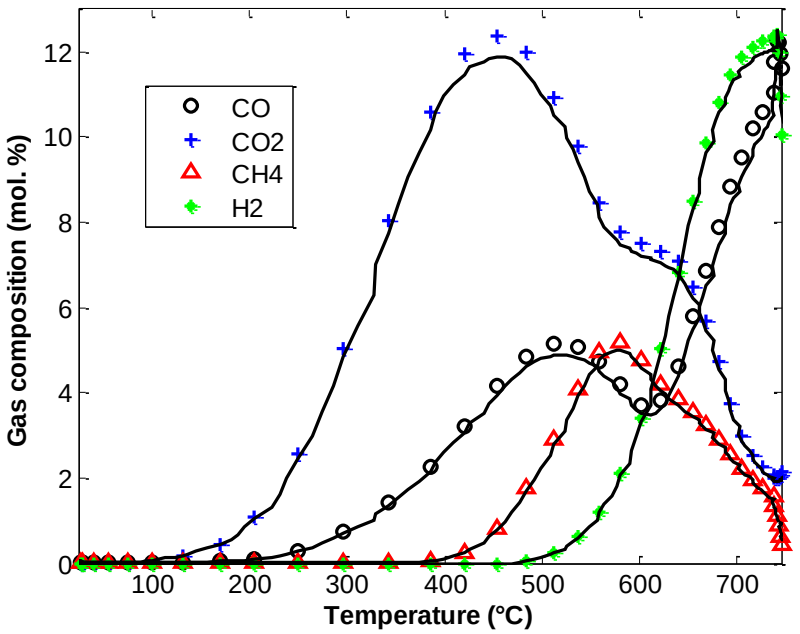

Figure 6.9 Model (o) vs. experiments (-): Temperature effect on individual gas product compositions

As explained previously in the pyrolysis section, the evolution of the CO concentration of suggest that there are two stages: (1) primary pyrolysis from up to 750°C and (2) tar cracking, from 560 to 750°C. During the first stage, the CO produced comes only from the primary pyrolysis. Nevertheless, an additional amount of CO was produced from tar cracking reactions during the second stage. However, the results are different for CO_2: only a small amount of CO_2 could potentially come from tar cracking, during the second stage. As reported in Table 6.3, the carbon monoxide is the major product (56%) that can be produced from the tar cracking reaction. The results are in agreement with the explanation derived from the experimental data in Figure 6.9. Tar cracking, CO shift and

steam methane reforming reactions continue taking place in the freeboard region. This is not considered in the present model.

Furthermore, starting at 485°C, the concentration of H_2 was to be increased as the temperature increased to reach 12.5% at 750°C. Carbon monoxide started to be released at 200°C, then increased as the temperature rose to reach 5.1% at 512°C, after which it decreased to 3.7% at 602°C and then increased to 12% at 750°C. Carbon dioxide increased to 12.4% at 700°C and then decreased to 2% at 750°C. Methane increased as the temperature increased, starting at 410°C to 5.2% at 580°C, then decreased considerably to 0.5% at 750°C.

For the second stage, the transient gas product yields are presented in Figure 6.10. The dotted and solid lines represent the experiments and model results respectively. The modeled and experimentally obtained results are in agreement and confirm the reliability of the fluidized bed TGA as standard equipment for studying the kinetics of coal gasification.

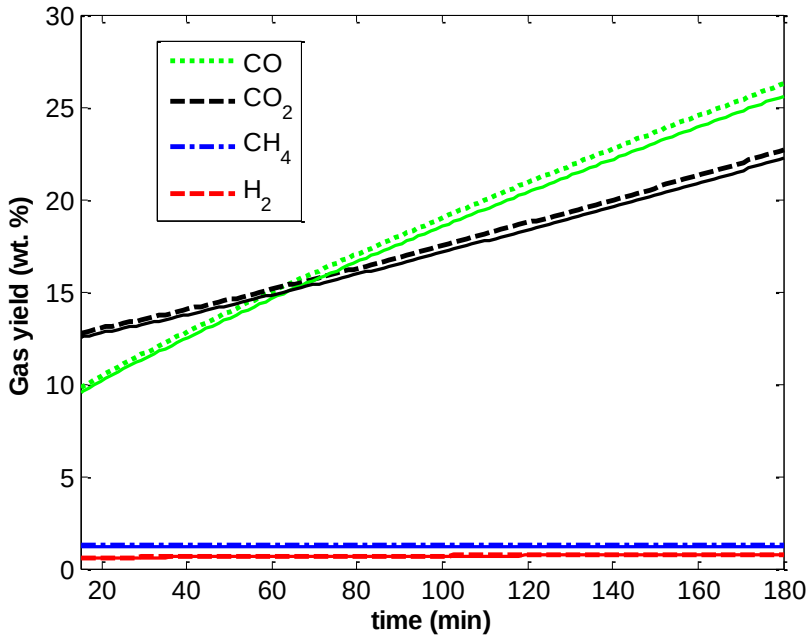

Figure 6.10 Transient product gas yields at 750°C

6.2.7 Equilibrium

It is worthwhile comparing the final product distributions with those that could be obtained if all the generated gas were in mutual equilibrium at the final stage of gasification. Equilibrium relations for reactions R8 and R9 are considered and represented in Figure 6.11.

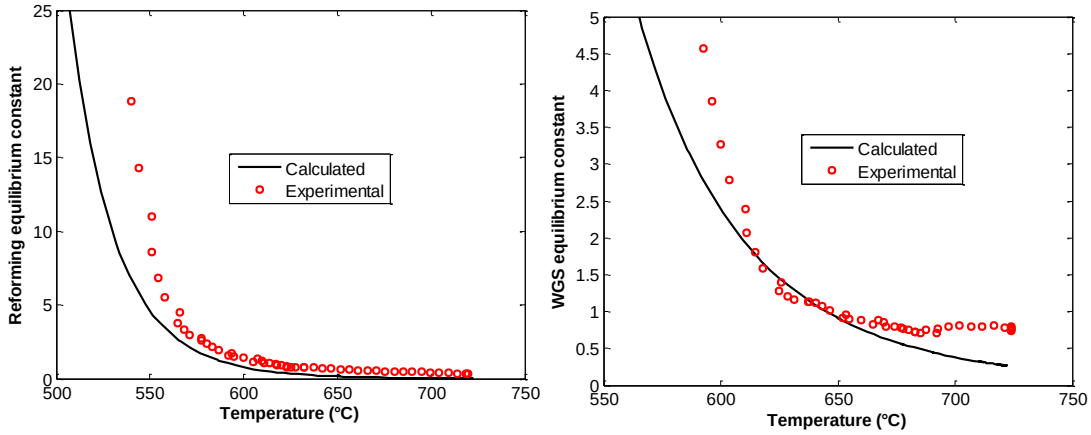

Figure 6.11 Comparison of gas composition and equilibrium values: (-) curves equilibrium and (o) experiments

Generally, the experimental results show more agreement with equilibrium data as the temperature increases. The equilibrium data for the reforming and water gas shift reactions are lower than the experimental results. Incomplete tar cracking in the fluidized bed TGA should explain the observed deviation [51, 86, 95, 96]. Such deviations from equilibrium have been reported for several types of gasifiers [51, 86, 95, 96]. The deviation shown for the water gas shift reaction can be attributed to the amount of CO that came from tar cracking reaction.

6.2.8 Conclusion

Coal gasification was investigated in the fluidized bed TGA. The results obtained from the weight loss were in reasonable agreement with those found from the total gas product. The kinetics of coal pyrolysis was developed from the fluidized bed TGA. The activation energies for individual gas pyrolysis were ranged from 7 to 14 kcal/mol for CO, 1.4 for CO_2, 13 for CH_4, and 9 for H_2 kcal/mol. The values found in the literature, for a similar coal, ranged from 44 to 60 kcal/mol for CO, 36-64 for CO_2, 52-69 for CH_4, and 89 kcal/mol for H_2. The kinetics of char gasification was determined. The activation energy was 3.15 kcal/mol, while the one reported in the literature was 3.25 kcal/mol for similar coal. A model for the micro fluidized bed TGA was proposed. The modeled and experimentally observed results were generally in good agreement, which confirms the reliability of the fluidized bed TGA. The equilibrium data for the water gas shift and the methane reforming reactions are lower than the experimental results.

6.2.9 Acknowledgements

The authors would like to thank Carbon Management Canada (CMC-NCE) for their financial support. They are also grateful to Dr. Rouzbeh Jafari, Dr. Moahammad Latifi, Dr. Milad Aghabaranejad, Dr. Abdelmajid Rakib, Dr. Sherif Farag, and Mr. Carlos Manuel Gil Castagnola for their valuable assistance.

6.2.10 NOTATION

B	Weight of the inert solid in the fluidized bed TGA (kg)
C_s	Concentration of the reactant solid in the fluidized bed TGA (kg solid/kg inert solid)
u_g	Superficial Gas velocity (m/s);
E	Activation energy (kJ/mol);
k_0	Pre-exponential factor (s-1);
R	Gas constant ($j.mol^{-1}.K^{-1}$);
T	Temperature (K);
M_i	Molecular weight of component i (kg/kmol);
r_j	Rate of reaction j ($kmol.m^3.s^{-1}$);
r^*_j	Rate of reaction j ($kg.m^3.s^{-1}$);
X	Conversion of char;
y_i	Fraction of component i in the gas;
z	Height of the bed (m);
V	Total Volatile yield (wt. %);
S	Yield of char (wt. %);
Q	Total gas flow rate (ST l/min);
WGS	Water Gas Shift

Subscripts

i	Indices specifying species (1=CO; 2=CO_2; 3=H_2; 4=H_2O; 5=CH_4)
j	Indices indicating the reactions

6.2.11 LIST OF FIGURES

CHAPITRE 7 ARTICLE 3: CATALYTIC ASH FREE COAL GASIFICATION IN A FLUIDIZED BED THERMOGRAVIMETRIC ANALYZER

7.1 Présentation de l'article

Ce chapitre reprend l'article intitulé **'catalytic ash free coal gasification in a fluidized bed thermogravimetric analyzer'**. Cet article a été soumis à la revue Fuel Journal.

Dans le présent article, une revue de littérature a été présentée, incluant les principales techniques pour le prétraitement du charbon afin d'en éliminer les cendres. Ensuite, un résumé des différents catalyseurs utilisés dans la gazéification du charbon, avec leurs effets sur les énergies d'activation des principales réactions a été arboré. Une description de la méthodologie expérimentale incluant le catalyseur, la technique de préparation du charbon sans cendre ainsi que son analyse élémentaire, le catalyseur utilisé (K_2TiO_3), et un rappel du montage expérimental ont été réalisées. Un résumé des principales réactions, qui pourraient avoir un effet sur l'analyse des résultats expérimentaux, dans les conditions expérimentales de cet article, ainsi que leurs cinétiques, ont été listées. Une discussion détaillée des résultats expérimentaux a été effectuée. Les différents paramètres cinétiques obtenus, des principales réactions considérées dans cet article, ainsi que ceux des principaux gaz produits de la pyrolyse du charbon ont été présentés. L'effet catalytique sur la conversion du charbon ainsi que la valeur énergétique des gaz produits a été étudié. En fin, une conclusion rappelant les principaux résultats du présent article a été présentée.

7.2 Catalytic ash free coal gasification in a fluidized bed thermogravimetric analyzer

Said Samih and Jamal Chaouki

(Soumis à Fuel Journal, manuscript number: JFUE-D-16-01225)

7.2.1 Abstract

Catalytic ash free coal gasification was investigated in the newly developed fluidized bed thermogravimetric analyzer. The total yield obtained from the fluidized bed TGA showed good agreement with the total gas product. For char gasification, the values of activation energy and pre-exponential factor were similar to those obtained from coal gasification in our previous work. The activation energy for the CO shift reaction decreased by 45% and 19% from the value reported in our previous work for coal gasification and in literature for catalytic coal gasification respectively. For the methane reforming reaction, the value of the activation energy was reduced by 40% from the one observed previously in our work, in the absence of a catalyst and decreased by 19% from the one reported in literature for catalytic gasification. The carbon conversion for the catalytic ash free coal gasification was 69% higher than the value obtained from the coal gasification for the same experimental conditions. This value was found to be 44.5% for the ash free coal gasification. The heating value of the gas product by using the catalyst for temperatures below 520°C was also higher than without catalyst. However, at higher temperature, using the catalyst had no effect on the heating value of the gas product.

7.2.2 Introduction

In recent years the impact of human activity on the climate has dramatically increased reaching its highest point in history. The temperature of the ocean and atmosphere has risen, leading to a decrease in snowfall and arctic ice levels and to rising sea levels. In September 2015, a record-setting number of temperature anomalies at the surface of the

earth was recorded [3]. Over the entire land and ocean surface, the combined average temperature was the highest in the 136-years of recordings, at 0.9°C above the 20th Century average of 15.0°C[3]. This value is increasing by 0.06 °C per decade. In Canada, temperatures were above average by up to 5°C across the province of Ontario. About 2.1°C above the 20th Century average was observed in the United States. September 2015 was, however, the coldest in Spain and the United Kingdom, at 0.8°C below the 1981-2010 national average [3].

The leading cause of the observed climatic change is the anthropogenic green house gas (GHG) emissions. Driven largely by economic and population growth, total anthropogenic green house gases (GHG) have continued to increase dramatically. About 78% of GHG emissions are due to the fossil fuel combustion and industriel processes [2, 3]. Coal accounted for the largest source of anthropogenic CO2 emissions, at about 44% [8].

The international challenge for today is to separate economic growth and social development from increasing anthropogenic green house gases (GHG) [5]. To reduce green house gas emissions and enhance resilience to climate change, innovation and investments in environmentally sound technologies are required [2]. The Canadian energy strategy focused on accelerating the development and deployment of energy research and technologies that enhance the use of clean and conventional energy sources [10]. Strategies are developped and implemented to meet the current and future needs of the energy sector human resource needs currenlty and the future [10].

Although renewable energy production will grow, fossil fuels are expected to continue playing a predominate role in the energy sector [56, 97]. Coal plants are still making a major contribution to the world energy portfolio and are projected to maintain their lead in the future [56, 97, 98]. In 2007, there were 420 operating gasifiers worldwide, of which 55% used coal as feed and 32% petroleum residue. With a gasification capacity of 30,825 MWth of syngas, there were 212 operating coal gasifiers. China accounts for the majority of coal gasification plants built in recent years [7].

There are however various problems associated with the use of coal gasification: low efficiency, the presence of tar and high capital and operating costs. The use of catalysts can significantly reduce the operating temperature of the coal gasifier. Neverthless, the presence of ash in coal decreases the power efficiency and also constitutes a major air pollutant [99]. Catalysts also become deactivated by ash, especially potassium, as these components react with alumina and silica from coal to form stable potassium or calcium-alumino silicates [97, 100, 101]. Another interesting new application of ash free coal is the direct carbon fuel cell (DCFC) that produces electricity using solid carbon [98, 102]. The use of ash free coal in DCFC significantly enhances the mass transport after the cell reactions[98, 102].

To characterize the kinetics and mechanism of catalytic gas-solid reactions, an innovative fluidized bed thermogravimetirc analzyer was recently developped [11]. In the present paper, gasification of coal and ash free coal are investigated in the newly developped fluidized bed TGA. The effect of the catalytic on ash free coal gasification is also studied. The experimental results are compared and discussed to derive interesting conclusions.

7.2.3 Coal beneficiation

In a low-grade coal gasification process, the formation of deposits is one of the major problems caused by ash. As a result, gas flow and heat transfer could be considerably prevented, greatly obstructing the operation of the process [103]. Different sintering phenomena can be considered as the origin of the forming deposits. When the particle size is reduced, the rate of sintering increases, whereas it decreases when the temperature rises. Reducing sulfur becomes imperative in order to obtain an environmentally acceptable sulfur oxide (SOx) emission, especially in the case of high sulfur content in raw coal [103-106]. Coal beneficiation should be considered as one inseparable part when discussing low-grade coal gasification.

Coal beneficiation, or cleaning, designs the various operations performed on the run-of-mine (ROM) coal to prepare it for specific end uses. It includes all technologies that reduce the sulfur and ash content of coals, without destroying its physical character.

Coal cleaning processes can be classified into physical or mechanical, chemical, and microbiological [104-106].

7.2.3.1 Processes of physcial coal benificiation

Physical beneficiation processes rely on the use of gravitational, centrifugal, and/or electrostatic forces to separate clean coal from the accompanying impurities [104-107]. Froth flotation also can be used for the beneficiation of a very fine size coal fraction (28 mesh) [104]. Table 7.1 gives a brief review of the physical coal beneficiation processes [104-106].

Table 7.1 Physical coal beneficiation processes [68-70]

Process name	Typical operating conditions			Impurities reduction (%)		
	T (K)	Pressure	Particle size	Pyritic Sulfur	Ash	Clean coal
Magnex process	338	Ambient	14	85	67	85
High gradient magnetic separation process	Ambient	Ambient	60-10	87	87	80
Microwave coal cleaning process	392-572	Ambient	30-100	40-50	-	-

7.2.3.2 Chemical coal beneficiation process

For the chemical (or microbiological) beneficiation processes, ROM coal is subjected to chemical (or microbiological) action to achieve this separation. The chemical reagents used, which generally include chlorinated solvents (methylene chloride1, 1,1-trichloroethylene, and perchlorethylene), affect only the sulfur and ash impurities present within the coal, and not the coal matrix [104-106, 108]. Table 7.2 summarizes these kinds of beneficiation processes [104-106].

Table 7.2 Chemical coal beneficiation processes [68-70]

Process name	Typical operating conditions			Chemical reagent	Impurities reduction (%)		
	T (K)	Pressure (psig)	Particle size (mesh)		Pyritic Sulfur	Ash	Clean coal
TRW-Meyers coal desulfurization	194-266	Up to 120	14	Ferric sulfate	up to 95	10-30	82-92
Battelle Hydrothermal process	430-650	350-2500	200	Sodium Hydroxide	90-98	-	97-100
PERC oxidative desulfuration	300-430	220-1500	200	Sulfuric acid	95	-	90
Low temperature chlorinolysis	165	15	200	Chlorine	up to 90	-	98

7.2.3.3 Performances of different coal beneficiation processes

Table 7.3 summarizes different information regarding coal beneficiation processes evaluated for grassroots facilities[105, 106, 109]. The economic analyses were performed, using the discounted cash-flow method, for a coal beneficiation plant designed to produce 15,000 tons/day, in which the cost of the ROM coal was $20/ton [105, 106, 109].

Table 7.3 Performances of different coal beneficiation processes [105, 106, 109].

Process description	% reduced		% recovered		Beneficiation cost	
	Sulfur	Ash	material	thermal	$/ton	$/MMBtu
Wet beneficiation	26.6	46.6	26.6	46.6	26.6	46.6
Deep cleaning	43.3	72.8	43.3	72.8	43.3	72.8
Battelle hydrothermal	79.3	-	79.3	-	79.3	-
TRW-Meyers fine coal	78.6	30.0	78.6	30.0	78.6	30.0

7.2.4 Catalytic gasification

Obtaining high process efficiency is possible theoretically and thermodynamically with low rank coal. Achieving it is a question of manipulating process configurations, using the best solid-gas contacting systems and catalysts.

The catalysts used to achieve these objectives can be classified into three categories: alkali metals, earth-alkaline metals, and transition metals. This includes metals, metal oxides, metal halides, alkali carbonates, and iron carbonyls, with a special emphasis on K_2CO_3, Na_2CO_3, KCl, NaCl and CaO.

The catalysts can affect the gasification rate by the following:

- Increasing the active site concentration;
- Lowering energy barriers of different steps;

- ❖ Providing an alternative route for gasification.

However, the following points should be taken into consideration:

- ✓ Increasing the gasification temperature decreases the relative catalytic effects;
- ✓ Operating the steam environment makes catalysts more effective than hydrogen alone;
- ✓ The catalyst concentration affects it reactivity, thus an optimum concentration must be found;
- ✓ The physical catalyst mixing with the carbon is less effective than its impregnation;
- ✓ The reaction conditions can affect the reactivity of different catalysts.

It is important to specify that two major aspects must be distinguished in evaluating the effect of catalysts: the carbon conversion and the thermal efficiency of a gasifier. Thermal efficiency decreases when increasing the carbon conversion in a catalyzed medium. In more concrete terms, the geater the catalyst reactivity is, the more negative the impact on thermal activity is (KCl, K_2CO_3, NaCl, $LiCO_3$, Fe_3O_4, Pb_3O_4, MgO and Ni [105, 106, 110, 111].

Finally, the use of a mixture of catalysts can be the best way for different reactions involved in coal gasification.

The desired loading for K_2CO_3 is 5 to 20 wt.%. Below 5%, the catalyst can be lost as a result of an irreversible reaction with the Al_2CO_3 and SiO_2 of the char ash, producing $K_2O.Al_2O_3.xSiO_2$ and $Na_2O.Al_2O_3.xSiO_2$ compounds. Above 20%, there is a saturation effect due to the catalyst blocking the pores in the carbon, therefore restricting the access of gas to the micropores' surface [105, 106, 112].

The effect of the catalysts, K_2CO_3 and Na_2CO_3, on CO_2 coal gasification is illustrated in Table 7.4.

Table 7.4 Effect of catalysts on kinetic parameters: K_2CO_3 vs. Na_2CO_3 [35]

Catalyst	Activation energy ($kJ.mol^{-1}$)	Pre-exponential factor (min^{-1})
None	122.0	1480
K_2CO_3	75.3	18.4
Na_2CO_3	80.3	75.1

Table 7.5 represents the effect of different catalysts on water gas shift reaction [36-40].

Table 7.5 Effect of catalysts on water shift reaction [36-40]

Catalyst	Activation energy ($kJ.mol^{-1}$)	Reference
Fe_2O_3/ZrO_2	105-111	[36]
Gold/ferrochrome	88.2	[37]
$13.5Ni{-}2K/10CeO_2{-}Al_2O_3$	155	[38]
Pt@SiO2	70	[39]
Li/MgO	158	[40]
K_2TiO_3	44.3	This work
None	101.9	Our previous work
None	162.6	[19, 86]

Table 7.6 illustrates the effect of the various catalysts on the methane reforming reaction [41-47].

Table 7.6 Effect of catalysts on methane reforming [41-47]

Catalyst	Activation energy ($kJ.mol^{-1}$)	Reference
K-based	113-124	[41-44]
Ni/y-Al2O3	133.9	[43]
Rh/Al_2O_3	111	[44]
Platinum	114	[47]
$Ce_{0.9}Gd_{0.1}O_{2-x}$ (CGO)	153	[45]
Ni/Mg/K/Al2O3	93	[46]
Ni/La/Al2O3	85.2	[42]
Ni/La-Co/Al2O3	99.4	[42]
K_2TiO_3	71.9	This work
None	108	Our previous work
None	124.7	[19, 86]

7.2.5 Experimental

7.2.5.1 Preparation of ash free coal

Ash free coal was produced by and obtained from the Department of Chemical and Materials Engineering, University of Alberta, Canada. Solvent extraction was the process used for ash free coal production [113, 114]. Dry pulverized coal and solvent were mixed (1/10 weight ratio), ball-milled, and vacuum dried at 80 °C for 12 hours. With continuous agitation and under nitrogen (N_2) atmosphere, the mixture was then heated up to 400 °C. Hot filtration was used to separate the solid residue from the dissolved liquid phase. To precipitate the coal-derived organic components, hexane was added to the dissolved liquid phase (1/40 volume ratio). The precipitated ash free coal was obtained after filtration and drying [113, 114].

7.2.5.2 Feed Material

Western Canadian lignite coal (WLC) was used as the solid fuel for the experiments reported in this paper. The proximate and ultimate analyses of the coal are presented in Table 7.7. More information on the bed material is given in the apparatus description and procedure sections.

Table 7.7 Analysis of the Western Canadian lignite coal

	Canadian lignite coal	Ash free coal
Proximate analysis (wt. % a.r.)		
Fixed Carbon	34.3	46.7
Volatile matter	39.3	53.2
Ash	15.4	Trace
Moisture	11.1	Trace
Ultimate analysis (wt. %)		
C	57.2	88.9
H	4.3	5.1
N	1.20	1.5
O	21.1	24.9
S	0.1	0.0

a.r. as received

The mass balance was carried out in the coal, ash free coal, and residue [113]. The results suggest that only 47.4% of the raw material was recovered, and the ash was reduced by 47.4%. The conclusion is that the preparation technique for ash free coal is not suitable for the process. More focus on the beneficiation techniques should be taken into account in the future. As presented previously, other methods could be used to recover up to 90% of the material and reduce up to 76% of the ash.

7.2.5.3 Catalyst

A commercial catalyst (K_2TiO_3) was used for the experiment reported in this article. The catalyst K_2TiO_3 was tested at 800 °C in a quartz reactor in the fluidized bed TGA. Twenty grams of the commercial catalyst was fluidized and heated up to 800 °C in air atmosphere for 5 hours. The results, obtained from the weight loss measurement and gas analysis,

showed that the commercial catalyst was stable under these conditions. The K/C weight ratio was 10 % in all of the experiments reported in this paper.

7.2.6 Apparatus description and procedures

The experimental apparatus that was used for all the experiments reported in this paper is presented in our previous paper [11].

For all the experiments reported in the present article, 40 g of olivine sand, > 180 μm and < 212 μm in size, was mixed and fluidized with 5 g of lignite coal and ash free coals > 500 μm and < 600 μm in size. The experiments for coal gasification were carried out in a gas mixture of 5% oxygen-balance nitrogen (N_2), while those for ash free coal gasification were tested in a gas mixture, of 3% oxygen-balance nitrogen. The particle density for the sand was 3290 $kg.m^{-3}$. The heating rate was about 40°C/min. The gas flow rate changed depending on the temperature in order to keep the bed at the minimum fluidization regime according to the strategy developed for the fluidized bed TGA [11].

The exiting gases from the fluidized bed TGA were analyzed by means of a GC/FT-IR system. More details are provided in our previous work.

7.2.7 Ash free coal gasification

A comparison of the reaction rates of the heterogeneous reactions is shown in Figure 7.1. The obtained results suggest that only the R1 reaction can be taken into account in the studied experimental data range.

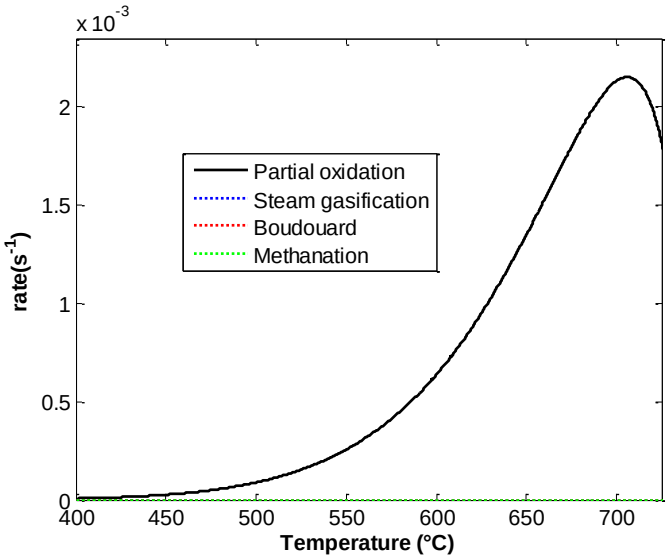

Figure 7.1 Comparison of gas-solid reaction rates

For the homogeneous reactions, only methane reforming and water shift reactions can be taken into account in the experimental data range. Indeed, the combustion reactions were considered to be instantaneous in the experimental data range. Figure 7.2 illustrates a comparison of the reaction rates of the homogenous reactions. Moreover and as shown in Figure 7.2, the CO shift reaction (R2) is more dominant than the methane reforming (R3) one in the studied experimental data range.

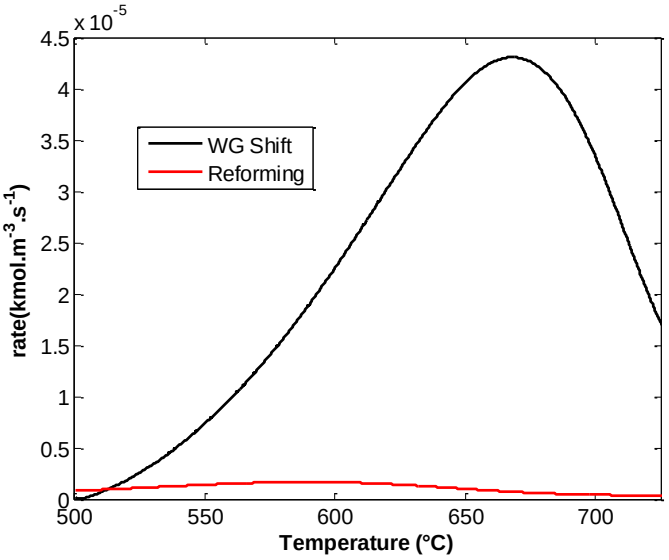

Figure 7.2 Comparison of reforming and water gas shift reaction rates

Consequently, Table 7.8 summarizes the list of the chemical reactions that are to be taken into consideration in the present study, in addition to the pyrolysis reactions.

Table 7.8 List of Heterogeneous and Homogeneous reactions

No	Chemical reaction	Kinetic	Reference
R1	$C+\alpha O_2 \rightarrow 2(1-\alpha)CO+(2\alpha-1)CO_2$	$r_1=\left(14.5\times10^{-3}\right)\cdot\exp\left(-\frac{13180}{T}\right)\cdot P_{O_2}\cdot\left(1-X_{1c}\right)^{2/3}$ $\frac{2(1-\alpha)}{2\alpha-1}=(2400)\cdot\exp\left(-\frac{6234}{T}\right)$	s^{-1} FBTGA
R2	$CO+H_2O\leftrightarrow H_2+CO_2$	$r_8=\left(2.89\times10^{2}\right)\cdot\exp\left(-\frac{162607}{RT}\right)\cdot\left([CO]\cdot[H_2O]-\left(\frac{[CO_2]\cdot[H_2]}{K*}\right)\right)$ $K*=12.64\cdot\exp\left(-\frac{196229}{RT}\right)$ $r_8=2.95\cdot\exp\left(-\frac{101847}{RT}\right)\cdot\left([CO]\cdot[H_2O]-\left(\frac{[CO_2]\cdot[H_2]}{K*}\right)\right)$ $K*=5.5\times10^{3}\cdot\exp\left(-\frac{9000}{T}\right)$	$kmol\cdot m^{-3}\cdot s^{-1}$ [19, 86] Our previous work
R3	$CH_4+H_2O\rightarrow3H_2+CO$	$r_9=\left(3\times10^{2}\right)\cdot\exp\left(-\frac{15000}{T}\right)\cdot[CH_4]\cdot[H_2O]$ $r_9=\left(8\times10^{3}\right)\cdot\exp\left(-\frac{13000}{T}\right)\cdot[CH_4]\cdot[H_2O]$	$kmol\cdot m^{-3}\cdot s^{-1}$ [19, 86] Our previous work
R4	Tar cracking $Tar\rightarrow\nu_{CO}CO+\nu_{CO_2}CO_2+\nu_{CH_4}CH_4+\nu_{H_2}H_2+\nu_{tar}tar_{inert}$	$r_{10}=\nu_i 10^{4.98}\exp\left(-\frac{93}{RT}\right)\cdot(\rho_{tar})$	$kg\cdot m^{-3}\cdot s^{-1}$ [29]

The molecular weight of tar, M_{HC}, is 90 kg/kmol, and ρ is the density of the tar (kg of tar/m^3 of gas), HC, in the gas stream. The stoichiometric coefficients for tar cracking reaction are reported in Table 7.9.

Table 7.9 Stoichiometric coefficients for tar cracking

Component	Coefficient
CO	0.56
CO2	0.11
CH4	0.09
H2	0.02
Secondary tar	0.22

7.2.8 Results and discussion

The experimental conditions for this section are detailed in the apparatus and procedures section. The comparison of the model and experiment results are carried out on two parts: (1) the first stage from 25 up to 750°C, and (2) the second stage, where the temperature was fixed at 750°C for two hours.

As explained in our previous work, the model of the continuous stirred-tank can realistically be used to describe the behavior of the reaction chamber on the fluidized bed TGA. The results of the modeling are presented in the following section.

7.2.8.1 Ash free coal gasification in a fluidized bed TGA

Ash free coal and catalytic ash free coal gasification were investigated in the fluidized bed TGA. A comparison of the experiment weight loss and total product gas yield is shown in Figure 7.3. The results are generally in good agreement. The difference reported in Figure 7.3 for ash free coal gasification is due to the amount of tar produced during the experiments.

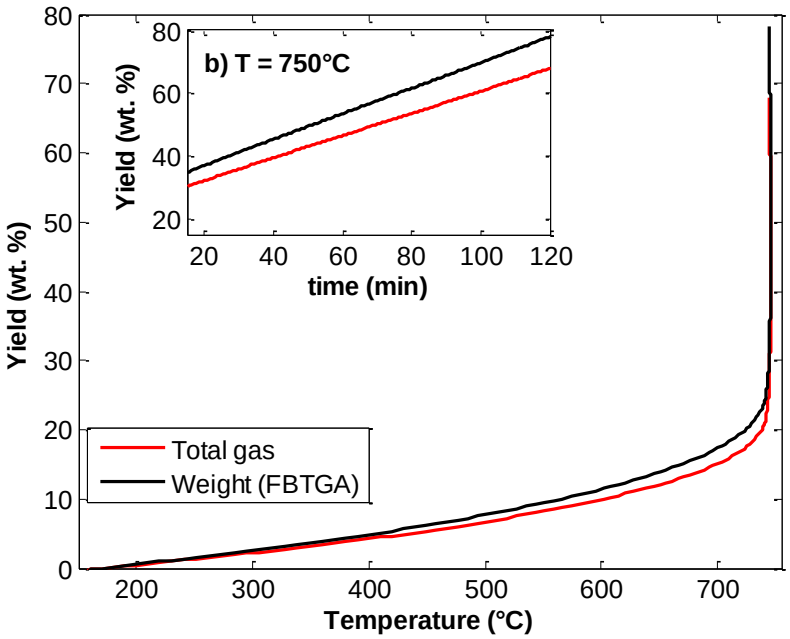

Figure 7.3 AFC gasification in a fluidized bed TGA: weight loss vs. total product gas

Figure 7.4 shows the effect of the catalyst on the ash free coal gasification in the fluidized bed TGA. The results indicate that the solid weight conversion was significantly enhanced when the catalyst was used in the experiments.

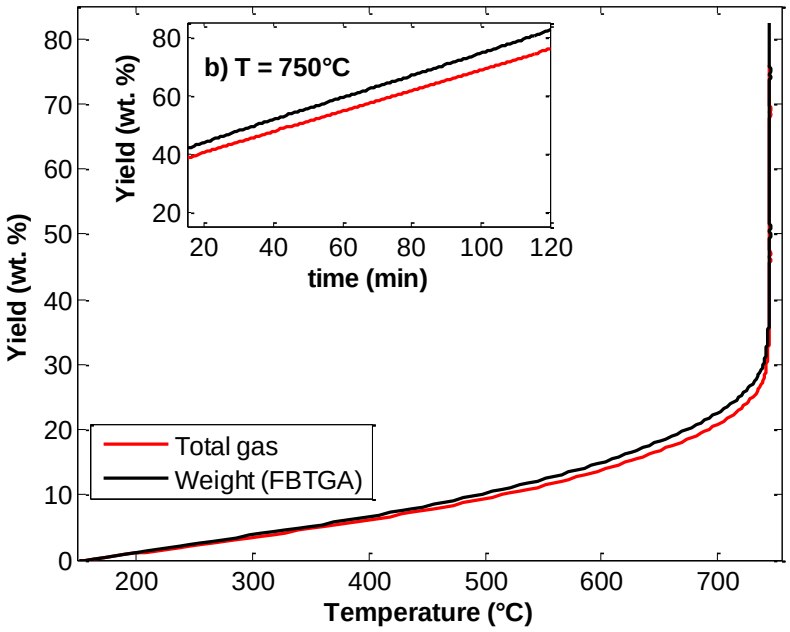

Figure 7.4 Catalytic ash free coal gasification in a fluidized bed TGA

7.2.8.2 Tar production

Tar production, or unconverted tar, was to be estimated from the following equation:

$$\boldsymbol{Tar\ production = 100 - total\ devolatilization - total\ gas\ produced} \quad (\mathbf{1})$$

Table 7.10 shows the effect of temperature on tar yield for coal, ash free coal (AFC) and AFC with the catalyst. The results suggest that more tar was produced during ash free coal gasification in comparison with the results obtained from coal gasification. Using the catalyst, however, tended to sharply reduce the amount of tar produced. In some, there is an important change in the yield of tar produced by using the catalyst in the ash free coal gasification.

Table 7.10 Temperature effect on tar yield: Coal, AFC and CatAFC

Temperature (°C)	**600**	**650**	**700**	**750**
Coal	1.6%	1.6 %	1.5%	1.4%
AFC	1.7%	2.0%	2.3%	2.3%
AFC with catalyst	1.3%	1.6%	1.6%	1.2%

AFC: ash free coal; CatAFC: ash free coal with catalyst

It should be indicated that all the experiments were repeated three times at least. The relative uncertainty was estimated to be 5%.

Table 7.11 summarizes the obtained kinetic parameters for ash free coal gasification in a fluidized bed TGA.

Table 7.11 Kinetic parameters from a fluidized bed TGA

No.	Chemical reaction	Kinetic	Reference
R1	$C+\alpha O_2 \rightarrow 2(1-\alpha)CO+(2\alpha-1)CO_2$	$r_1=\left(14.5\times10^{-3}\right)\cdot\exp\left(-\frac{13180}{T}\right)\cdot P_{O_2}\cdot\left(1-X_{1c}\right)^{2/3}$ $\frac{2(1-\alpha)}{2\alpha-1}=(2400)\cdot\exp\left(-\frac{6234}{T}\right)$ $r_1=\left(7.58\times10^{4}\right)\cdot\exp\left(-\frac{13592}{T}\right)\cdot P_{O_2}\cdot\left(1-X_{1c}\right)^{2/3}$ $\frac{2(1-\alpha)}{2\alpha-1}=(2400)\cdot\exp\left(-\frac{6234}{T}\right)$	s^{-1} This work [19, 20]
R2	$CO+H_2O\leftrightarrow H_2+CO_2$	$r_2=(2.55)\cdot\exp\left(-\frac{5323}{T}\right)\cdot\left([CO]\cdot[H_2O]-\left(\frac{[CO_2]\cdot[H_2]}{K*}\right)\right)$ $K*=5.5\times10^{3}\cdot\exp\left(-\frac{9000}{T}\right)$ $r_2=(2.95)\cdot\exp\left(-\frac{12250}{T}\right)\cdot\left([CO]\cdot[H_2O]-\left(\frac{[CO_2]\cdot[H_2]}{K*}\right)\right)$ $K*=5.5\times10^{3}\cdot\exp\left(-\frac{9000}{T}\right)$	$kmol\cdot m^{-3}\cdot s^{-1}$ This work Our previous work
R3	$CH_4+H_2O\rightarrow3H_2+CO$	$r_3=\left(1.5\times10^{2}\right)\cdot\exp\left(-\frac{8650}{T}\right)\cdot[CH_4]\cdot[H_2O]$ $r_3=\left(8\times10^{3}\right)\cdot\exp\left(-\frac{13000}{T}\right)\cdot[CH_4]\cdot[H_2O]$	$kmol\cdot m^{-3}\cdot s^{-1}$ This work Our previous work

The results for char gasification are similar to those reported in literature [19, 20]. However, the obtained activation energies for gas-water shift and methane reforming reactions, R2 and R3, are

56.5 and 77 kJ/mol, respectively. These values are significantly lower than those found in literature [36, 44]. The lowest activation energy for water-gas shift reaction is 70 kJ/mol [36, 44]. This value is 1.24 times higher than the one obtained in the fluidized bed TGA.

For the methane reforming reaction, the lowest activation energy found in literature is 85 kJ/mol. This is 10% higher than the one obtained from the fluidized bed TGA.

In general, the effect of the catalyst was to reduce the activation energies of the CO shift and the methane reforming reactions by 56% and 71%, respectively. These results are in general agreement with those reported in literature for the same catalyst applied in other reactions, especially CO_2 gasification. The activation energy was decreased by 43 to 75% in a previous work from the literature [35].

For the pre-exponential factors, the values obtained from the fluidized bed TGA are generally lower than those published previously. The results are in agreement with those found in a previous work using a micro-fluidized bed analyzer [93, 94]. This result can be attributed to the fact that the rate of collisions, which occur between the gaseous reactants and the well dispersed catalyst (K2TiO3), is extremely low because of the appropriate mixing in the fluidized bed TGA. It should be indicated that the pre-exponential factor measures the rate of the collisions that occur between the reactants [43].

7.2.8.3 Product gas yields

In this section, only the first stage of the experiments will be discussed. It should be noted that during this stage the temperature increased from 25 to 750°C at a heating rate of 40°C/min. A comparison of the model and the experimental gas yields is shown in Figure 7.5.The model and the experimental results are generally in good agreement for H_2 and CH_4, and reasonable agreement for CO and CO_2.

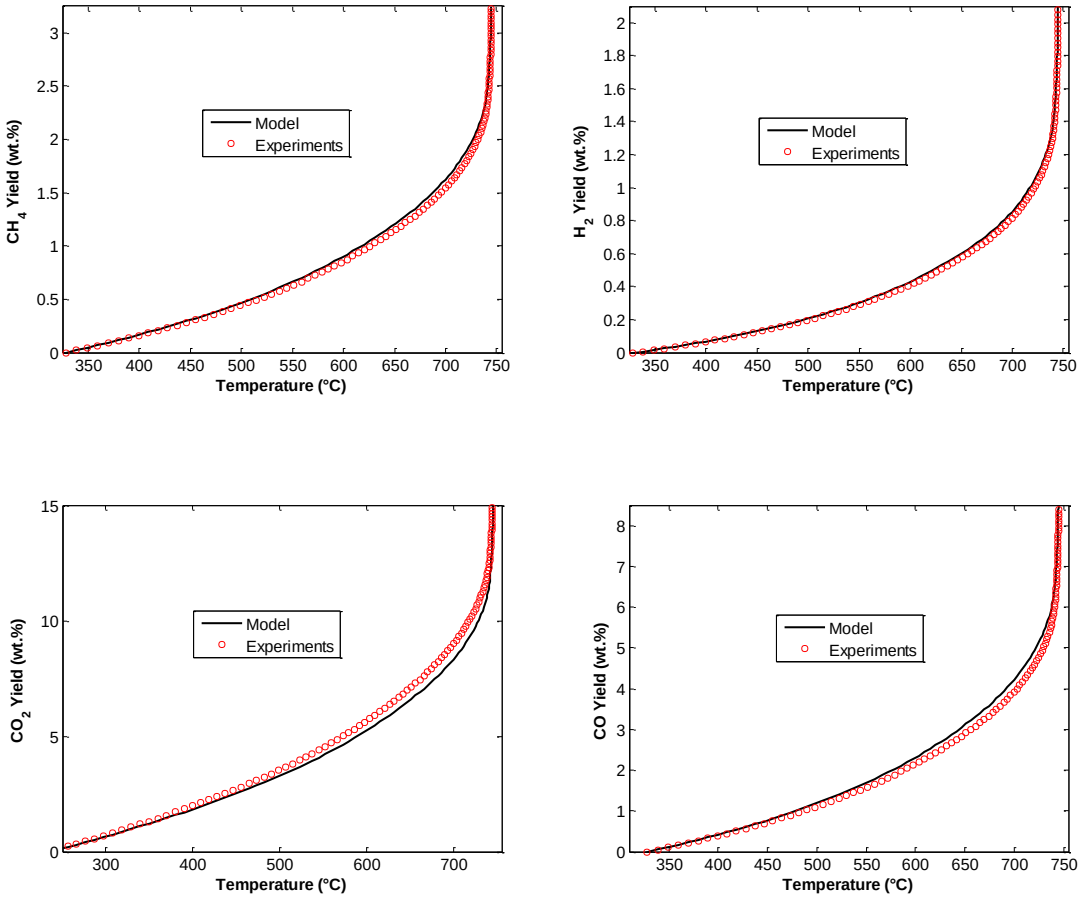

Figure 7.5 Temperature effect on gas yields: experiments vs. model

7.2.8.4 Product gas compositions

Table 7.12 represents the temperature effect on the gas product composition, N_2 free.

The experiments and the model results are in complete agreement. Hydrogen production is exceedingly promoted with temperature. As expected, the CO to CO_2 ratio is increased when the temperature rises. Methane production, however, was decreased with temperature.

Table 7.12 Effect of temperature on N_2 free gas composition: model vs. experiments

Temperature (°C)		**650**		**750**
Gas	Model	Experiments	Model	Experiments
CO	25.5%	26.3 %	17 %	17.5 %
CO_2	30.6%	30.4 %	14.5%	13.9%
CH_4	18.0 %	18.4%	10.8%	11%
H_2	2.1 %	2.1%	37.3%	38%

The experiments and the model results are in complete agreement. Hydrogen production is greatly promoted due to the temperature. As expected, the CO to CO_2 ratio is increased when the temperature rises. Methane production, however, decreased with temperature.

7.2.8.5 Transient gas yields

The experimental results for the second stage are used for this section, where the temperature was fixed at 750°C for two hours. Figure 7.6 indicates the transient product gas yields at 750°C. The model and the experimental gas yields are generally in good agreement, which confirms the reliability of the kinetic parameters that deviated from the fluidized bed TGA.

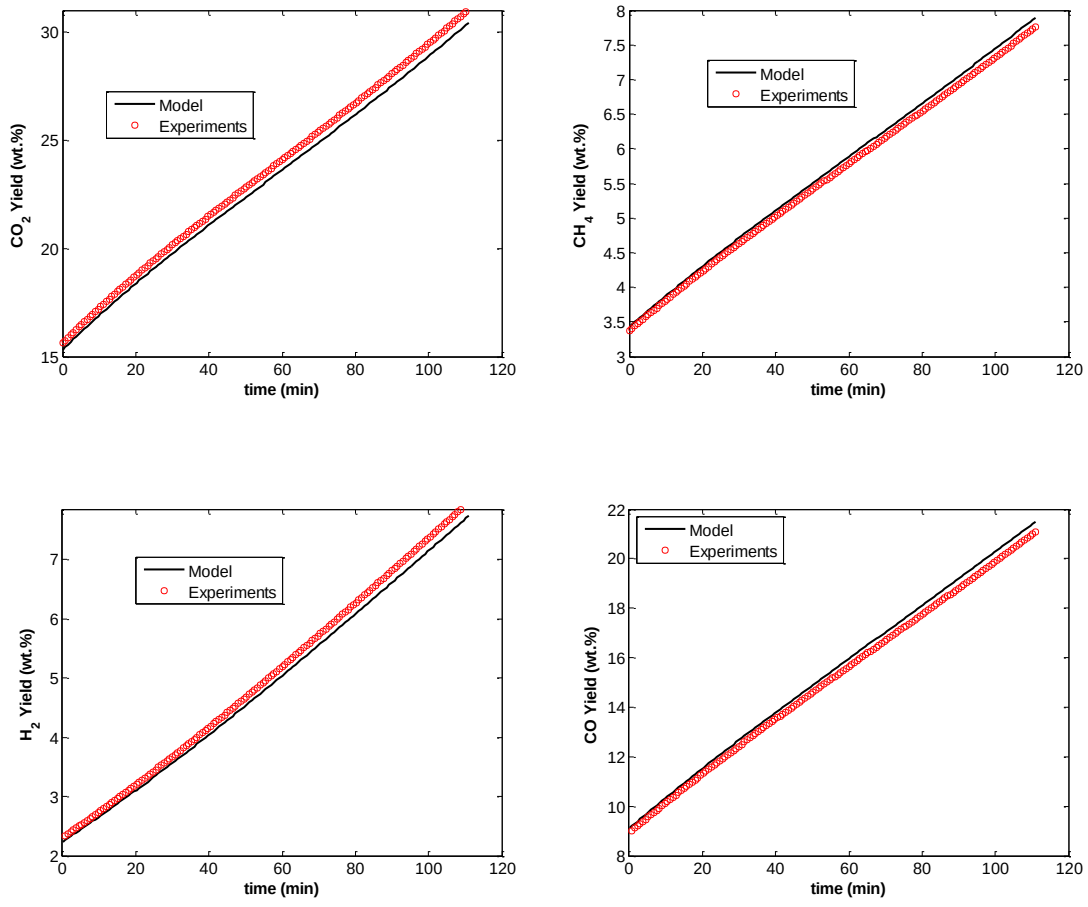

Figure 7.6 Transient gas yields at 750°C: experiments vs. model

7.2.8.6 Carbon conversion

The carbon and hydrogen conversions can be calculated as follows [56]:

$$Y_C = 12 \times \left(Y_{CO}/28 + Y_{CO_2}/44 + Y_{CH_4}/16 + 2 * Y_{C_2H_6}/30\right)$$

A comparison of the carbon conversion of coal, ash free coal and ash free coal with the catalyst is shown in Figure 7.7. CatAFC, AFC, and coal stand for the results obtained from the catalyst with ash free coal, ash free coal and coal gasification, respectively. Ash free coal has the lowest carbon conversion at temperatures below 730°C, after which this behavior was particularly changed and the carbon conversion became the lowest for coal gasification. In summary, coal beneficiation had a negative impact on carbon conversion. The results are however impressive for the catalytic ash free coal gasification. At 700°C, carbon conversion was respectively increased by 15.3% and 52.6%, for coal and ash free gasification. These values were continuously increasing to reach 44.5% and 69.1% at 750°C.

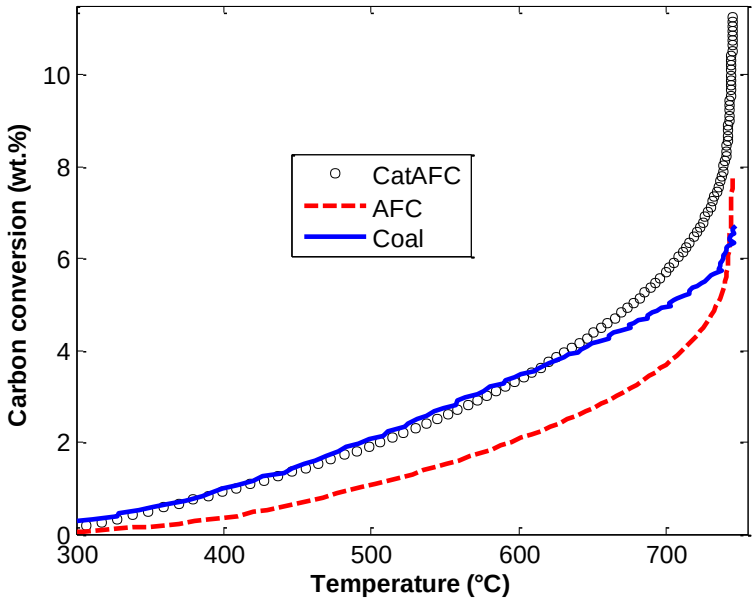

Figure 7.7 Temperature effect on carbon conversion

7.2.8.7 Higher heating value

The higher heating value (HHV) of the dry gas, N_2 free, under standard conditions could be approximated as follows [56, 115]:

$$HHV\ (MJ/Nm^3) = 12.7\ \times y_{H_2} + 12.6\ \times y_{CO} + 39.8\ \times y_{CH_4} + 70\ \times y_{C_2H_6}$$

Figure 7.8 demonstrates a comparison of the results obtained from coal, ash free coal (AFC), and catalytic ash free coal (CatAFC) gasification. Overall, the higher heating value of the gas product was significantly enhanced by removing ash from coal. The use of the catalyst, however, greatly increased the heating value of the gas product, but only for temperatures below 520°C. The maximum heating value was 14, 14.8 and 13.5 Mj/Nm^3 at temperatures of 528, 551, and 577°C for catalytic AFC, ash free coal, and coal gasification, respectively.

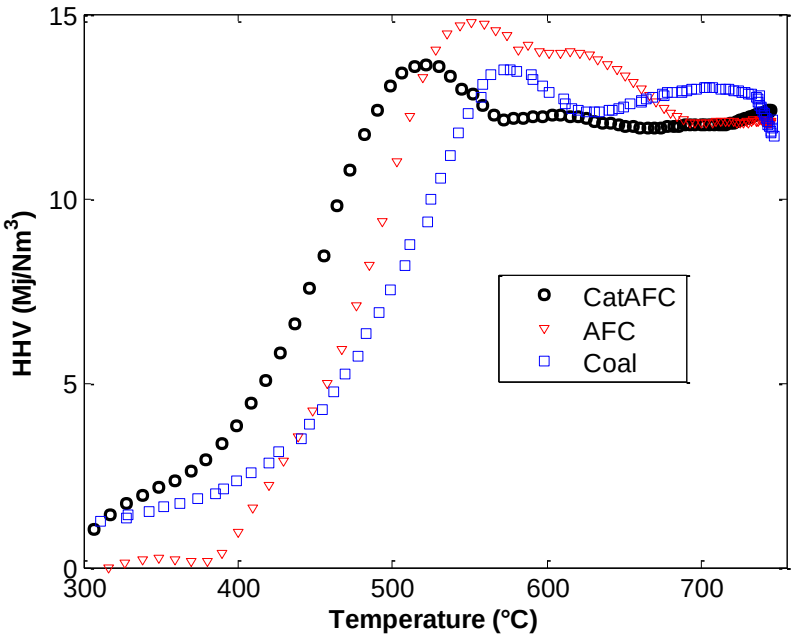

Figure 7.8 Temperature effect on HHV

Carbon conversion is similar for coal and catalytic ash free coal gasification for temperatures below 625°C. Nonetheless, a higher heating value was observed for the gas produced from catalytic ash free coal gasification for temperatures below 556°C.

7.2.9 Conclusion

The effect of a potassium catalyst (K_2TiO_3) on ash free coal gasification was studied in the fluidized bed TGA. The results obtained from the weight loss were in reasonable agreement with those found in the total gas product. The activation energy, 109.6 kJ/mol, and the pre-exponential factor, $1.45*10^{-3}$ s^{-1}, were found to be similar to those reported for coal gasification in our previous work. The effect of the catalyst was to reduce the activation energy of the CO shift reaction from 102 to 56.5 kJ/mol. For the methane reforming reaction, the activation energy decreased from 108 to 77 kJ/mol from using the catalyst. The catalytic effect on the carbon conversion was a 69% enhancement at 750°C. The use of the catalyst significantly increased the higher heating value of the gas product for temperatures below 520°C.

7.2.10 Acknowledgements

The authors are grateful to Dr. Moshfiqur Rahman for providing the ash free coal. Financial support from Carbon Management Canada (CMC-NCE) is gratefully acknowledged.

CHAPITRE 8 DISCUSSION GÉNÉRALE

Les croissances démographique et économique mondiales sont directement liées à la consommation d'énergie. Les émissions des gaz à effet de serre, en particulier le dioxyde du carbone (CO_2), suivent la même tendance : plus qu'on se développe économiquement, plus qu'on émit de CO_2. Le charbon contribue, et continuera à contribuer, majoritairement dans le portfolio de la consommation mondiale de l'énergie. Parmi toutes les sources d'énergies fossiles, l'industrie du charbon est la plus polluante.

La situation actuelle de notre globe terrestre est extrêmement alarmante. En 2015-2016, on note un record des anomalies de la température à la surface de la terre. Comme nous l'avons déjà souligné, découpler la croissance économique et le développement social de l'augmentation des emissions anthropiques des gaz à effet de serre (GES) est un défi majeur pour la communaté scientifique [2, 4, 5]. Pour ce faire, Canada, un des cinq pays les plus grands producteurs d'energie au monde, a adopté une stratégie de l'énergie qui vise à accélérer le développement et le déploiement de technologies de pointe, favorisant l'utilisation des sources d'énergie propres et fossiles [10].

C'est dans cette optique que s'inscrit notre travail, visant à developper une technologie de gazéification, pour faire extraire de l'energie du charbon d'une manière plus écologique.

L'analyseur thermogravimétrique (ATG) à lit fluidisé, developpé dans ce travail, permet d'étudier la cinétique et les méchanismes des réactions gaz-solide. La gazéification du charbon, une des applications parmi les nombreuses traitements thermiques des déchets solides, a fait l'objet de la première application de l'ATG à lit fluidisé.

Dans un premier temps, l'ATG à lit fluidisé a été testé, pour validation, sur la décomposition thermique de l'hydroxyde de calcium $Ca(OH)_2$. Les résultas on été remarquables: les limitations de transfert de matière et chaleur, observées dans l'ATG convetionnel, ont été surmontées par l'utilisation de l'ATG à lit fluidisé.

Ensuite, une étude de la cinétique de la gzéification du charbon a eu lieu dans l'ATG à lit fluidisé. Les energies d'activation obtenues ont été largement inférieures à celles reportées dans la litérature. Des resultats similaires ont été récement obtenus pour la pyrolyse de de la biomasse dans un micro-réacteur à lit fluidisé. Le deuxième volet du premier article traite l'équilibre de la gazéification du charbon dans l'ATG à lit fluidisé. Les deux réactions de réformage du méthane et de déplacement du monxyde de carbone ont été loin de leur état d'équilibre. Ce résultat est du au craquage incomlpet du gourdon, facteur classé hors équilibre.

Parce que la cendre et le goudron constituent un probleme majeur pour le developpement de la technologie de gazéification, et aucune étude n'a eu lieu sur la gazéification catalytique du charbon sans cendre, nous avons décidé d'en faire la troisième application dans l'ATG à lit fluidisé. Le charbon sans cendre a été obtenu de l'Université d'Alberta.

La technique utilisée pour enlever la cendre du charbon a été l'extraction thermique avec un solvant commercial. Cette technique n'est toutefois pas souhaitable pour des projets industriels. Un bilan de matière a montré que le taux de récupération du charbon sans cendre a été inférieur à 50%. D'autres méthodes de prétraitement du charbon pourraient être utilisées dans le futur.

L'effet du catalyseur (K_2TiO_3) sur la gazéification du charbon sans cendre a été étudié dans l'ATG à lit fluidisé. Les résultats obtenus montrent une conversion supérieure du carbone à basse température (<520°C), avec des gaz produits de meuilleure valeur energétique.

Un autre résultat important à souligner est l'utilisation du catalyseur a permis de réduire relativement la quantité du goudron produite du charbon, par 48%.

Un deuxième aspect, interessant, lié toujours à l'utilisation du catalsyeur (K_2TiO_3) est celui des énergies d'activation des réactions de la gazéification. L'applicatin du catalyseur a réduit considérablement les énergies d'activation de la réaction du réformage du methane, ainsi que celle de déplacement du monxyde de carbone (CO shift).

CHAPITRE 9 CONCLUSION ET RECOMMANDATIONS

Ce travail s'inscrit dans un grand projet, ambitieux, sur la gazéification du charbon Canadian, intitulé 'gazéification du charbon avec catalyseurs et captage de CO_2 via des adsorbants'. Le projet a été réalisé en collaboration avec plusieurs universités, dont l'Université de la Colombie Britannique, l'Université de Calgary, l'Université d'Alberta ainsi que Polytechnique Montréal. Notre travail a mis l'accent sur le développement de l'ATG à lit fluidisé y étudier la cinétique de la gazéification catalytique du charbon et charbon sans cendre.

Ainsi, les principales contributions du présent travail peuvent être présentées comme suit :

- Un analyseur thermogravimétrique à lit fluidisé (ATGLF) a été développé. C'est le premier équipement au monde qui regroupe deux technologies déjà existantes : le lit fluidisé et l'analyseur thermogravimétrique. Ces deux technologies sont difficilement assemblables par leurs principes de fonctionnement. Avant la réalisation de ce projet, cette idée apparait comme une grande contradiction à la communauté scientifique ;
- L'ATGLF a été validé par la décomposition de l'hydroxyde de calcium. Les limitations diffusionnelles ont été éliminées par le mélangeage approprié au sein de la chambre réactionnelle de l'ATG à lit fluidisé ;
- Une étude de la pyrolyse du charbon, ainsi que la gazéification du char, a été réalisée dans l'ATG à lit fluidisé. Les différents paramètres cinétiques, incluant les énergies d'activations et les facteurs pré-exponentiels, ont été développés.
- L'effet catalytique (K_2TiO_3) sur la gazéification du charbon sans cendre a permis d'obtenir une meilleure conversion à basse température avec une production des gaz d'une plus grande valeur énergique que dans le cas sans catalyseur.
- L'utilisation du catalyseur, K_2TiO_3, a permis de diminuer les énergies d'activation des réactions de réformage du méthane ainsi que celle de déplacement du monoxyde du carbone.

- Le catalyseur (K_2TiO_3) a permis de diminuer la quantité du goudron produite de la gazéification du charbon sans cendre.

Le procédé utilisé pour la production du charbon sans cendre, par l'Université d'Alberta, nous a permis d'obtenir un charbon sans cendre adéquat pour ce travail de doctorat. Cependant, ce procédé n'est pas approprié pour un projet industriel. Plus de 50% de la quantité initiale du charbon a été rejetée. Vue l'importance des résultats trouvés dans ce travail, il serait intéressant de continuer sur cette voie de prétraitement du charbon avant de le gazéifier. D'autres procédés pourraient être utilisés pour l'élimination de la cendre, ainsi que le soufre, du charbon. Tel que déjà mentionné dans la revue de littérature, le taux de rejet de charbon pourrait être inférieur à 10% de la quantité initiale. Ce taux pourrait même atteindre 3% pour le procédé « Battle Hydrothermal». Le coût de production est toutefois plus élevé pour ce procédé.

Le taux de chauffe utilisé pour les expériences reportées dans cette thèse est faible par rapport aux valeurs industrielles (40 °C/min vs. 1000 °C/s). Ainsi, il serait intéressant de faire des expériences dans l'ATG à lit fluidisé en utilisant des taux de chauffe élevés. Ce qui permettra de mieux comprendre les mécanismes des réactions étudiées.

Il serait également d'une extrême importance de faire une révision de la cinétique des différentes réactions gaz-solide, avec et sans catalyseur, dans l'ATGF. Un ATG à lit fluidisé à haute pression (ATGFP) pourrait aussi être réalisé.

Tous les équipements du laboratoire qui fonctionnent à lit fixe, dont la calorimétrie différentielle à balayage (differential scanning calorimetry, DSC), pourraient être un équipement idéal à lit fluidisé.

BIBLIOGRAPHIE

[1] "GIEC, 2013: Résumé à l'intention des décideurs. Changements climatiques 2013: Les éléments scientifiques."

[2] "United Nations Intergovernmental Panel on Climate Change. Climate change 2014: Synthesis Report. Summary for Policymakers."

[3] *NOAA National Centers for Environmental Information, State of the Climate: Global Analysis for September 2015*.

[4] (2015). *International Energy Agency Climate Change*. Available: http://www.iea.org/topics/climatechange/

[5] The way forward, five key actions to achieve a low-carbon energy sector [Online]. Available: http://www.iea.org/publications/freepublications/publication/The_Way_forward.pdf

[6] G. d. e. i. s. l. é. d. climat, "Résumé à l'intention des décideurs," 2005.

[7] R. Fernando. (October 2008). *Coal gasification*. Available: http://bookshop.iea-coal.org.uk/report/82678//82110/Coal-gasification,-CCC-140

[8] Key coal trends: excerpt from coal information [Online]. Available: http://www.iea.org/publications/freepublications/publication/KeyCoalTrends.pdf

[9] I. E. Agency. (2013). *World Energy Outlook*

[10] (2015). *Canadian Energy Strategy*. Available: http://www.canadaspremiers.ca/phocadownload/publications/canadian_energy_strategy_eng_fnl.pdf

[11] S. Samih and J. Chaouki, "Development of a fluidized bed thermogravimetric analyzer," *AIChE Journal*, vol. 61, pp. 84-89, 2015.

[12] O. Ebrahimpour, J. Chaouki, and C. Dubois, "Diffusional effects for the oxidation of SiC powders in thermogravimetric analysis experiments," *Journal of Materials Science,* vol. 48, pp. 4396-4407, 2013/06/01 2013.

[13] D. B. Anthonys, "Coal devolatilization and hydrogasification " *AIChE* vol.

22, pp. 625-656, 1976.

[14] D.Neogi, C. C. Chang, W. P. Walawender, and L. T. Fan, "Study of coal gasification in a experimental fluidized bed reactor " presented at the Annual Meeting-AIChE, San Francisco, CA, USA, 1984.

[15] B. Prabir, *Combustion and gasificaion in fluidized beds*: Taylor and Francis Group, 2006.

[16] J. L. Johnson, *Kinetics of coal gasification*. New York: John Wiley & Sons, 1979.

[17] D. B. Anthony and J. B. Howard, "Coal devolatilization and hydrogastification," *AIChE Journal,* vol. 22, pp. 625-656, 1976.

[18] E. M. Suuberg, W. A. Peters, and J. B. Howard, "Product Composition and Kinetics of Lignite Pyrolysis," *Industrial & Engineering Chemistry Process Design and Development,* vol. 17, pp. 37-46, 1978/01/01 1978.

[19] J. C. Wurzenberger, S. Wallner, H. Raupenstrauch, and J. G. Khinast, "Thermal conversion of biomass: Comprehensive reactor and particle modeling," *AIChE Journal,* vol. 48, pp. 2398-2411, 2002.

[20] J. M. Lee, Y. J. Kim, W. J. Lee, and S. D. Kim, "Coal-gasification kinetics derived from pyrolysis in a fluidized-bed reactor," *Energy,* vol. 23, pp. 475-488, 6// 1998.

[21] G. Groppi, E. Tronconi, P. Forzatti, and M. Berg, "Mathematical modelling of catalytic combustors fuelled by gasified biomasses," *Catalysis Today,* vol. 59, pp. 151-162, 2000.

[22] J. Macak and J. Malecha, "Mathematical Model for the Gasification of Coal under Pressure," *Industrial & Engineering Chemistry Process Design and Development,* vol. 17, pp. 92-98, 1978/01/01 1978.

[23] D. Neogi, C. C. Chang, W. P. Walawender, and L. T. Fan, "Study of coal gasification in an experimental fluidized bed reactor," *AIChE Journal,* vol. 32, pp. 17-28, 1986.

[24] A. Inayat, M. M. Ahmad, S. Yusup, and M. I. A. Mutalib, "Biomass Steam Gasification with In-Situ CO2 Capture for Enriched Hydrogen Gas Production: A Reaction Kinetics Modelling Approach," *Energies,* vol. 3, pp. 1472-1484, 2010.

[25] Y. J. Kim, J. M. Lee, and S. D. Kim, "Modeling of coal gasification in an internally circulating fluidized bed reactor with draught tube," *Fuel,* vol. 79, pp. 69-77, 1// 2000.

[26] J. Adanez and F. G. Labiano, "Modeling of moving-bed coal gasifiers," *Industrial & engineering chemistry research,* vol. 29, pp. 2079-2088, 1990.

[27] J. Corella and A. Sanz, "Modeling circulating fluidized bed biomass gasifiers. A pseudo-rigorous model for stationary state," *Fuel Processing Technology,* vol. 86, pp. 1021-1053, 5/25/ 2005.

[28] T. R. Nunn, J. B. Howard, J. P. Longwell, and W. A. Peters, "Product compositions and kinetics in the rapid pyrolysis of sweet gum hardwood," *Industrial & Engineering Chemistry Process Design and Development,* vol. 24, pp. 836-844, 1985/07/01 1985.

[29] M. R. Hajaligol, J. B. Howard, J. P. Longwell, and W. A. Peters, "PRODUCT COMPOSITIONS AND KINETICS FOR RAPID PYROLYSIS OF CELLULOSE," *Industrial & Engineering Chemistry, Process Design and Development,* vol. 21, pp. 457-465, 1982.

[30] K. M. Bryden and K. W. Ragland, "Numerical modeling of a deep, fixed bed combustor," *Energy & Fuels,* vol. 10, pp. 269-275, 1996.

[31] J. Neeft, H. Knoef, and P. Onaji, "Behaviour of tar in biomass gasification systems. Tar related problems and their solutions; Novembre Report No. 9919. Energy from Waste and Biomass (EWAB), The Netherlands," 1999.

[32] Z. Abu El-Rub, E. Bramer, and G. Brem, "Review of catalysts for tar elimination in biomass gasification processes," *Industrial & engineering chemistry research,* vol. 43, pp. 6911-6919, 2004.

[33] L. Devi, K. J. Ptasinski, and F. J. J. G. Janssen, "A review of the primary measures for tar elimination in biomass gasification processes," *Biomass and Bioenergy,* vol. 24, pp. 125-140, 2// 2003.

[34] C. Pfeifer and H. Hofbauer, "Development of catalytic tar decomposition downstream from a dual fluidized bed biomass steam gasifier," *Powder Technology,* vol. 180, pp. 9-16, 1/14/ 2008.

[35] S. Li and Y. Cheng, "Catalytic gasification of gas-coal char in CO2," *Fuel,* vol. 74, pp. 456-458, 3// 1995.

[36] A. A. Hakeem, L. Mu, R. J. Berger, F. Kapteijn, and M. Makkee, "Kinetics of the high temperature water-gas shift over Fe2O3/ZrO2, Rh/ZrO2 and Rh/Fe2O3/ZrO2," *Chemical Engineering Journal,* vol. 263, pp. 427-34, 03/01 2015.

[37] G. N. Vajani, S. L. Ng, and C. R. F. Lund, "Rate expression for water-gas shift over a gold/ferrochrome catalyst," *Industrial and Engineering Chemistry Research,* vol. 50, pp. 10493-10499, 2011.

[38] N. A. Pechimuthu, K. K. Pant, S. C. Dhingra, and R. Bhalla, "Characterization and activity of K, CeO2, and Mn promoted Ni/Al2O3 Catalysts for carbon dioxide reforming of methane," *Industrial and Engineering Chemistry Research,* vol. 45, pp. 7435-7443, 2006.

[39] Y. Wang, Y. Zhai, D. Pierre, and M. Flytzani-Stephanopoulos, "Silica-encapsulated platinum catalysts for the low-temperature water-gas shift reaction," *Applied Catalysis B: Environmental,* vol. 127, pp. 342-350, 2012.

[40] I. Balint and K.-i. Aika, "Temperature-programmed desorption study of water-gas shift and methane steam-reforming reactions over Li/MgO catalyst," *Applied Catalysis A:General,* vol. 196, pp. 209-215, 2000.

[41] M. H. Halabi, M. H. J. M. de Croon, J. van der Schaaf, P. D. Cobden, and J. C. Schouten, "Intrinsic kinetics of low temperature catalytic methane–steam reforming and water–gas shift over Rh/CeαZr1−αO2 catalyst," *Applied Catalysis A: General,* vol. 389, pp. 80-91, 12/1/ 2010.

[42] M. H. Park, B. K. Choi, Y. H. Park, D. J. Moon, N. C. Park, and Y. C. Kim, "Kinetics for steam and CO2 reforming of methane over Ni/La/Al2O3 catalyst," *Journal of Nanoscience and Nanotechnology,* vol. 15, pp. 5255-5258, 2015.

[43] T. W. Kim, J. C. Park, T.-H. Lim, H. Jung, D. H. Chun, H. T. Lee, *et al.*, "The kinetics of steam methane reforming over a Ni/γ-Al2O3 catalyst for the development of small stationary reformers," *International Journal of Hydrogen Energy,* vol. 40, pp. 4512-4518, 4/13/ 2015.

[44] J. Wei and E. Iglesia, "Structural requirements and reaction pathways in methane activation and chemical conversion catalyzed by rhodium," *Journal of Catalysis,* vol. 225, pp. 116-127, 7/1/ 2004.

[45] E. Ramirez-Cabrera, A. Atkinson, and D. Chadwick, "Partial oxidation and steam reforming of methane over Ce0.9Gd0.1O2-x [SOFC catalyst]," in *Fourth European Solid Oxide Fuel Cell Forum. Proceedings, 10-14 July 2000*, Oberrohrdorf, Switzerland, 2000, pp. 49-58.

[46] A. M. Robinson, M. E. Gin, and M. M. Yung, "Methane steam reforming kinetics on a Ni/Mg/K/Al2O3 catalyst," in *Special Issue Honoring Umit Ozkan - ACS Distinguished Researcher in Petroleum Chemistry. Editors: Burcu Bayram, John N. Kuhn, and Matthew M. Yung*, 2013, pp. 1708-1715.

[47] K. Gosiewski, U. Bartmann, M. Moszczyński, and L. Mleczko, "Effect of the intraparticle mass transport limitations on temperature profiles and catalytic performance of the reverse-flow reactor for the partial oxidation of methane to synthesis gas," *Chemical Engineering Science,* vol. 54, pp. 4589-4602, 10// 1999.

[48] M. Barrio, M. Fossum, and J. E. Hustad, "A samll scale stratifier downdraft gasifier coupled to a gas engine for combined heat and power production," *Norwegian Universiy of Science and Technology,* 2000.

[49] R. Radmanesh, "Fluidized bed biomass gasification," Ph.D., University of Montreal, Ecole Polytechnique, Montreal, 2006.

[50] W. R. Smith and R. W. Missen, "Chemical reaction equilibrium analysis: theory and algorithms," *John Wiley and Sons, xvi+ 364, 23 x 15 cm, illustrated,* 1982.

[51] X. T. Li, J. R. Grace, C. J. Lim, A. P. Watkinson, H. P. Chen, and J. R. Kim, "Biomass gasification in a circulating fluidized bed," *Biomass and Bioenergy,* vol. 26, pp. 171-193, 2// 2004.

[52] C. R. Altafini, P. R. Wander, and R. M. Barreto, "Prediction of the working parameters of a wood waste gasifier through an equilibrium model," *Energy Conversion and Management,* vol. 44, pp. 2763-2777, 2003.

[53] D. Bacon, J. Downie, J. Hsu, and J. Peters, "Modelling of fluidized bed wood gasifiers," in *Fundamentals of thermochemical biomass conversion*, ed: Springer, 1985, pp. 717-732.

[54] K. Mansaray, A. Al-Taweel, A. Ghaly, F. Hamdullahpur, and V. Ugursal, "Mathematical modeling of a fluidized bed rice husk gasifier: Part I-Model development," *Energy Sources,* vol. 22, pp. 83-98, 2000.

[55] M. Ruggiero and G. Manfrida, "An equilibrium model for biomass gasification processes," *Renewable energy,* vol. 16, pp. 1106-1109, 1999.

[56] M. S. Masnadi, J. R. Grace, X. T. Bi, C. J. Lim, N. Ellis, Y. H. Li, *et al.*, "Single-fuel steam gasification of switchgrass and coal in a bubbling fluidized bed: A comprehensive parametric reference for co-gasification study," *Energy,* vol. 80, pp. 133-147, 2/1/ 2015.

[57] R. Radmanesh, J. Chaouki, and C. Guy, "Biomass gasification in a bubbling fluidized bed reactor: Experiments and modeling," *AIChE Journal,* vol. 52, pp. 4258-4272, 2006.

[58] M. L. de Souza-Santos, "Comprehensive modelling and simulation of fluidized bed boilers and gasifiers," *Fuel,* vol. 68, pp. 1507-1521, 1989/12/01 1989.

[59] D. Fiaschi and M. Michelini, "A two-phase one-dimensional biomass gasification kinetics model," *Biomass and Bioenergy,* vol. 21, pp. 121-132, 2001.

[60] S. Hamel and W. Krumm, "Mathematical modelling and simulation of bubbling fluidised bed gasifiers," *Powder technology,* vol. 120, pp. 105-112, 2001.

[61] R. Radmanesh, R. Mabrouk, J. Chaouki, and C. Guy, "Effect of temperature on solids mixing in a bubbling fluidized bed reactor," *International Journal of Chemical Reactor Engineering,* vol. 3, 2005.

[62] K. S. Lim, V. S. Gururajan, and P. K. Agarwal, "Mixing of homogeneous solids in bubbling fluidized beds: theoretical modelling and experimental investigation using digital image analysis," *Chemical Engineering Science,* vol. 48, pp. 2251-2265, 1993.

[63] J. Grace, "Fluidized Bed Reactor Modeling," ed, 1981.

[64] O. Sitnai, "Solids mixing in a fluidized bed with horizontal tubes," *Industrial & Engineering Chemistry Process Design and Development,* vol. 20, pp. 533-538, 1981.

[65] J. A. Yu, J. R. Yue, Z. E. Liu, L. Dong, G. W. Xu, J. H. Zhu, *et al.*, "Kinetics and Mechanism of Solid Reactions in a Micro Fluidized Bed Reactor," *Aiche Journal,* vol. 56, pp. 2905-2912, Nov 2010.

[66] M. Pantoya, J. J. Granier, A. Rai, K. Park, and M. Zachariah, "The effect of heating rate on the reaction kinetics of nanoscale aluminothermic reaction," *AIChE* 2005.

[67] V. Despina, K. Evaggelia, S. Stelios, and S. Piero, "Gasification of waste biomass chars by carbon dioxide via thermogravimetry-effect of catalysts," *Combustion Science and Technology,* vol. 184, pp. 64-77, 2012.

[68] S. Katarzyna, B. Pietro, and F. Francesco, "Thermogravimetric analysis and kinetic study of poplar wood pyrolysis," *Applied Energy,* vol. 97, pp. 491-497, 2012.

[69] J. P. Sanders and P. K. Gallagher, "Kinetics of the oxidation of magnetite using simultaneous TG/DSC," *Journal of Thermal Analysis and Calorimetry,* vol. 72, pp. 777-789, 2003.

[70] P. Sivakumar, P. Sivakumar, K. Anbarasu, R. Mathiarasi, and S. Renganathan, "An eco-friendly catalyst derived from waste shell of scylla tranquebarica for biodiesel production," *International Journal of Green Energy,* vol. 11, pp. 886-897, 2014.

[71] Y. M., D. N.D., and P. D., "Co-pyrolysis of lignite and sugar beet pulp," *Energy Conversion and Management,* vol. 51, pp. 1060-4, 2010.

[72] F. Wang, X. Zeng, J.-Z. Han, J.-W. Zhang, Y.-Y. Liu, Y. Wang, *et al.*, "Comparation of char gasification kinetics studied by micro fluidized bed and by thermogravimetric analyzer," *Ranliao Huaxue Xuebao/Journal of Fuel Chemistry and Technology*, vol. 41, pp. 407-413, 2013.

[73] R. Radmanesh, Y. Courbariaux, J. Chaouki, and C. Guy, "A unified lumped approach in kinetic modeling of biomass pyrolysis," *Fuel*, vol. 85, pp. 1211-1220, 6// 2006.

[74] Y. Jian, Y. Changbin, Z. Xi, G. Shuang, D. Li, W. Yin, *et al.*, "Biomass pyrolysis in a micro-fluidized bed reactor: characterization and kinetics," *Chemical Engineering Journal*, vol. 168, pp. 839-47, 04/01 2011.

[75] J. Yu, X. Zeng, J. Zhang, M. Zhong, G. Zhang, Y. Wang, *et al.*, "Isothermal differential characteristics of gas-solid reaction in micro-fluidized bed reactor," Langford Lane, Kidlington, Oxford, OX5 1GB, United Kingdom, 2013, pp. 29-36.

[76] Y.-h. Lin, Z.-c. Guo, H.-g. Tang, S. Ren, and J.-w. Li, "Kinetics of Reduction Reaction in Micro-Fluidized Bed," *Journal of Iron and Steel Research International*, vol. 19, pp. 6-8, 06/ 2012.

[77] J. R. Grace, J. Chaouki, and T. Pugsley, "Fluidized Bed Reactor," *Particle Technology and Applications*, p. 199, 2012.

[78] C. Higman and M. Van der Burgt, *Gasification*: Gulf professional publishing, 2011.

[79] X. Zeng, F. Wang, Y. Wang, A. Li, J. Yu, and G. Xu, "Characterization of char gasification in a micro fluidized bed reaction analyzer," 2540 Olentangy River Road, P.O. Box 3337, Columbus, OH 43210-3337, United States, 2014, pp. 1838-1845.

[80] Y. Courbariaux, *Étude et mise au point d'un procédé de traitement des brasques de l'industrie de l'aluminium*, 2005.

[81] F. Fotovat, J. Chaouki, and J. Bergthorson, "Distribution of large biomass particles in a sand-biomass fluidized bed: Experiments and modeling," *AIChE Journal*, vol. 60, pp. 869-880, 2014.

[82] G. G. Joseph, J. Leboreiro, C. M. Hrenya, and A. R. Stevens, "Experimental segregation profiles in bubbling gas-fluidized beds," *AIChE journal*, vol. 53, pp. 2804-2813, 2007.

[83] P. Rowe and A. Nienow, "Particle mixing and segregation in gas fluidised beds. A review," *Powder Technology*, vol. 15, pp. 141-147, 1976.

[84] J. Shabanian, R. Jafari, and J. Chaouki, "Fluidization of ultrafine powders," *International Review of Chemical Engineering*, vol. 4, pp. 16-50, 2012.

[85] J. Desypris, P. Murdoch, and A. Williams, "Investigation of the flash pyrolysis of some coals," *Fuel*, vol. 61, pp. 807-816, 9// 1982.

[86] A. P. Watkinson, J. P. Lucas, and C. J. Lim, "A prediction of performance of commercial coal gasifiers," *Fuel*, vol. 70, pp. 519-527, 4// 1991.

[87] M. Aghabararnejad, G. S. Patience, and J. Chaouki, "Transient modeling of biomass steam gasification with Co3O4," *Fuel*, vol. 140, pp. 354-364, 1/15/ 2015.

[88] K. Kato and C. Wen, "Bubble assemblage model for fluidized bed catalytic reactors," *Chemical engineering science*, vol. 24, pp. 1351-1369, 1969.

[89] C. Wen and Y. Yu, "A generalized method for predicting the minimum fluidization velocity," *AIChE Journal*, vol. 12, pp. 610-612, 1966.

[90] J. Werther, "47 Modeling and scale-up of industrial fluidized bed reactors," *Chemical Engineering Science*, vol. 35, pp. 372-379, 1980.

[91] D. Kunii and O. Levenspiel, "Bubbling bed model for kinetic processes in fluidized beds. Gas-solid mass and heat transfer and catalytic reactions," *Industrial & Engineering Chemistry Process Design and Development*, vol. 7, pp. 481-492, 1968.

[92] S. Farag, L. Kouisni, and J. Chaouki, "Lumped approach in kinetic modeling of microwave pyrolysis of kraft lignin," *Energy & Fuels*, vol. 28, pp. 1406-1417, 2014.

[93] J. Yu, J.-h. Zhu, F. Guo, Z.-k. Duan, Y.-y. Liu, and G.-w. Xu, "Reaction kinetics and mechanism of biomass pylolysis in a micro-fluidized bed reactor," *Journal of Fuel Chemistry and Technology*, vol. 38, pp. 666-672, 12// 2010.

[94] X. Zeng, F. Wang, Y. Wang, A. Li, J. Yu, and G. Xu, "Characterization of char gasification in a micro fluidized bed reaction analyzer," *Energy & Fuels,* vol. 28, pp. 1838-1845, 2014.

[95] C. Von Fredersdorff, M. Elliot, and H. Lowry, "Chemistry of Coal Utilization," *Supplementary VolumeJohn Wiley, New York,* p. 939, 1963.

[96] R. Coates, C. Chen, and B. Pope, "Coal devolatilization in a low pressure, low residence time entrained flow reactor," *Coal gasification,* pp. 92-98, 1974.

[97] J. Kopyscinski, J. Lam, C. A. Mims, and J. M. Hill, "K2CO3 catalyzed steam gasification of ash-free coal. Studying the effect of temperature on carbon conversion and gas production rate using a drop-down reactor," *Fuel,* vol. 128, pp. 210-219, 7/15/ 2014.

[98] I. Lee, S. Jin, D. Chun, H. Choi, S. Lee, K. Lee, *et al.*, "Ash-free coal as fuel for direct carbon fuel cell," *Science China Chemistry,* vol. 57, pp. 1010-1018, 2014/07/01 2014.

[99] K. M. Steel and J. W. Patrick, "The production of ultra clean coal by chemical demineralisation," *Fuel,* vol. 80, pp. 2019-2023, 11// 2001.

[100] K. Formella, P. Leonhardt, A. Sulimma, K. H. van Heek, and H. Jüntgen, "Funcat Cogas '86: the international symposiumInteraction of mineral matter in coal with potassium during gasification," *Fuel,* vol. 65, pp. 1470-1472, 1986/10/01 1986.

[101] K.-T. Kim, K.-H. Kim, and J.-O. Choi, "K 2 CO 3-catalysed steam gasification of a coal char," *Fuel,* vol. 68, pp. 1343-1346, 1989.

[102] X. Li, Z. Zhu, R. De Marco, J. Bradley, and A. Dicks, "Modification of Coal as a Fuel for the Direct Carbon Fuel Cell," *The Journal of Physical Chemistry A,* vol. 114, pp. 3855-3862, 2010/03/25 2010.

[103] E. Kurkela, K. Sipilä, and J. Koljonen, "Synthesis gas production from Finnish peat by fluid-bed gasification," *Proc. Energy from biomass and wastes, Washington,* 1986.

[104] S. P. N. Singh and G. R. Peterson, "ADVANCES IN COAL BENEFICIATION," *Coal Processing Technology,* vol. 5, pp. 24-30, 1979.

[105] B. MISHRA, B. DAS, S. BISWAL, and P. REDDY, "Overview of Beneficiation, Utilization and Environmental Issues in Relation to Coal Processing," in *Proc Indian Natn Sci Acad*, 2015, pp. 725-737.

[106] P. Meshram, B. K. Purohit, M. K. Sinha, S. K. Sahu, and B. D. Pandey, "Demineralization of low grade coal – A review," *Renewable and Sustainable Energy Reviews,* vol. 41, pp. 745-761, 1// 2015.

[107] D. Gidaspow, D. Wasan, S. Saxena, Y. Shih, R. P. Gupta, and A. Mukherjee, "ELECTROSTATIC DESULFURIZATION OF COAL IN FLUIDIZED BEDS AND CONVEYORS," in *American Institute of Chemical Engineers 1986 Annual Meeting.*, Miami, FL, USA, 1986, pp. AIChE, New York, NY, USA.

[108] R. J. Nankee, "CHLORINATED SOLVENTS FOR COAL BENEFICIATING," in *Soc of Mining Engineers, Preprints for Presentation at the SME Annual Meeting.*, Denver, CO, USA, 1987, pp. Soc of Mining Engineers of AIME, Littleton, CO, USA.

[109] A.Moilanen, "Ash behaviour in gasification," in *Symposium on Low-Grade Fuels. Part 2*, Finlande, 1989, pp. 423-430.

[110] F. Kapteijn and J. A. Moulijn, "Kinetics of catalysed and uncatalysed coal gasification " in *Carbon and Coal Gasification: Science and Technology*, 1986.

[111] J. L. Johnson, "Kinetics of coal gasification: a compilation of research," 1979.

[112] F. Kapteijn and J. A. Moulijn, "KINETICS OF CATALYSED AND UNCATALYSED COAL GASIFICATION," in *Carbon and Coal Gasification: Science and Technology.*, Alvor, Port, 1986, pp. 291-360.

[113] J. Kopyscinski, M. Rahman, R. Gupta, C. A. Mims, and J. M. Hill, "K2CO3 catalyzed CO2 gasification of ash-free coal. Interactions of the catalyst with carbon in N2 and CO2 atmosphere," *Fuel,* vol. 117, Part B, pp. 1181-1189, 1/30/ 2014.

[114] N. Okuyama, N. Komatsu, T. Shigehisa, T. Kaneko, and S. Tsuruya, "Hyper-coal process to produce the ash-free coal," *Fuel Processing Technology,* vol. 85, pp. 947-967, 2004.

[115] D. Lide, "CRC Handbook of Chemistry and Physics 2004-2005: A Ready-Reference Book of Chemical and Physical Data," ed: CRC press Boca Raton, 2004.

ANNEXE A – MOMENTUM BALANCE ON THE MICRO-REACTOR OF THE FLUIDIZED BED TGA

As indicated in the first article, the pseudo variation of the weight of the fluidized bed TGA is due to the fluidizing agent that is flowing into the reactor. More precisely, the pseudo variation of the weight is due to the total weight of the FB-TGA, i.e., when there is fluidizing agent flowing over the reactor and when there isn't. Hence, a differential momentum balance on the reactor is carried out in order to derive a mathematical formulation for this concept of the pseudo variation of the weight of the FB-TGA.

The control volume is represented by figure A.1. It includes the triplet reactor-distributor-filter.

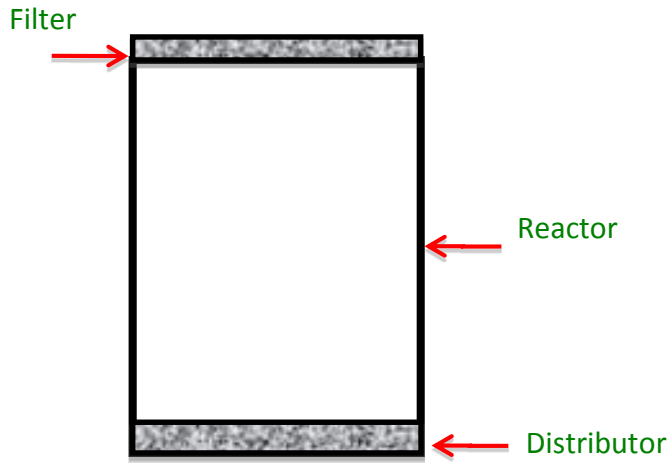

Figure A. 1 Control volume for the momentum balance

When there is no fluidizing agent that is flowing (U_g=0), the total weight of the reactor, which is measured by the load cell, can be formulated as follows:

$$m_{real}\left(t,T,U_g=0\right)=m_{reactor}\left(t,T,U_g=0\right)+m_{bed}\left(t,T\right) \qquad (1)$$

However, when the fluidizing agent flows to the reactor, it applies an ascending force on the reactor in the *z* direction. The expression of this force is given by the momentum balance shown in figure 2.

As illustrated in figure A. 2, the different terms of the momentum balance can be classified into three groups: (1) pressure effect, (2) convection effect and (3) gravity effect. The pressure effect regroups the following:

- The whole pressure before the distributor: $\Delta P_{dist.} + \Delta P_{bed} + \Delta P_{filter}$;
- The whole pressure after the distributor: $\Delta P_{bed} + \Delta P_{filter}$;
- The whole pressure before the filter ΔP_{filter};

However, the convection terms include the following:

- The force applied by convection on the reactor before the distributor: $\rho_{g0} U_{g0}^2 S$;
- The force applied by convection on the reactor after the distributor: $\rho_{g1} U_{g1}^2 S$;
- The force applied by convection on the reactor before the filter: $\rho_{g2} U_{g2}^2 S$;
- The force applied by convection on the reactor after the filter: $\rho_{g3} U_{g3}^2 S$;

Finally, the gravity term, applied by the fluidizing agent on the reactor, represents the weight of the fluid inside the reactor.

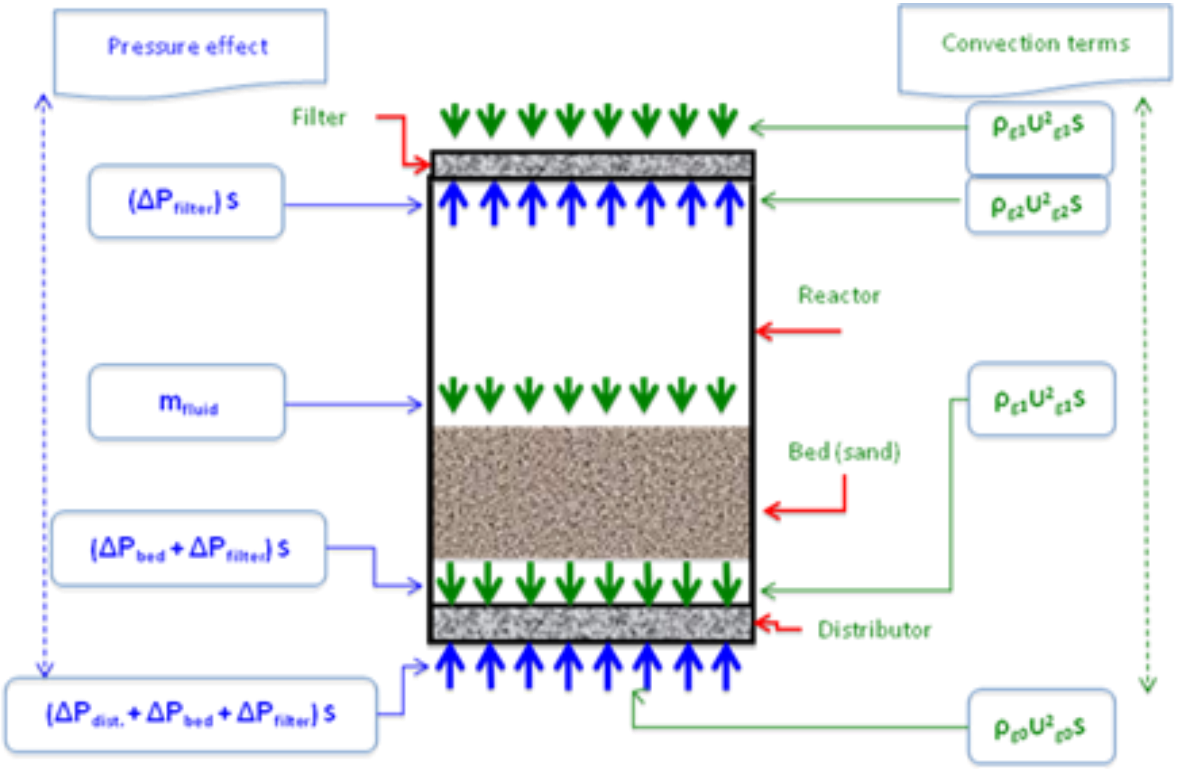

Figure A.2 Momentum balance on the fluidized bed reactor (FB-TGA)

As shown in figure A. 2, the ascending force applied by the fluidizing agent on the reactor, in the z direction, can be expressed as follows:

$$F_{fluid\rightarrow reactor}\Big|_z = \left[\left(\Delta P_{dist.} + \Delta P_{bed} + \Delta P_{filter}\right)\times S + \left(\Delta P_{filter}\right)\times S + \rho_{g0}U_{g0}^2 \times S + \rho_{g2}U_{g2}^2 \times S\right] - \left[\left(\Delta P_{bed} + \Delta P_{filter}\right)\times S + \rho_{g1}U_{g1}^2 \times S + \rho_{g3}U_{g3}^2 \times S\right] - m_{fluid}\times g \quad (2)$$

After simplification, the above expression becomes:

$$F_{fluid\rightarrow reactor}\Big|_z = \left[\left(\Delta P_{dist} + \Delta P_{filter}\right)\times S + \beta U_{g0}^2 \times S\right] - m_{fluid}\times g$$

$$Where, \beta = \left(\rho_{g0} + \rho_{g2}\frac{U_{g2}^2}{U_{g0}^2}\right) - \left(\rho_{g1}\frac{U_{g1}^2}{U_{g0}^2} + \rho_{g3}\frac{U_{g3}^2}{U_{g0}^2}\right) \quad (3)$$

By neglecting the convection term and the weight of the fluid inside the reactor, the final expression of the force applied by the fluidizing gas on the reactor is given by equation 4.

$$F_{fluid\rightarrow reactor}\Big|_z = \left(\Delta P_{dist} + \Delta P_{filter}\right)\times S \quad (4)$$

The concept of the pseudo variation of the weight of the reactor is due to the force expressed by equation 4. Therefore, equation 5 gives the expression of such pseudo variation of the weight, denoted Δm_P, as a function of the pressure drop across the distributor and filter of the reactor.

$$\Delta m_P = \alpha_P \times \left(\Delta P_{dist.} + \Delta P_{filter}\right); \alpha_P = \frac{S}{g} \qquad (5)$$

Furthermore, the apparent weight of the reactor, which is measured by the load cell, can be expressed by equation 6.

$$m_{app.}(t,T,U_g) = m_{real}(t,T,U_g) - \Delta m_P(t,T,U_g) \qquad (6)$$

Where:

$$m_{real}(t,T,U_g) = m_{reactor}(t,T,U_g) + m_{bed}(t,T) \qquad (7)$$

And Δm_P denotes the pseudo variation of the weight of the reactor given by equation 5.

In more concrete terms, the model that gives the real weight of the reactor is expressed in equation 8.

$$m_{real}\left(t,T,U_g\right) = m_{app.}\left(t,T,U_g\right) + \Delta m_P\left(t,T,U_g\right) \qquad (8)$$

To include the effect of the pseudo variation of the reactor weight in the FB-TGA results, the pressure drop along distributor and filter should be measured, converted to weight, and subtracted from the total weight loss of the reactor.

ANNEXE B – CERTIFICAT DE CALIBRATION DE LA CELLULE DE CHARGE 101AH

Calibration Data

Input Resistance: 837 Ω
Output Resistance: 470 Ω
Calibration Factor: 20.7915mV/V
Operator(s): Bernard Smallwood
Calibration Date: 09/06/2011
Calibration Procedure: 072-LC75-10, Rev -, Date 02/19/2008

% Capacity	Load (grams)	Raw (mV/V)	Normalized (mV/V)
0	0.00	0.1904	0.0000
50	125.00	10.5835	10.3931
100	250.00	20.9830	20.7926
50	125.00	10.5918	10.4014
0	0.00	0.1929	0.0025

Shunt Calibration Data

Line No.	Shunt Resistor	Shunt Sense	Zero	Shunt Zero	Shunt Cal	Shunt Cal. Capacity
1	10kΩ	N/A	N/A	N/A	11.5133 mV/V	N/A

Calibration Standards

NIST Traceable #	Inst. ID#	Description	Model	Cal Date	Date Due
4782169	100563	HOOK HANGER WEIGHT SET	1 KG,500,200,100,50,25	01/18/2011	01/18/2013
4540811	100157	HOOK HANGER WEIGHT SET	25,100,200,500	10/11/2010	10/11/2013
4540980	100569	STAINLESS STEEL HANGER W	F CLASS	10/11/2010	10/11/2012
4540953	100581	STAINLESS STEEL HANGER W	CLASS 6	10/11/2010	10/11/2012
3928655	100108	STAINLESS STEEL WEIGHT S	25,50,100,200,500,1000G	02/26/2010	02/26/2012
4396960	101565	WEIGHT STD W / HANGER 45	9484T	08/16/2010	08/16/2013
4396971	101566	WEIGHT STD W / HANGER 45	9484T	08/16/2010	08/16/2013
5106576	7241234	DECADE RESISTOR	0-10M OHMS	05/04/2011	05/04/2012
4751105	100751	DIGITAL MULTIMETER	34401A	01/05/2011	01/05/2012
4751095	100820	DIGITAL MULTIMETER	34401A	01/05/2011	01/05/2012

Environmental Data

Temperature: 73 °F
Humidity: 47 %RH
Pressure: 14.30 psiA

Certificate No
1346201--001

PRINT DATE: 9/6/2011
Page 2 of 2
Document No. 086-1000-09

ANNEXE C – CERTIFICAT CSA POUR LE FOUR ET LE CONTRÔLEUR ZCP560

Zesta Engineering Limited
Control Systems Division
212 Watline Avenue Mississauga Ontario Canada L4Z 1P4
905-568-3100 **Email** slock@zesta.com **Fax** 905-568-3100

Zesta Engineering Limited
Control Systems Division
212 Watline Avenue Mississauga Ontario Canada L4Z 1P4
905-568-3100 **Email** slock@zesta.com **Fax** 905-568-3

Validation for ZCP560

Control panel functional specification for ZCP560
Date: November 27, 2012

Volts 240 **Phase** 1 **Amps** 12 **Hertz** 60

puts shall be connected to the panel. All sensor inputs shall oads shall be connected to the panel. The panel shall ll comply with the specifications before being released.

Standard Specifications

e 4.72"(120mm)H x 11.81"(300mm)W x 7.87"(200mm)D and have a NEMA rati t requires special inputs or outputs that Zesta Engineering L meter) power cord c/w a twist-lock plug (L6-15P NEMA configuration) as mea nts shall be discussed before construction begins. single phase and a current rating of 15 amps.

nd limit zones will be one, using the Watlow **series EZ-ZONE PM Integrated c** l accept two type "K" Thermocouples. Process and Limit temperature sensors req

s will be the **Zesta ZPAC Solid State Relay Assembly** (PN ZPAC-600-15-C current rating of 15 Amps .

ill be connected via Zesta supplied twist-lock power receptacle (L6-15R NEMA co

nections will be connected via Zesta supplied type K thermocouple universal jacks

Custom specifications for ZCP560

he following custom programmable features:
nd Soak Temperature and Limit Controller.
nication port.

For more information, see drawings numbered ZCP56002.PRJ, ZCP56015.SCH & ZCP560L

on for programming controllers:
ure in degrees °C or °F _____?
ure set point _____?
alarm set point _____?

the authorized person or persons agrees with the specifica provide a signature and date on each drawing and this form.

Zesta Engineering is a CSA Approved Panel Shop
File LR91385

Zesta Engineering is a CSA Approved Panel Shop
File LR91385